THE UNIVERSITY OF MICHIGAN

INDUSTRY PROGRAM OF THE COLLEGE OF ENGINEERING

THE VIBRATORY TRANSPORT OF BULK MATERIALS

(Arthur Donald)

Arthur D. Brickman

A dissertation submitted in partial fulfillment
of the requirements for the degree of
Doctor of Philosophy in the
University of Michigan
Department of Mechanical Engineering
1963

November, 1963

IP-639

Doctoral Committee:

Professor Joseph E. Shigley, Chairman
Professor Robert M. Haythornthwaite
Professor Robert C. Juvinall
Assistant Professor Robert B. Keller
Professor J. Raymond Pearson

ACKNOWLEDGMENTS

The author acknowledges with graditude the wise counsel of his doctoral thesis committee, particularly that of its chairman, Professor Shigley, during the execution of this research.

Thanks are also extended to the National Science Foundation, the Ford Foundation, and the Syntron Company of Homer City, Pennsylvania, whose financial support made the author's work possible.

TABLE OF CONTENTS

TABLE OF CONTENTS CONT'D

LIST OF TABLES

LIST OF FIGURES

LIST OF FIGURES CONT'D

LIST OF FIGURES CONT'D

NOMENCLATURE

A	=	amplitude of surface vibration, in.
A_w	=	orifice area, $in.^2$
A_x	=	A cos α, horizontal component of vibration amplitude, in.
A_y	=	A sin α, vertical component of vibration amplitude, in.
b	=	width of conveyor channel occupied by transport material, in.
C_w	=	dimensionless orifice discharge coefficient.
F	=	instantaneous tangential force acting on lower face of material element, lb.
F_a	=	maximum instantaneous value of F available from dry friction, lb.
F_r	=	maximum instantaneous value of F required to prevent sliding, lb.
g	=	gravitational constant, in/sec^2.
G	=	instantaneous normal force acting on lower face of material element, lb.
h	=	nominal depth of transport material on conveying surface, in.
k	=	dimensionless specific heat ratio for perfect gases, 1.4 for air.
K	=	permeability coefficient for air flow through transport material, sec.
m	=	mass of transport material element, $lb\text{-}sec^2/in.$
n	=	frequency of vibration, cycles/sec.
N	=	frequency of vibration, cycles/min.
p	=	instantaneous absolute pressure of air in clearance between transport material and vibrating surface, $lb/in.^2$
p_o	=	absolute pressure of ambient air, $lb/in.^2$

p_s = absolute stagnation pressure, lb/in.^{2}

$r, \dot{r}, \ddot{r}$ = instantaneous vertical displacement, velocity, and acceleration of transport material relative to vibrating surface: in, in/sec, and in/sec^2.

R = perfect gas constant, in/deg R.

$s, \dot{s}, \ddot{s}$ = instantaneous horizontal displacement, velocity, and acceleration of transport material relative to vibrating surface: in, in/sec, and in/sec^2.

S = horizontal surface area of transport material, in.^{2}

t = elapsed time, sec.

T = instantaneous absolute temperature of air in clearance under transport material, deg R.

T_o = absolute temperature of ambient air, deg R.

T_s = absolute stagnation temperature, deg R.

U = average horizontal flow velocity of transport material, ft/min.

v = $\dot{r}/\omega A_y$, dimensionless instantaneous vertical velocity of transport material element relative to vibrating surface,

V = $\omega^2 A_y/g$, maximum vertical acceleration component of vibrating surface, g's (dimensionless).

w = instantaneous mass flow rate of air through transport material, lb-sec/in.

w_i = mass flow rate of a perfect gas in an isentropic nozzle, lb-sec/in.

W = average horizontal flow rate of transport material, lb/min.

$x, \dot{x}, \ddot{x}$ = instantaneous absolute horizontal displacement, velocity, and acceleration: in, in/sec, in/sec^2.

$y, \dot{y}, \ddot{y}$ = instantaneous absolute vertical displacement, velocity, and acceleration: in, in/sec, in/sec^2.

α = inclination of surface vibration, deg.

β = $\tan^{-1}\lambda$, dimensionless damping factor.

λ = $\rho_o/\rho K\omega$, dimensionless damping factor.

μ = coefficient of dry friction for transport material on conveying surface, dimensionless.

ρ = density of transport material, lb-sec^2/in.^{4}

ρ_o = density of ambient air, lb-sec^2/in.^{4}

φ = ωt, elapsed angle in vibration cycle, rad.

φ_a, φ_b = respective values of φ at which transport material loses and regains contact with surface, deg.

φ_0, φ_1 = respective values of φ at which transport material begins and stops sliding in the forward direction on the conveyor surface, deg.

φ_2, φ_3 = respective values of φ at which transport material begins and stops sliding in the backward direction on the conveyor surface, deg.

ω = $2\pi n$, circular frequency of vibration, rad/sec.

NOTE: Where certain infrequently used symbols not listed above appear in the thesis, their meanings will be obvious from the context.

ABSTRACT

This investigation deals with the mechanism by which a bulk material can be transported across a level vibrating surface. An understanding of this phenomenon is essential for determining optimum operation as well as practical limitations in vibratory conveyor design. It is shown that for a specified material, surface, and vibration, the transport flow rate can be predicted with engineering accuracy from an appropriate theoretical model of the dynamic system.

An experimental conveyor in which material depth, vibration inclination, amplitude, and frequency could be independently varied was operated with a single material comprised of 0.008-inch diameter glass beads. Flow rates were measured for depths up to 2 in., inclination angles up to 60 deg. amplitudes up to 0.068-inch, and frequencies up to 4000 cpm; friction and air transmission measurements were made of the test material and its behavior observed during a purely vertical vibration.

Idealized dynamic models of the bulk material, some not previously studied, were analyzed to determine how density, friction, and permeability affect the cyclic hopping-sliding motion that characterizes the transport mechanism. Theoretical performance based on the measured properties of the glass bead material is compared with test data.

Both experimental and theoretical results show that the most important operating parameter for a conveyor is the peak vertical acceleration of its vibrating surface. When this acceleration is less

than 1.0g the material moves by pure sliding so that the frictional effects at the material-surface interface become important. Above 1.0g however, material motion is due primarily to cyclic hopping of the material with sliding having little effect on the flow rate.

All results indicate that the upper limit on the material flow rate is equal to the peak horizontal velocity attained by the vibrating surface, and maximum flow occurs for vertical accelerations above 3g.

Test results indicate that the transport velocity attained by a relatively five-grained material is lower than that predicted by simple dynamic theory, particularly at large conveyor amplitudes. A unique analysis of cyclic air flow through such a material is used to establish the effect of material permeability on the transport mechanism.

I. INTRODUCTION

The problem of transporting materials and parts from one place to another during an industrial operation falls within the domain of the materials handling engineer. He must be concerned with the continuous movement of not only objects of large unit size but also relatively fine-grained bulk solids such as pulverized coal and sand.

A practical device which has a number of inherent advantages for moving granular materials but whose operating principles are not fully understood is the so-called vibratory conveyor. This thesis deals with the basic phenomenon by which such conveyors utilize a mechanical vibration to impart motion to an aggregate material.

A. General Aspects of Vibratory Transport

A great deal of engineering study has been given in recent years to improved methods for transporting materials over variable distances. In general, the conveyor transport systems that have evolved for industrial service can be divided into two categories according to whether the conveying surface has continuous or oscillatory motion. The first category is typified by belt conveyors which are essentially moving platforms that involve little relative motion between the conveyed material and the belt. In the second category are the shaker and vibratory conveyors where relative motion of the material on the conveying surface is a prerequisite of operation.

Shaker conveyors consist of a long rigid trough mounted on rollers and driven in a type of horizontal back-and-forth motion calculated to slide the material forward a certain distance each cycle. The

total stroke of shaker conveyors is large, around 10 inches, and the frequency of oscillation is low, about 100 cpm. Vibratory conveyors are a more recent development in the field of materials handling and in contrast to the shaker type, generally operate with displacement amplitudes less than 0.1 inch and frequencies in the 1000 to 10,000 cpm range.

The construction and operation of a vibratory conveyor can best be examined in terms of an idealized kinematic model, Figure 1, having the same essential features. It consists of a rigid trough or channel supported horizontally on bars that form a parallelogram linkage. A free hinge of the linkage is driven at constant speed by a crank or eccentric so that the entire mechanism undergoes a small-amplitude vibration. Because of the arrangement of the parallelogram links, however, the channel vibration is not horizontal but somewhat inclined. If an aggregate material is now introduced at the closed end of the channel, it will acquire what appears to be a steady motion toward the open end, and the rate of material flow can be accurately controlled by adjustment of a gate placed across the channel near the inlet.

Each point on the channel may be considered as vibrating sinusoidally along a short inclined trajectory, and the motions of all points on the channel are identical. On the rightward and slightly upward stroke of the vibratory cycle, the transport material is thrown completely clear of the channel and momentarily acquires a trajectory of its own. Because of the gravitational force however, the material ultimately drops back into contact but only at some later time in the

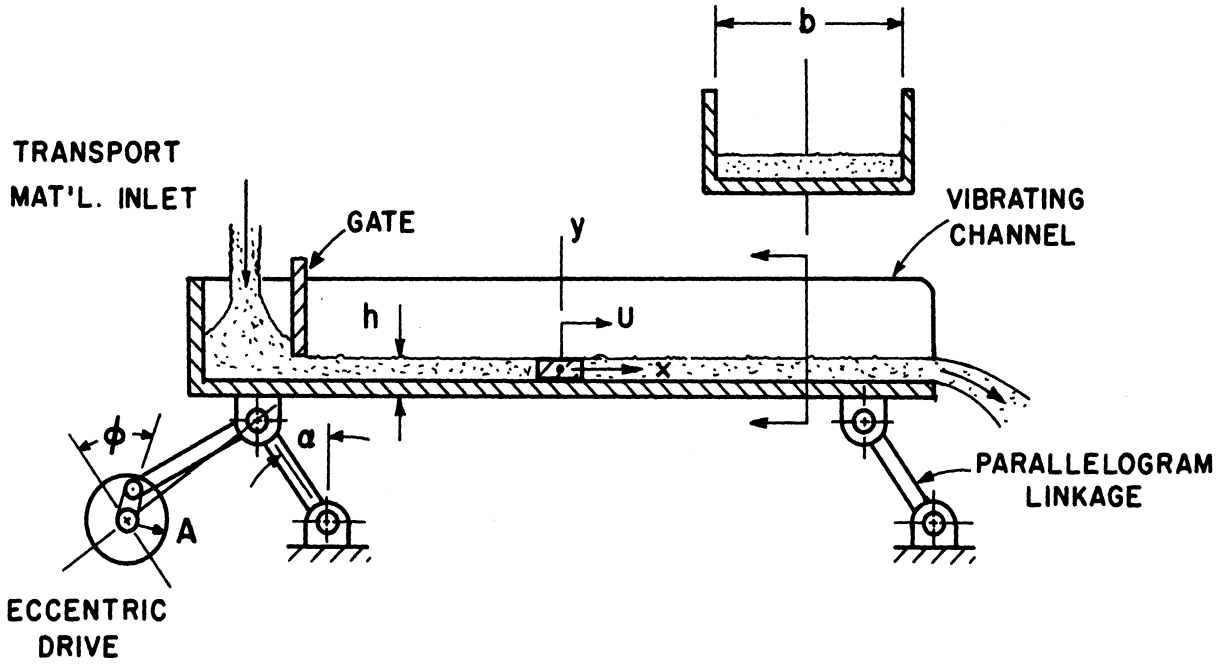

Figure 1. Sketch of an Elementary Vibratory Conveyor.

cycle when the channel has completed a portion of its return stroke. Once frictional contact between the material and vibrating surface has been re-established, the channel begins another forward stroke and the cycle is repeated. The result of this action during continuous operation of the conveyor is that the transport material, by a succession of tiny hops and slides, moves intermittently along the channel from inlet to discharge.

Commercial vibratory conveyors using the foregoing principle are uniquely adapted for parts and material transport in many industrial situations. They have found wide application in the conveying of high-temperature aggregates like foundry sand, hot coke, and rolling mill scale. The vibrating channel can be enclosed or made in a tubular form to transport powder-like, sterile, or noxious materials which might otherwise involve severe dust, contamination, or fume problems. Since the conveyor will clean itself of a material no longer supplied to its inlet end, different materials can be run in succession without fear of contamination. Many vibratory conveyors are applied in transporting materials simultaneously undergoing a secondary process such as mixing, cooling, screening, drying, or coating.

Industrial versions of this conveyor are available in a range of sizes from less than one foot to over 100 feet in length although economic and design factors impose severe limitations on maximum length. In most applications the conveyor is confined to operation with the vibrating channel horizontal since upgrade and downgrade transport of only about 10 degrees of slope can be achieved. Use of the conveyor

for transport of unit or packaged loads is not too common though it is increasing. Bulk solids susceptible to aeration do not convey well by vibration because they tend to float above a thin layer of material moving along the surface of the channel. Compared with continuous-motion conveyors, the vibratory type is characterized by relatively low power requirements, good control of transport flow rate, and minimum wear even when handling abrasive materials.

B. Work of Previous Investigators

Vibratory methods of transporting bulk materials, mostly shaker conveyors, were first used in mining operations[21,18] about forty years ago. The development and widespread application of the modern vibratory conveyor, however, did not occur until the time of World War II[1,20,27,26], and many variations of these conveyors are on the market today[9,5,29,13].

The design of a practical vibratory conveyor is complicated not only by great differences in the conveyability and other properties of bulk materials, but also by the related problems of generating and isolating the required mechanical vibration. Thus the most common conveyor configuration, unlike the kinematic model of Figure 1, is that of a two-mass dynamic system: a vibrating channel elastically coupled to a massive base and excited by an electromagnetic, rotating-weight, or eccentric drive motor. The base absorbs reactions from the drive mechanism and is itself elastically connected to the ground structure. Except for secondary effects such as internal friction and the reactive effect of the transport material on the channel, the prediction of bare conveyor vibrations from the two-mass model involves no serious theoretical problems, and a

considerable number of dynamic analyses of conveyor systems, but exclusive of material effects, have been undertaken[6,10,25,11,7,4].

Although the relationships between bulk solid properties and ease of transport are not fully understood, vibratory conveyors have been successfully used with hundreds of different materials. For the most part, selection of suitable conveyor specifications and prediction of performance are made on the basis of trial-and-error and experience. There is a considerable effort underway, however, to identify material flow properties in such a way that they can be used with theoretical principles to predict material behavior and hence become a worthwhile adjunct in equipment design. With this objective, properties which affect storage and gravity flow[15,14,22], conveyability[8,12,16], and power loss in conveyors[16,23] have been investigated from both experimental and theoretical viewpoints, but only with limited success.

At the same time that material properties have been under study, some attention has been given in the last ten years to the phenomenon of vibratory transport itself, namely the specific motions and dynamic interactions of the transport material with respect to the vibrating surface. About 25 years ago, Bachmann[2] used a mechanically driven conveyor in which to study the motion of transport material by stroboscopic light. He obtained maximum vertical vibratory accelerations of about 1.5 g (one g is the acceleration of gravity) and concluded that the material, once thrown free of the conveyor surface during the vibration cycle, obeys the law of free fall in a vacuum. This observation has served as a basic assumption for most modern investigators.

About ten years ago, Klockhaus[17] considered the motion of a particle on a level surface vibrating sinusoidally at some inclination to the horizontal. By neglecting all sliding motion, velocity gradients, impact effects, and air resistance, he obtained expressions for the phase and duration of the intermittent hopping displacement of the particle and used these to derive an equation for the mean flow velocity of the conveyed material. At approximately the same time, Jung[16] studied the theoretical operation of a comparatively low-speed inclined conveyor in which a sliding mode of material transport was to take place. Jung's analysis of the material sliding mechanism was not carried to the point where direct relationships could be drawn between conveyor performance and design specifications, and is somewhat obscured by his simultaneous consideration of drive motor dynamics and other aspects of the over-all problem. More recently, Wolff[28] performed an analysis of a similar conveyor using a sliding particle model, but his dynamic concepts relating to simple friction do not agree with those of previous investigators.

Both Jung[16] and Schraud[23] have made theoretical analyses of the power requirements of vibratory conveyors. Jung evaluates power consumption from the excess of frictional power due to sliding over the rate at which the material loses potential energy due to conveyor channel inclination. On the other hand, Schraud's particle analysis precludes sliding and he calculates power consumption from energy losses due to inelastic impact between the transport material and conveying surface. In neither case were experimental data reported to substantiate predicted results.

Vibratory transport of relatively fine-grained materials has long been known to be an unpredictable and erratic operation, even on conveyors that give satisfactory performance with coarse aggregates. The reason for this has been attributed by Kroll[19] and Böttcher[3] to the reluctance of powder-like materials to transmit a flow of air. Such a lack of permeability would apparently prevent a layer of fine material from being thrown free of the conveyor surface as readily during the vibration cycle as an equally thick layer of coarse material. Thus the displacements of the fine material relative to the surface would be diminished if not completely stopped, and conveyor output reduced.

Kroll's results clearly indicate that fine aggregates placed on a vibrating surface do not behave like particles in a vacuum and that the assumption of negligible air resistance is not always a very realistic one in a transport analysis. The results of Böttcher's experiments with cement on a 50 cps conveyor further demonstrate the turbulent and unstable behavior that occurs with fine stock for vibratory acceleration levels just slightly greater than 1.0 g and nominal flow depths.

The property of air permeability, though an important general factor in vibratory transport, is not significant for many conveyor combinations of material coarseness, flow depth, and acceleration levels. This fact has been substantiated by Böttcher[3] and Schultz[24], who, using filter gravel and 50-mesh sand respectively, obtained test results agreeing in many respects with predictions of simple particle theory. A similar situation exists with respect to the frictional characteristic of the transport material and the vibrating surface: in certain ranges

of operation, variation in the friction coefficient has a marked effect on conveyor performance but in others only a nominal effect. Thus as Erisman[8] has pointed out, continuing progress in materials handling depends not only on the recognition of specific material properties affecting the transport mechanism, but also on the incorporation of these properties into the analysis and design of conveyor systems.

C. Scope and Purpose of this Research

This research was undertaken to investigate the mechanism by which a dry granular material is transported across a level vibrating surface. A thorough understanding of this phenomenon is necessary to establish optimum operating conditions as well as practical limitations in the design of vibratory conveyor systems. The experimental phases of the study consisted of the following:

1. A special-purpose vibratory conveyor was constructed and tests performed to observe the relationship between the mean transport velocity of the material and the independent operating variables of flow depth, vibration angle, amplitude, and frequency. The ranges of numerical values for these independent variables over which the test data extend are 1/4 to 2 inches, 20 to 60 degrees, .01 to .07 inch, and 800 to 4000 cpm, respectively. A commercial sand-like material, glass spheres .008 inch in diameter, was used as the transport material in all tests.

2. In order to identify the material properties that most strongly influence the mechanism of transport, measurements were made to determine the density, friction coefficient, and air permeability

of the test medium. Frictional drag data were observed for steady motion of the material on the actual conveyor surface, and permeability data were obtained from measurements of steady-state air flow through a sample of the material.

3. A series of tests were run to observe the dynamic behavior of the bulk material under the influence of a perfectly vertical vibration of the transport surface. Photographs of signals corresponding to surface displacement and contact force as functions of time were made during these tests. In addition, high speed motion pictures of the test material were made for certain conditions of vertical vibration.

In view of the work reported by previous investigators, an attempt was made to compare the observed performance results with those predicted from a theoretical analysis of the vibratory transport mechanism. Operation of the conveyor-material combination was extended over those ranges in which sliding friction and air permeability of the material would become influential factors. This afforded test data for comparison with calculated results in which the effect of such material properties had been taken into account. Three equivalent dynamic models of the transport system were examined and in all of them the material motion was assumed to be that of a rigid body in pure translation. Each model, however, accounts for a separate feature of conveyor operation and introduces a characteristic independent variable on which the material flow velocity depends, as follows:

1. The "hopping model" idealization formulated by previous investigators assumes that the material does not slide at all on the vibrating support, but that a relative forward displacement takes place

during that part of the vibration cycle when the material may be thrown free of the surface.

2. A "sliding model" of the transport material was studied to determine the role of frictional drag in the transport mechanism. When Coulomb friction is assumed to act between the material and vibrating support, both forward and backward sliding as well as hopping can take place during the vibration cycle and affect the mean flow velocity. Previous investigations had not accounted for all these effects.

3. Fine-grained materials, because they are relatively impervious to air flow, do not exhibit as much motion relative to the conveying surface as coarse materials. A unique "porous plate model" of the transport material was devised and studied in an attempt to account for the effects of this performace factor.

II. THEORETICAL DEVELOPMENT

Before a complicated dynamic phenomenon can be studied by means of mathematical equations, the major interacting parts comprising the system must be identified and their characteristics defined. Then a succession of idealizing assumptions regarding the operation of the system can be made so that the derived equations are as simple as possible but still predict system behavior with reasonable accuracy.

Such an approach is used in this chapter to study the motion of a bulk solid on a vibrating surface. Three idealized models of the transport mechanism are presented and results derived from the analysis of each are put in a form suitable for comparison in a later chapter with test results.

A. Basic Elements of the Transport System

Figure 1 shows a schematic representation of an elementary vibratory conveyor. It consists of a horizontal channel mounted on a parallelogram linkage and capable of executing a small-amplitude vibration produced by an eccentric drive. During operation, bulk material introduced at the closed end of the channel is propelled by the motion through a rectangular opening of height h and width b formed by a gate retained across the sides of the channel, and then proceeds toward the right to be discharged at the open end of the channel.

Because of the comparatively long linkage arms, it will be assumed that the channel vibrates in a straightline motion inclined at angle α to the horizontal. Moreover the channel will be assumed

completely rigid so each of its points has exactly the same motion. The vibration will be taken as a purely sinusoidal motion of amplitude A (one-half the total stroke) and constant circular frequency ω. Time and displacement will be measured from the mid-travel point in the vibration such that at any subsequent time t, the instantaneous displacement of the surface is $A \sin \omega t$ and the elapsed angle in the vibration is $\varphi = \omega t$.

B. Idealization of the Transport Material

Motion of the conveyed material along the vibrating surface will be reckoned from the fixed axes xy shown in Figure 1. Preliminary tests and the experience of other investigators indicate that the average transport velocity of relatively coarse aggregates does not vary appreciably in the y direction and that frictional drag from the sides of the channel does not produce much transverse, or z-direction, gradient either. Thus it is reasonable to assume that advancing sections of the material remain plane and vertical, so that the motion for purposes of analysis is that of a rigid body traveling at average velocity U in pure translation.

Three characteristic properties are attributed to the hypothetical material on which the mathematical analyses are based. These are density ρ, friction coefficient μ, and permeability factor K. The material is assumed incompressible and of uniform grain size so that density changes due to settling and aeration are negligible. Friction on the underside of the material layer is assumed to be of the Coulomb or dry type defined by a single coefficient that characterizes a particular combination of material and vibrating surface. The permeability coeffi-

cient is an index of how readily the material will transmit air flow at relatively low pressure drops and is thus related to air drag effects on the material motion.

C. The Hopping Particle Model

An extremely useful representation of the vibratory transport mechanism, apparently originating with Klockhaus[25], is one which neglects all sliding on the conveyor surface but assumes instead that the motion takes place by virtue of cyclic hopping of the transport material. A complete analysis for this hopping particle model will be made on the basis of the following specific assumptions: (a) transport material is a particle of concentrated mass, (b) particle responds inelastically to impact with surface, (c) air resistance is negligible, (d) particle does not slide on surface, and (e) surface vibration is sinusoidal.

1. Criterion for Hopping

First consider the forces which would be built up if the particle were prevented from moving at all on the vibrating surface. Under such a condition, the particle would have maximum displacement components in the horizontal and vertical directions defined by $A_x = A\cos\varphi$ and $A_y = A \sin \varphi$, respectively. For any time instant, the components x and y of the particle displacement are given by

$$x = A_x \sin \omega t \qquad \text{and} \qquad y = A_y \sin \omega t \tag{1}$$

and the force balance on the particle is as shown in Figure 2(a). Here $\ddot{x}$ and $\ddot{y}$ are the horizontal and vertical accelerations and the five

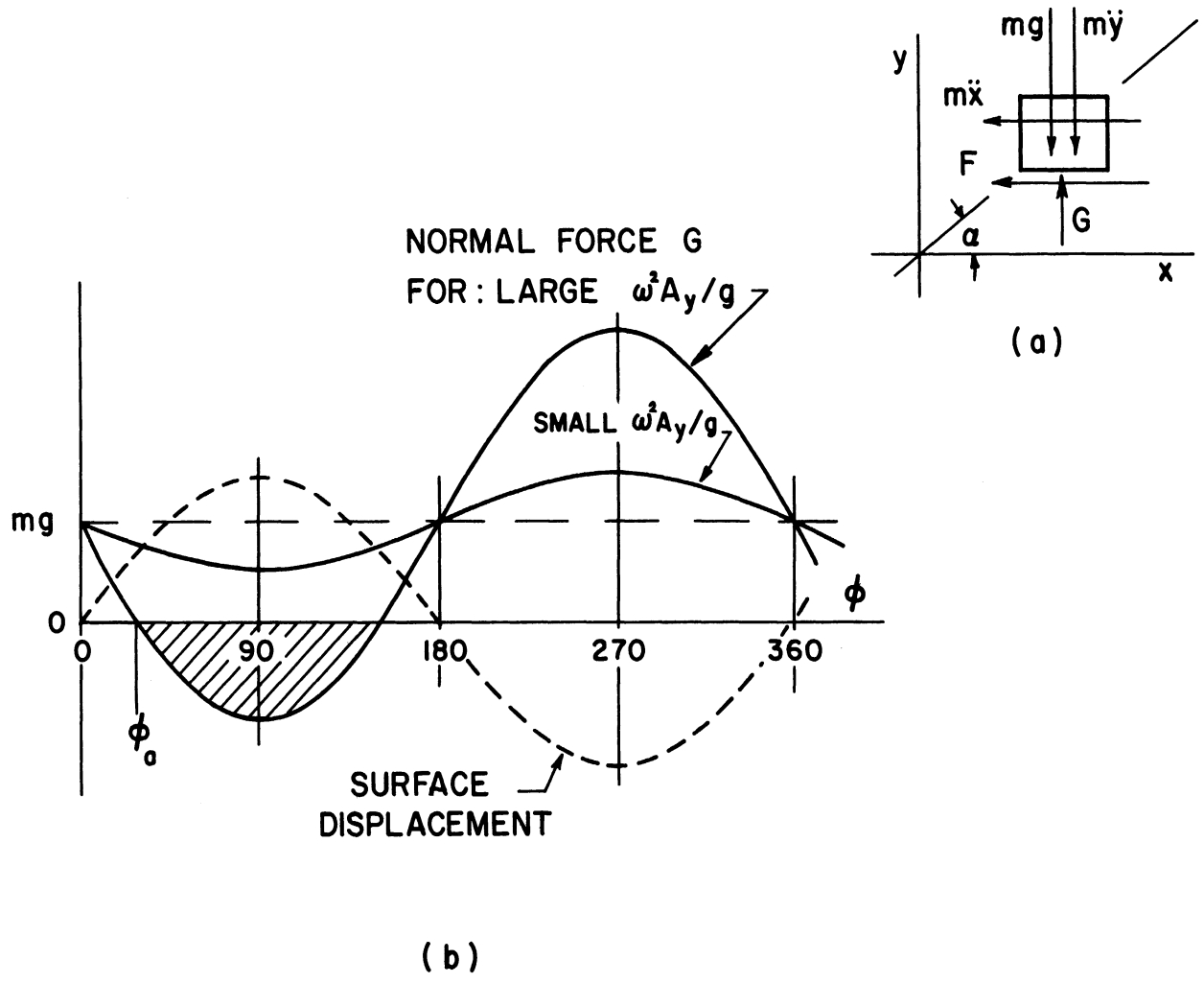

Figure 2. (a) Force Diagram for Particle of Transport Material; (b) Variation of Normal Force on Particle During Vibration Cycle.

instantaneous forces are as follows: gravity force mg , horizontal inertia force $m\ddot{x}$, vertical inertia force $m\ddot{y}$, tangential contact force F , and normal contact force G . A vertical force balance on the particle of mass m requires that

$$G = mg + m\ddot{y} \tag{2}$$

By differentiating Equation (1) twice to obtain $\ddot{y}$ and substituting the result into Equation (2), one obtains

$$G = mg \left[1 - \frac{A_y \omega^2}{g} \sin \varphi \right] \tag{3}$$

where $\varphi = \omega t$, the elapsed angle in the vibration cycle.

Variation of the normal force G during the vibration cycle ($0 < \varphi < 360$ degree) is shown by the solid-line curves of Figure 2(b). For sufficiently small values of the quantity $A_y \omega^2/g$, the normal force is always positive, i.e., upward on the particle. However when $A_y \omega^2/g$ is large, Equation (3) and the cross-hatched zone in Figure 2(b) indicate that the normal force becomes negative after some point φ_a in the cycle. Since it is physically impossible for G to ever be negative, the significance of φ_a is that it represents the elapsed angle at which the particle loses contact with the vibrating surface and begins a discrete jump or hop of its own.

The dimensionless quantity $A_y \omega^2/g$, representing the maximum vertical acceleration of the surface, is thus a most important operating variable in this model system. When this acceleration number is less

than unity, no particle transport takes place; and when greater than unity, hopping of the particle can be expected. For the latter case, Equation (3) shows that hopping commences when $G=0$ and at an angle φ_a defined by

$$\sin \varphi_a = \frac{1}{A_y \omega^2/g} \tag{4}$$

The particle will regain contact with the surface later in the cycle when their absolute vertical displacements become equal and $\varphi = \varphi_b$, as indicated in Figure 3. While in flight, the particle will have a ballistic trajectory defined by accelerations $\ddot{x} = 0$ and $\ddot{y} = -g$. Noting that the instantaneous displacements and velocities of the particle at the start of the hop ($\varphi = \varphi_a$) are respectively

$$\begin{aligned} x &= A_x \sin \varphi_a & \qquad y &= A_y \sin \varphi_a \\ x &= A_x \omega \cos \varphi_a & \qquad y &= A_y \omega \cos \varphi_a \end{aligned} \tag{5}$$

one can obtain a complete set of equations for the particle motion by successive integration as follows:

$$\left.\begin{aligned} \ddot{x} &= 0 \\ \dot{x} &= A_x \omega \cos \varphi_a \\ x &= (\varphi - \varphi_a) A_x \cos \varphi_a + A_x \sin \varphi_a \end{aligned}\right\} \tag{6}$$

$$\left.\begin{aligned} \ddot{y} &= -g \\ \dot{y} &= -\frac{g}{\omega}(\varphi - \varphi_a) + A_y \omega \cos \varphi_a \\ y &= -\frac{1}{2}\frac{g}{\omega^2}(\varphi - \varphi_a)^2 + (\varphi - \varphi_a) A_y \cos \varphi_a + A_y \sin \varphi_a \end{aligned}\right\} \tag{7}$$

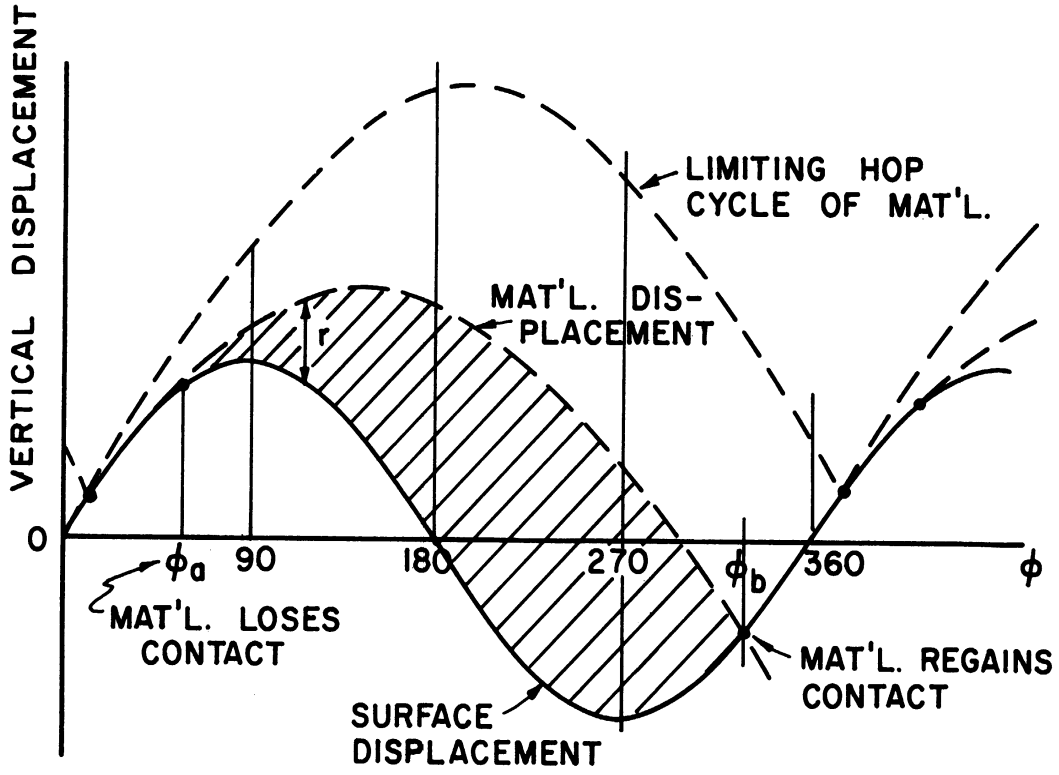

Figure 3. Vertical Motion of Material Particle and Surface During Vibration Cycle.

The particle displacement of Equation (7) can now be set equal to the surface displacement of Equation (1) to obtain the vibration angle $\varphi=\varphi_b$ denoting the end of particle flight, as follows:

$$-\frac{1}{2}\frac{g}{\omega^2}(\varphi_b-\varphi_a)^2 + (\varphi_b-\varphi_a)A_y \cos\varphi_a + A_y \sin\varphi_a = A_y \sin\varphi_b \qquad (8)$$

An implicit but unique relation between the hopping angles φ_a and φ_b is obtained by substituting Equation (1) in (8) and rearranging so that

$$\sin\varphi_b - \sin\varphi_a - (\varphi_b-\varphi_a)\cos\varphi_a = \frac{1}{2}(\varphi_b-\varphi_a)^2 \sin\varphi_a \qquad (9)$$

Digital computer values of φ_a and φ_b as a function of the maximum vertical acceleration were obtained from Equations (4) and (9) by Schultz[29] and are listed in Table I and shown graphically by the uppermost curve of Figure 4. It is seen that incipient hopping of the particle occurs at $\varphi = 90$ degree when the acceleration reaches a value of 1.0 g. For higher accelerations, φ_a occurs earlier and φ_b later in the vibration cycle, until particle flight persists during the entire cycle. The limiting case is shown by the upper dotted line in Figure 3 and the vertical line in Figure 4 at $A_y\omega^2/g = 3.3$. For accelerations greater than this, the particle model analysis breaks down as the hopping motion is no longer cyclic.[25,28]

2. Relative Horizontal Motion

Once the takeoff and landing points for the hopping motion are known it becomes possible to predict the motions of the particle relative to the surface that take place during each cycle. In particular, the relative x-direction velocity $\dot{s}$ during hopping is merely the instanta-

TABLE I

COMPUTED RESULTS FOR HOPPING PARTICLE MODEL (29)

$V = A_y\omega^2/g$	φ_a		φ_b		$U/\omega A_x$
	deg	rad	deg	rad	
1.000	90.0	1.571	90.0	1.571	0
1.003	85.9	1.500	102.2	1.783	.0063
1.015	80.2	1.400	119.5	2.085	.0368
1.038	74.5	1.300	136.9	2.389	.0908
1.073	68.8	1.200	154.4	2.697	.1661
1.122	63.0	1.100	172.7	3.013	.260
1.189	57.3	1.000	191.1	3.338	.365
1.278	51.5	.900	210.5	3.676	.480
1.395	45.9	.800	231	4.032	.595
1.553	40.1	.700	253	4.412	.705
1.770	34.4	.600	277	4.828	.805
2.09	28.6	.500	304	5.301	.878
2.57	22.9	.400	336	5.872	.926
3.30	17.65	.308	378	6.591	.950

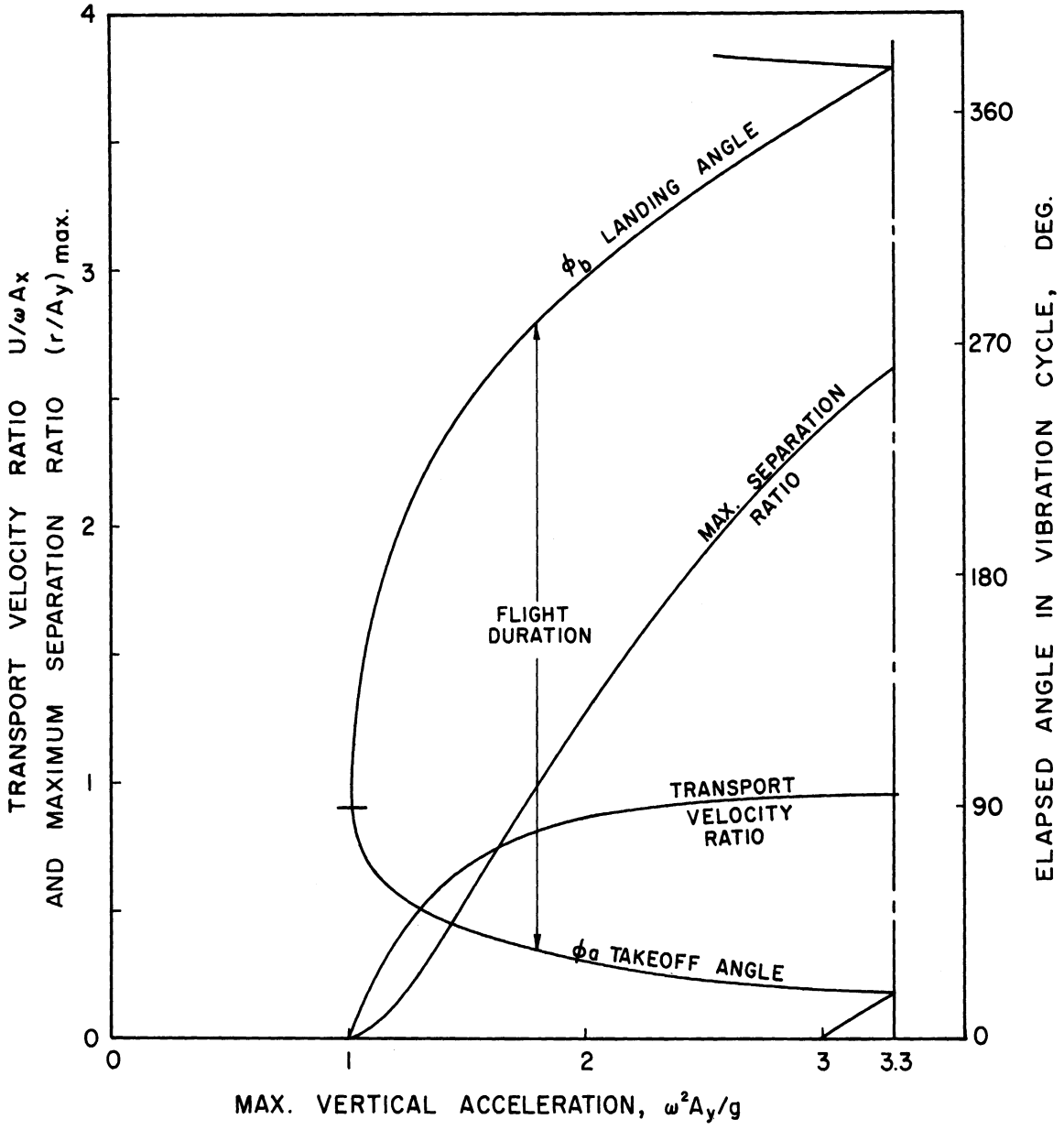

Figure 4. Behavior of Transport Material as Calculated from the Hopping Particle Model.

neous difference between the particle and surface velocities:

$$\dot{s} = A_x\omega \cos \varphi_a - A_x\omega \cos \varphi \tag{10}$$

This velocity, integrated with respect to time over the interval of hopping, yields the net forward displacement s_m per cycle:

$$s_m = \int \dot{s}\, dt = \int_{\varphi_a}^{\varphi_b} (\dot{s}/\omega) d\varphi$$

$$= A_x [(\varphi_b - \varphi_a) \cos \varphi_a - (\sin \varphi_b - \sin \varphi_a)] \tag{11}$$

The average transport velocity U of the particle is the product of this displacement and the frequency of vibration $\omega/2\pi$. A convenient dimensionless ratio representing this velocity can be formed after first combining Equations (9) and (11) as follows:

$$\frac{U}{\omega A_x} = \frac{1}{4\pi} (\varphi_b - \varphi_a)^2 \sin \varphi_a \tag{12}$$

Table I lists numerical values calculated from this equation and Figure 4 shows a plot of the velocity ratio which approaches a limiting value of unity for large values of vertical acceleration. This bears out the intuitive conclusion that the transport material velocity can never exceed the maximum horizontal velocity of the conveying surface.

3. Relative Vertical Motion

The instantaneous separation r between the material and surface during hopping is identified graphically in Figure 3 and defined as the difference between the displacements given by Equations (7) and (1):

$$r = -\frac{1}{2}\frac{g}{\omega^2}(\varphi-\varphi_a)^2 + (\varphi-\varphi_a) A_y \cos\varphi_a + A_y \sin\varphi_a - A_y \sin\varphi \quad (13)$$

The separation reaches a maximum at some value $\varphi = \varphi_m$ when the derivative $dr/d\varphi$ becomes zero and changes sign. Differentiation of Equation (13) shows that the angle of maximum separation is defined implicitly as a function of φ_a by

$$(\varphi_m-\varphi_a) \sin\varphi_a = \cos\varphi_a - \cos\varphi_m \quad (14)$$

By substituting Equation (14) into (13) and simplifying, one can obtain an expression for the maximum separation experienced by the particle during its hop as a multiple of the vertical displacement of the vibrating surface, as follows:

$$\left(\frac{r}{A_y}\right)_{max} = \frac{(\sin\varphi_a - \sin\varphi_m)^2}{2 \sin\varphi_a} \quad (15)$$

Figure 4 shows a plot of this separation ratio calculated from Equations (4), (14), and (15). It indicates an almost linear increase of separation with acceleration level.

Although Figure 4 represents all the important operating features of the hopping particle model, the calculated results in dimensionless form are not readily comparable with conveyor test data. The theoretical results can be easily converted to numerical form however by first selecting values for conveyor parameters α, A, and ω ; then using Equations (4) and (9) to obtain hop angles φ_a and φ_b ; finally calculating transport velocity U from Equation (12). Such a procedure is the basis for Figure 5 which shows typical performance curves for a hypothetical conveyor operating like the hopping particle model.

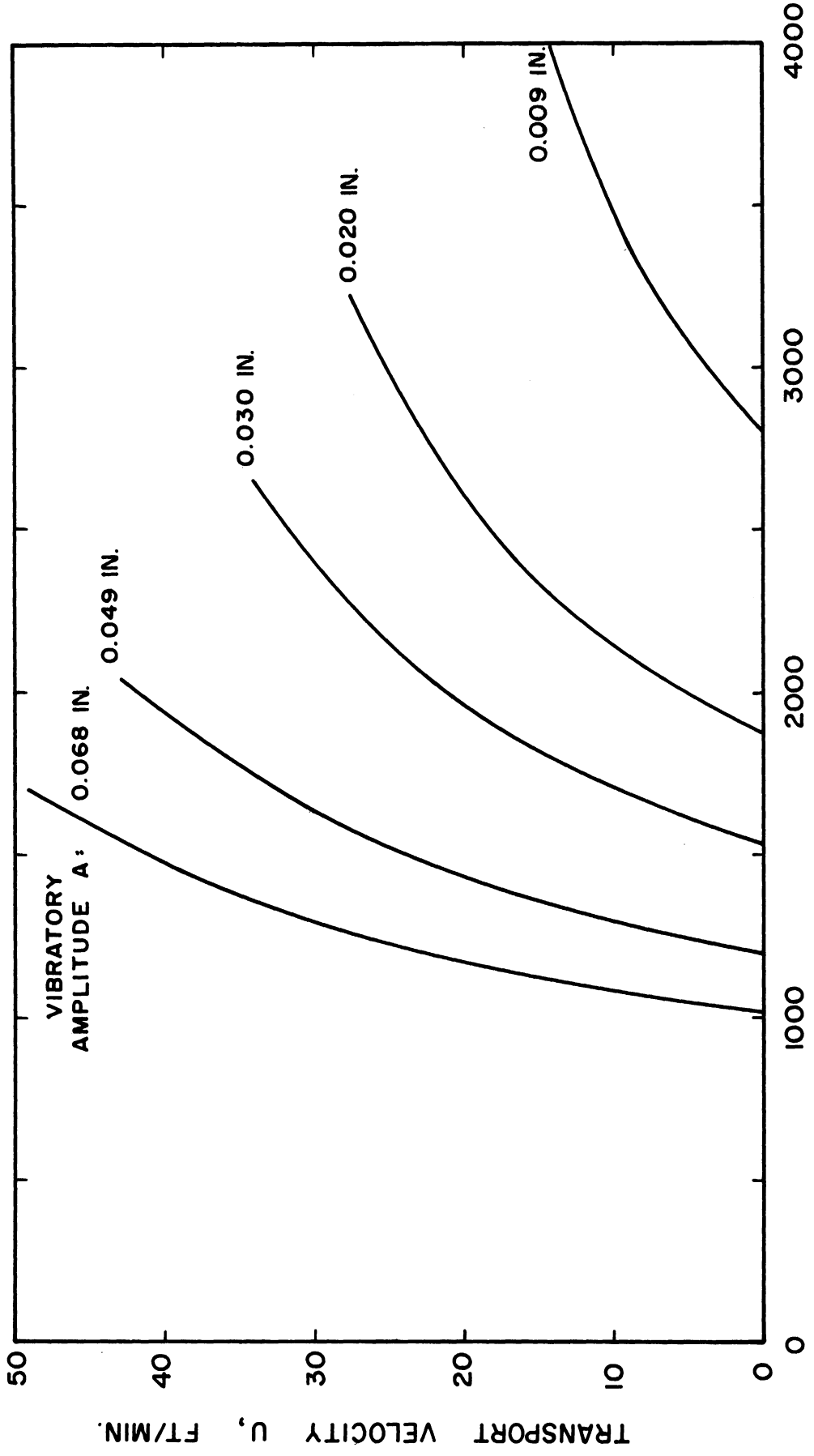

Figure 5. Performance of Vibratory Conveyor Based on Hopping Particle Model and 30 Degree Vibration Angle.

D. The Sliding Particle Model

It is evident from basic principles that a component of horizontal force must act on the transport material in order to initiate and maintain its motion relative to the conveyor surface. In the foregoing model analysis this friction force was assumed sufficiently large to prevent any slipping of the material during periods of contact with the vibrating surface. The purpose of the following analysis is to assess the role of friction at the material-surface interface by means of an idealized model in which relative motion by sliding is possible.

1. Criteria for Forward Slide

In order to account for the effects of surface friction in a simple way, the transport material will again be idealized as a single particle. However it will now be assumed that sliding of the particle can take place according to the laws of dry or Coulomb friction. No attempt will be made to include the effect of relative velocity on the dry friction coefficient μ .

Consider once more a particle that is constrained to move with the vibrating surface of a conveyor and for which the typical force diagram is shown in Figure 2(a). The normal force G on the particle varies with φ according to Equation (3), and the maximum value that the surface friction force F could ever attain is simply μG , or

$$F_a = \mu mg(1 - V \sin \varphi) \tag{16}$$

where V has been used as a shorthand symbol for the vertical acceleration number $A_y\omega^2/g$. The value of force F that would be required to

prevent any sliding of the particle can now be written from a horizontal force balance as

$$F_r = - m\ddot{x} \tag{17}$$

Since the acceleration $\ddot{x}$ can be obtained from successive differentiation of Equation (1) as

$$\ddot{x} = - A_x\omega^2 \sin \omega t \tag{18}$$

the cyclic variations of force F_r can be put in the form

$$F_r = \mu mg \left[\frac{V}{\mu \tan \alpha} \right] \sin \varphi \tag{19}$$

The true friction force on the particle will depend on the comparative size of F_a and F_r given by Equations (16) and (19) for a particular material and set of operating conditions. If, for example, the vertical acceleration V is quite low, the force F_r required to keep the particle from sliding will at all times in the cycle be smaller in magnitude than the available friction force F_a. Under such conditions, no forward motion of the particle on the conveying surface could be expected and the friction force $F = F_r$.

On the other hand, the upper part of Figure 6 shows the comparison of available and required forces for a higher acceleration level. Here the sinusoidal values of F_r in the vicinity of $\varphi = 90$ degrees exceed the corresponding values of F_a. This implies that the particle, instead of being locked on the vibrating surface as initially assumed, must break free and at the instant $\varphi = \varphi_o$ begin a sliding motion. It is evident

from the force curves in Figure 6 that the limiting value of φ_o is 90 degrees, and that the criterion for incipient slip can therefore be obtained by equating Equations (16) and (19) at that vibration angle. This results in the conclusion that forward slide of the particle will occur at some time in the vibration cycle for all

$$V \geq \frac{\mu \tan \alpha}{1 + \mu \tan \alpha} \tag{20}$$

An expression for the value of $\varphi = \varphi_o$ at which sliding begins is also obtained by equating the two forces and reduces to

$$\sin \varphi_o = \frac{1}{V} \left[\frac{\mu \tan \alpha}{1 + \mu \tan \alpha} \right] \tag{21}$$

Once sliding has been initiated at $\varphi_o < 90$ degrees, the particle moves forward on the conveyor surface under the retarding influence of a friction force $F = F_a$ so that its equation of motion changes from Equation (17) to

$$F_a = - m\ddot{x} = \mu mg(1 - V \sin \varphi) \tag{22}$$

Noting that $\ddot{x} = d\dot{x}/dt = \omega d\dot{x}/d\varphi$, one can rearrange and integrate Equation (22) as

$$\int_{\dot{x}_o}^{\dot{x}} d\dot{x} = - \frac{\mu g}{\omega} \int_{\varphi_o}^{\varphi} (1 - V \sin \varphi)\, d\varphi \tag{23}$$

to obtain the absolute velocity $\dot{x}$ of the particle for any angle φ. As indicated by the cross-hatched zone in Figure 6 the relative forward velocit

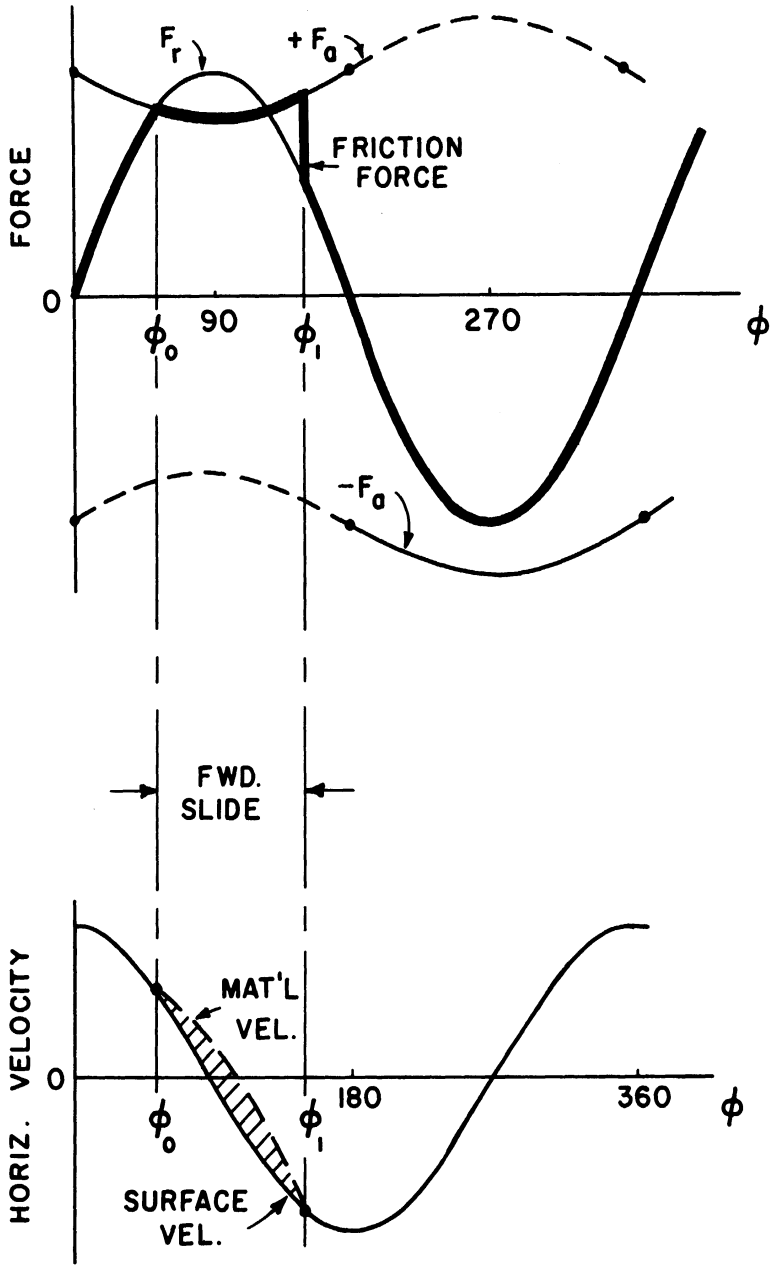

Figure 6. Force and Velocity Diagrams for Material Particle Having Forward Slide.

s of the material particle is merely its absolute velocity less the surface velocity $\omega A_x \cos \varphi$. The resulting dimensionless expression for $\dot{s}$ is

$$\frac{\dot{s}\omega}{\mu g} = V\left[\frac{1 + \mu \tan \alpha}{\mu \tan \alpha}\right](\cos \varphi_o - \cos \varphi) - (\varphi - \varphi_o) \qquad (24)$$

Forward slide of the material will persist until $\varphi = \varphi_1$, when the particle velocity has been reduced by friction to that of the vibrating surface. Thus the criterion for the end of sliding is that the relative velocity $\dot{s}$ of Equation (24) becomes zero. Combining Equations (21) and (24) for $\dot{s} = 0$ and $\varphi = \varphi_1$, one finds that this criterion results in the following implicit expression defining φ_1 in terms of φ_o :

$$(\varphi_1 - \varphi_o) \sin \varphi_o = \cos \varphi_o - \cos \varphi_1 \qquad (25)$$

Table II shows some numerical values of φ_1 and φ_o calculated from Equations (21) and (25) for various friction factors $\mu \tan \alpha$ and accelerations $A_y\omega^2/g$.

It is interesting to note in Figure 6 that at the instant sliding stops, the force F_a available from friction exceeds force F_r required to produce relative motion so that the friction force F drops abruptly to F_r as indicated. This condition persists through the second half of the vibration cycle where $|F_a| > |F_r|$ as shown, so no further sliding occurs until one cycle later when once again $\varphi = \varphi_o$. A knowledge of φ_o and φ_1 thus permits calculation as before of the forward displacement s_m of the particle per cycle and finally its average horizontal velocity according to

$$s_m = \int \dot{s}\, dt = \int_{\varphi_o}^{\varphi_1} (\dot{s}/\omega)\, d\varphi \qquad (26)$$

TABLE II

COMPUTED TRANSITION ANGLES FOR SLIDING PARTICLE

Forward Slide				Backward Slide			
$V = A_y\omega^2/g$ for		φ_0	φ_1	$V = A_y\omega^2/g$ for		φ_2	φ_3
$\mu\tan\alpha = .1$	$\mu\tan\alpha = .2$	deg	deg	$\mu\tan\alpha = .1$	$\mu\tan\alpha = .2$	deg	deg
.0909	.1667	90.0	90.0	.1112	.250	270	270
.0911	.1670	86.0	98.6	.1116	.251	265	280
.0922	.1690	80.2	110.0	.1130	.254	260	290
.0943	.1730	74.5	121	.1150	.259	255	300
.0975	.1790	68.8	133	.1183	.266	250	310
.1020	.1870	63.0	145	.1225	.276	245	321
.1080	.198	57.3	157	.1283	.289	240	331
.1161	.213	51.5	169	.1358	.305	235	342
.1268	.232	45.8	181	.1450	.326	230	352
.1410	.257	40.1	194	.1572	.353	225	363
.1608	.295	34.4	208	.1731	.389	220	374
.1900	.348	28.6	222	.1938	.436	215	386
.233	.428	22.9	238	.2225	.500	210	399
.307	.563	17.2	253	.263	.591	205	412
.455	.835	11.5	274	.325	.730	200	426
.915	1.678	5.7	299	.429	.966	195	442
∞	∞	0.0	360	.640	1.440	190	460

and

$$U = ns_m = (\omega/2\pi)s_m \tag{27}$$

By substituting for $\dot{s}$, φ_o, and φ_1 from Equations (24), (21), and (25) respectively into Equation (26), performing the integration indicated to get s_m, and then simplifying the result in Equation (27), one can express the average velocity in terms of a ratio as

$$\frac{U}{\omega A_x} = \frac{\mu \tan \alpha}{4 \pi V} \left[\frac{\sin \varphi_1 - \sin \varphi_o}{\sin \varphi_o} \right]^2 \tag{28}$$

It must be emphasized that this transport velocity ratio holds only for a comparatively small range of conveyor operation whose lower limit is given by Equation (20) and whose upper limit is fixed by the onset of backward slide as considered below.

2. Criteria for Backward Slide

If a condition involving only forward slip of the particle is established in the model system, and then the acceleration level V is increased somewhat, a situation corresponding to Figure 7 can be brought about. Here the magnitude of the hypothetical required force F_r not only exceeds the available force F_a at $\varphi=\varphi_1$, thus initiating a forward slide, but also exceeds F_a later in the cycle at $\varphi=\varphi_2$, this time producing a backward slide of the particle. From the shape of the force curves it is evident that the limiting condition for the occurrence of back slide is when $\varphi_2 = 270$ degrees. Setting Equation (19) equal to minus F_a from Equation (16) for this condition yields

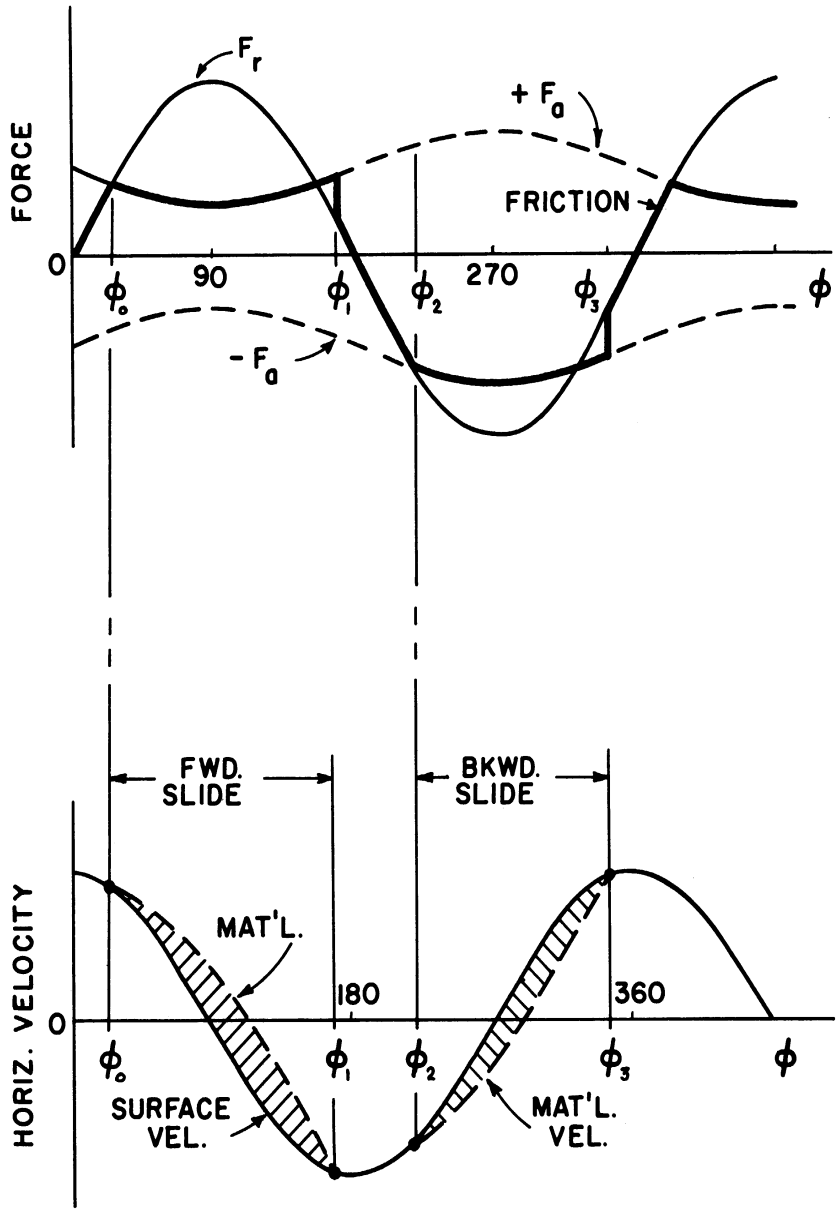

Figure 7. Force and Velocity Diagrams for Material Particle Having Both Forward and Backward Slide.

$$V \geq \frac{\mu \tan \alpha}{1 - \mu \tan \alpha} \tag{29}$$

as the criterion for the existence of backward slide and

$$\sin \varphi_2 = -\frac{1}{V}\left[\frac{\mu \tan \alpha}{1-\mu \tan \alpha}\right] \tag{30}$$

as the general expression for the angle φ_2 when slide begins.

As indicated by Figure 6, the true friction force F on the particle during the slide interval is minus F_a, so the equation of horizontal motion becomes

$$-F_a = -m\ddot{x} = -\mu mg\,(1 - V \sin \varphi) \tag{31}$$

which is similar to Equation (22) except for signs. As in the case of forward slide, the equation of motion can be integrated and a dimensionless expression obtained for the relative velocity of the particle, as follows:

$$\frac{\dot{s}\omega}{\mu g} = V\left[\frac{1 - \mu \tan \alpha}{\mu \tan \alpha}\right](\cos \varphi_2 - \cos \varphi) + (\varphi - \varphi_2) \tag{32}$$

The cross-hatched zone for backward slide in Figure 7 indicates that sliding ends, and the friction force F changes abruptly to F_r, when the relative velocity dwindles to zero. At this instant $\varphi = \varphi_3$ and $\dot{s} = 0$ in Equation (23) which can be combined with Equation (30) to give the following implicit relation for φ_3 defining the end of the slip:

$$(\varphi_3 - \varphi_2) \sin \varphi_2 = \cos \varphi_2 - \cos \varphi_3 \tag{33}$$

Table II shows typical calculated values for φ_2 and φ_3 obtained from Equations (30) and (33) for some values of friction and acceleration level.

Finally, the negative displacement s_m experienced by the particle during backslip can be obtained from Equations (33) and (26) by a procedure identical to that in the previous section, and a new transport velocity ratio analogous to Equations (28) computed. The new velocity ratio takes account of both forward and backward slip, and is as follows:

$$\frac{U}{\omega A_x} = \frac{\mu \tan \alpha}{4\pi V} \left[\left(\frac{\sin \varphi_1 - \sin \varphi_0}{\sin \varphi_0} \right)^2 - \left(\frac{\sin \varphi_3 - \sin \varphi_2}{\sin \varphi_2} \right)^2 \right] \qquad (34)$$

A comparison of this result with that of Equation (28) shows that the occurrence of backward slide, as expected, reduces the transport velocity attributable to a purely forward slide.

The relationship between the regions of conveyor operation in which periods of forward and backward slide occur can be visualized graphically in a plot of vibration angle φ versus acceleration number V as shown in Figure 8. Here, variations of φ_0, φ_1, φ_2, and φ_3 computed from the defining Equations (21), (25), (30), and (33) for various values of friction parameter $\mu \tan \alpha$ are shown as a function of vertical acceleration in g's . Sections of each curve corresponding to the four angles are marked off by short horizontal lines. Suppose, for example, a conveyor is run at a constant acceleration level of 0.3 g with a material producing a $\mu \tan \alpha = .2$. The appropriate curve in Figure 8 shows that forward slide of the material particle will begin early in the vibration cycle, at about $\varphi_0 = 35$ degrees, and end at $\varphi_1 = 210$ degrees. Following a short dwell on the conveyor surface, the particle at $\varphi_2 = 235$ degrees

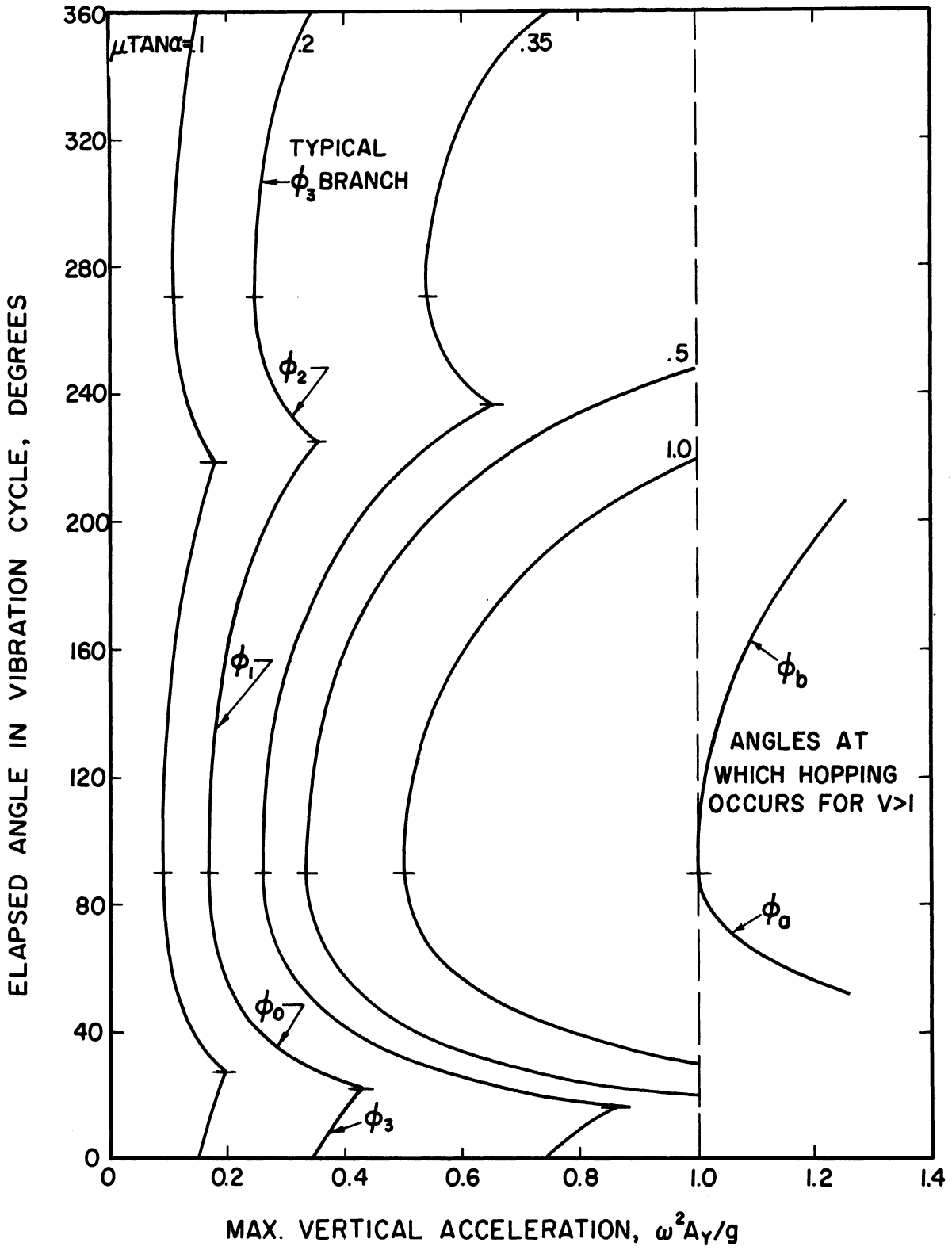

Figure 8. Occurrence of Sliding During Vibration at Low Acceleration Levels in Sliding Particle Model.

will go into a backward slide that persists to $\varphi_3 = 340$ degrees. Then the entire cycle repeats itself.

It is evident from the same curve that at a lower value of V , say 0.2 g, relative motion of the particle takes place only through a comparatively short forward slide. On the other hand, when the acceleration level exceeds the values corresponding to the cusps of the curve (V = .35 and .43), the dwell between periods of sliding vanishes completely and the solutions developed thus far for transport velocity are no longer valid. Moreover, for an acceleration less than V = .17 g the curve shows that no sliding at all will occur. In general, for increasing values of friction coefficient, higher levels of acceleration are required to produce particle slide and the sliding that does take place is predominantly forward. When the acceleration level exceeds 1.0 g, consideration of both hopping and sliding must be made to predict particle motion.

3. Conditions of Continuous Slide

The results of the previous section suggest that a acceleration levels approaching 1.0 g, the intervals of particle slide can take up such a large part of the vibration period that the dwell periods between slides vanish completely. Under this condition the material particle slides continuously, first forward then backward, acquiring some net forward increment of displacement on the conveyor surface each cycle. As

shown in Figure 9, the angles φ_1 and φ_2 become coincident and φ_o differs from φ_3 by exactly 360 degrees. At the end of each slide interval, the force F_r required to produce dwell is always less than the available friction force F_a, so the friction force jumps intermittently as indicated between plus F_a and minus F_a, and no dwell occurs.

An analysis of the particle motion in this range of operation is given in Appendix A. The results show that the angles φ_o and φ_1 defining the reversal of slide must satisfy the following transcendental relations:

$$\varphi_1 - \varphi_o = \pi (1 + \mu \tan \alpha) \tag{35}$$

$$\frac{\cos \varphi_o - \cos \varphi_1}{\varphi_o + 2\pi - \varphi_1} = \frac{1}{V} \frac{\mu \tan \alpha}{1 - \mu \tan \alpha} \tag{36}$$

The first of these equations indicates that the forward slide interval $(\varphi_1 - \varphi_o)$ exceeds 1/2 cycle by an amount proportional to $\mu \tan \alpha$ and is constant for a given combination of material and surface. However, the vertical acceleration V also affects the values of φ_o and φ_1 through Equation (36), and thus the transport velocity is a function of V. Typical values of the slide angles calculated by trial and error from Equations (35) and (36) are listed in Table III.

4. Combined Sliding and Hopping

The study of the particle model can readily be extended to operation at conveyor acceleration levels higher than 1.0 g where both sliding and hopping of the transport material is predicted. For such a

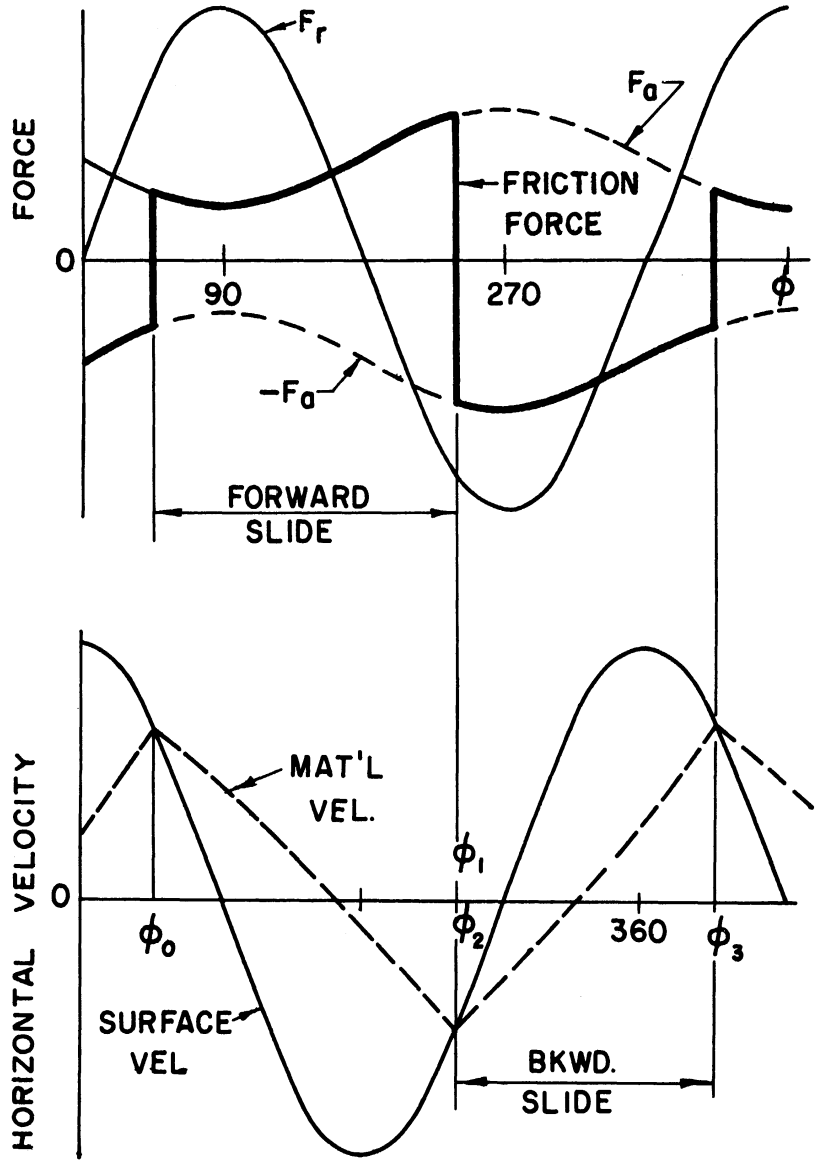
FORCE
F_r
F_a
FRICTION FORCE
0
90
270
ϕ
$-F_a$
FORWARD SLIDE
HORIZONTAL VELOCITY
MAT'L VEL.
ϕ_1
0
ϕ_0
ϕ_2
360
ϕ_3
SURFACE VEL
BKWD. SLIDE

TABLE III

COMPUTED ANGLES FOR SLIDE HOP PARTICLE MOTION

$\mu\tan\alpha = .1$			$\mu\tan\alpha = .2$		
V	φ_o	φ_1	V	φ_o	φ_1
.20	29.0	226.8	.44	22.5	239.7
.25	41.7	239.5	.45	24.7	240.7
.30	49.3	246.1	.50	30.6	246.6
.40	57.5	255.3	.60	38.6	254.6
.50	62.6	260.4	.70	43.8	259.8
.60	65.7	263.5	.80	47.6	263.6
.70	68.0	265.8	.90	50.4	266.4
.80	69.4	267.2	1.00	52.6	268.6
.90	70.9	268.7	1.05	53.0	271.0
1.00	72.1	269.7	1.15	51.5	276.5
1.05	71.4	271.4	1.35	45.5	289.0
1.10	65.0	274.0	1.55	38.0	300.5
1.20	56.0	280.0	2.00	21.0	323.5
1.40	46.0	292.0	2.50	6.0	342.5
1.60	39.0	304.0	2.75	0.7	348.7
2.00	30.0	324.5	3.00	-2.5	354.5
2.25	19.0	335.0			
2.50	10.5	344.5			
2.75	4.0	352			

case the available friction F_a, being proportional to the normal force G on the particle, becomes negative as shown in Figure 10 at the same angle φ_a for which hopping begins. At this instant the actual friction force must go to zero and remain there until the end of the hop at $\varphi=\varphi_b$ But at φ_b the available force F_a is not sufficiently large $(F_a < F_r)$ to capture the particle and therefore forward sliding, started before the hop, continues until φ_1. Then an immediate reversal to a backward slide condition lasting until $\varphi_3(\varphi_o + 260$ degrees) takes place. At φ_3 the particle motion reverses again, this time to a forward slide persisting until the cycle is repeated at φ_a.

Figure 10 shows that the friction force on the particle changes intermittently between plus F_a and minus F_a except for the hopping interval when the force is zero. The lower part of Figure 10 shows the cyclic variations in the surface velocity (solid curve) and the particle velocity components (dotted curves for $\dot{x}$ and $\dot{y}$) on a normalized basis. It is evident from these curves that the type of operation under consideration here is a combination of the purely hopping motion described in Figure 3 and the continuous sliding motion of Figure 9.

Because hopping of the particle is not dependent in any way on the friction force, the angles φ_a and φ_b defining this event in the cycle can be obtained from Equations (4) and (9) derived in a previous section. On the other hand, an analysis of the motion given in Appendix B shows that angles φ_o and φ_1 at the slide reversal points in the cycle must satisfy Equation (36) as well as

$$\varphi_1-\varphi_o = \pi(1+\mu \tan \alpha) + \left[\frac{1-\mu \tan \alpha}{2}\right]\left[(\varphi_b-\varphi_a)-V(\cos \varphi_a - \cos \varphi_b)\right] \quad (38)$$

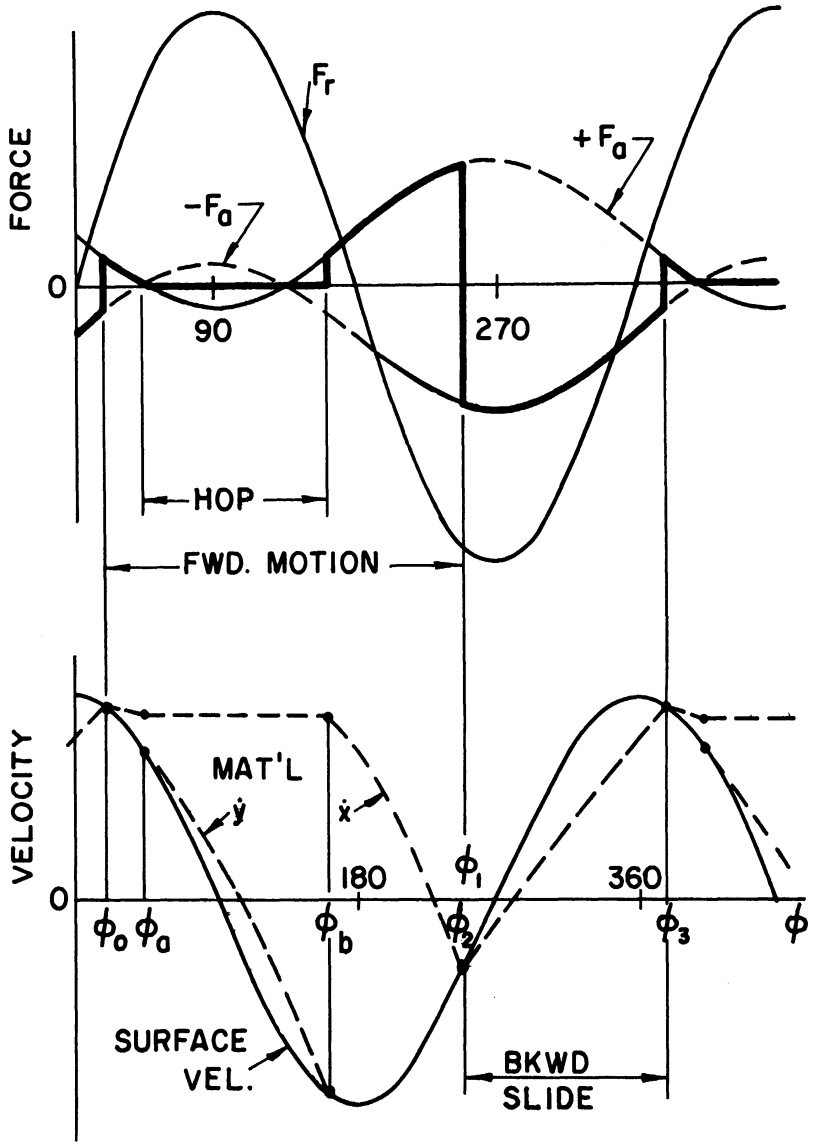

Figure 10. Force and Velocity Diagrams for Material Particle Having Combined Sliding and Hopping.

A series of numerical values for these angles, calculated by means of a simultaneous solution of Equations (36) and (38), is listed in Table III.

It is now possible to examine the predicted behaviour of the particle model in a general way over a large range of conveyor acceleration levels. For this purpose the events taking place each cycle in the transport of two hypothetical materials ($\mu \tan \alpha = .1$ and $\mu \tan \alpha = .2$) have been plotted using the calculated values given in Tables I, II, and III. The resulting curves, Figure 11, show how the six vibration angles denoting a transition in the particle motion vary with vertical acceleration. For any given value of the friction parameter, the curves delineate zones in which either no motion or a particular type of motion takes place. In the figure, the boundary of the hopping zone is shown as a solid line whereas the sliding zone boundaries appear as either dashed ($\mu \tan \alpha = .1$) or dot-dash ($\mu \tan \alpha = .2$) lines.

Consider conveyor operation with $\mu \tan \alpha = .2$ at successively increasing values of acceleration level $V = A_y \omega^2/g$. For a very low acceleration, say $V = .1$, no motion will occur at any time during the cycle since an imaginary vertical line through $V = .1$ will not intersect any branch of the dot-dashed curve. A somewhat larger acceleration however, say $V = .3$ g, will bring about a motion characterized by alternate forward and backward sliding separated by dwell periods as explained in a previous section. If the conveyor is run with $V = .6$ g, the particle will enter a forward slide zone at about $\varphi = 40$ degreesand then without any momentary dwell go into a backward slide zone around $\varphi = 250$ degrees.

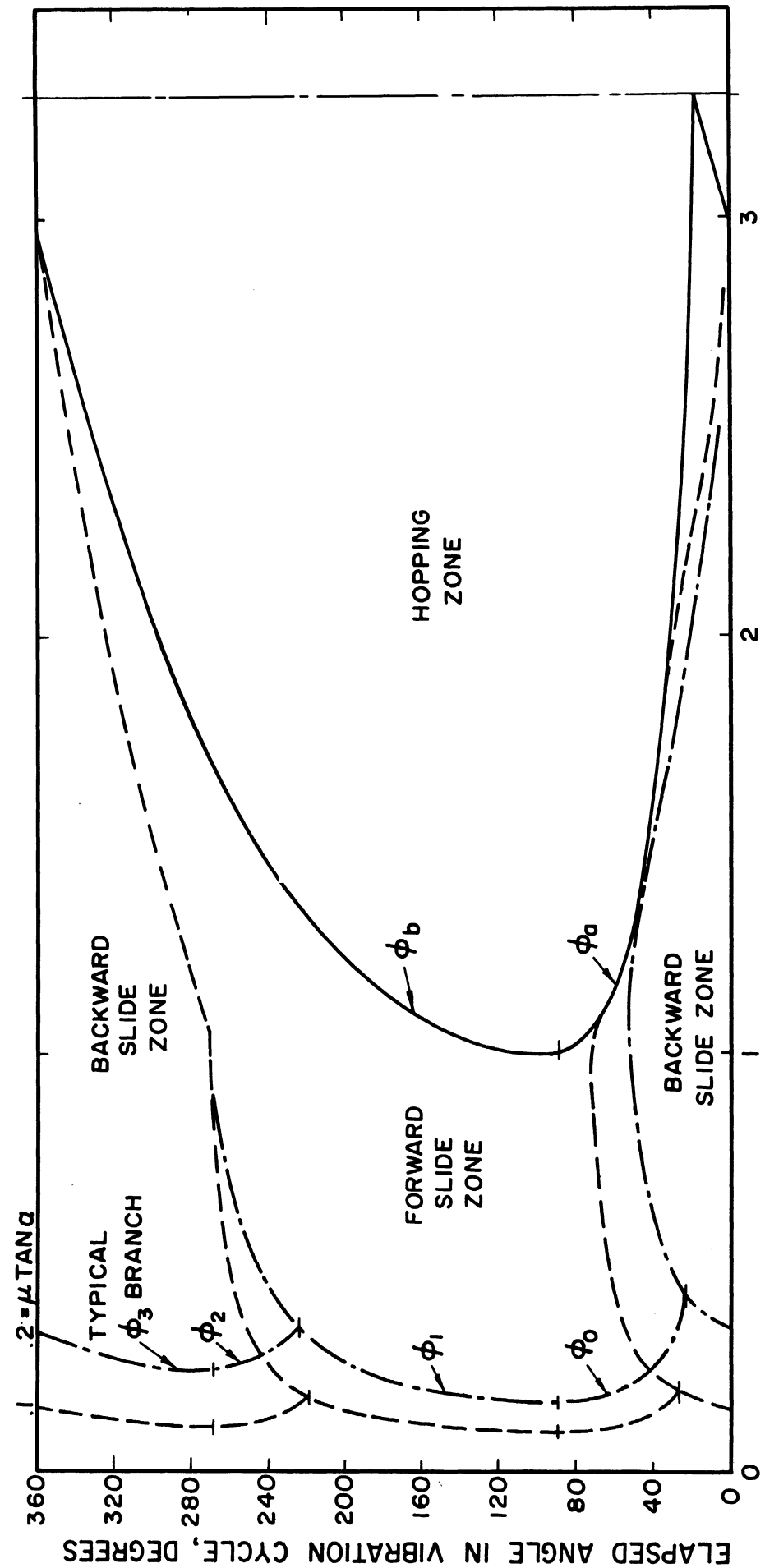

Figure 11. Behavior of Transport Material as Calculated from the Sliding Particle Model.

When the acceleration is increased just above 1.0 g, it is evident that the particle is thrown clear of the surface during part of the cycle and that forward sliding occurs both before and after the hopping motion. However as V is increased further, the hopping phase becomes more and more predominant. For the lower value of $\mu \tan \alpha = .1$ the dashed curve indicates that sliding will be initiated at smaller values of V, and that above 1.0 g the transition angles between sliding zones are nearly the same as for $\mu \tan \alpha = .2$.

Once the angles such as φ_o and φ_1 have been evaluated for a given friction parameter, it is possible as indicated by Equations (28) and (34) to predict a value of the transport velocity ratio for any given conveyor acceleration in the range $0 < V < 3.3$. Appendixes A and B show equations for the velocity ratio derived for the cases of continuous sliding and combined hopping-sliding motions, respectively. From these equations the calculated values appearing in Table IV have been obtained and the corresponding theoretical curves of Figure 12 plotted. For comparison, the transport velocity ratio for the hopping particle model is also shown.

A direct contrast of conveyor performance with the theoretical prediction can be made if the results of the sliding particle analysis are put into a more practical form. For this purpose the data of Table IV were used to calculate transport velocity as a function of frequency for a hypothetical conveyor having $\alpha = 30$ degrees and three different vibratory amplitutes. A plot of these results, along with the corresponding hopping-model curves from Figure 5, is shown in Figure 13.

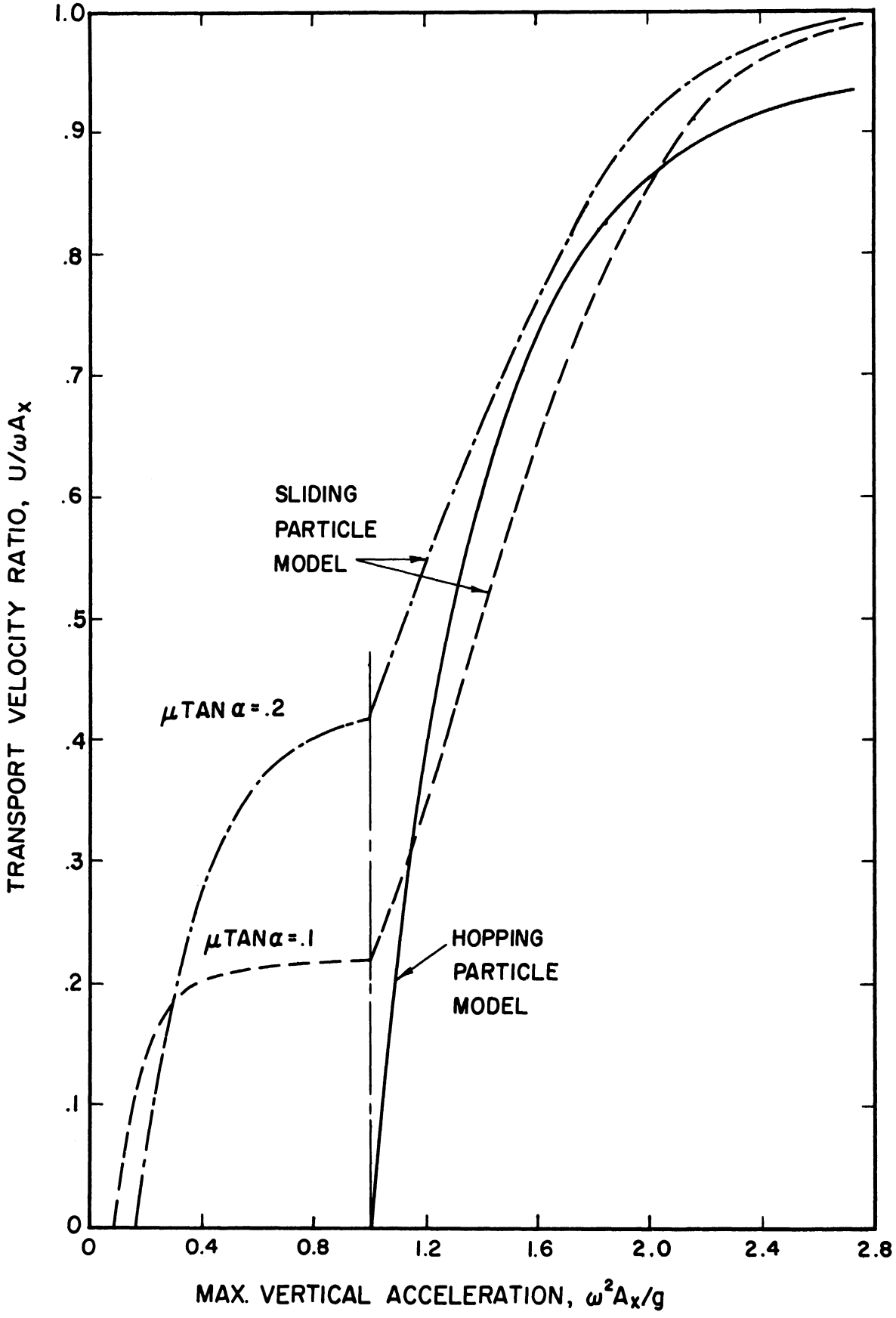

Figure 12. Predicted Effect of Sliding on Velocity of Transport Material.

TABLE IV

TRANSPORT VELOCITY RESULTS FOR SLIDING PARTICLE MODEL

$\mu\tan\alpha = .1$		$\mu\tan\alpha = .2$	
V	$U/A_x\omega$	V	$U/A_x\omega$
.09	0	.17	0
.20	.137	.44	.297
.25	.170	.45	.300
.30	.179	.50	.332
.40	.202	.60	.368
.50	.208	.70	.390
.60	.212	.80	.402
.70	.219	.90	.411
.80	.215	1.00	.417
.90	.216	1.14	.504
1.00	.218	1.40	.660
1.20	.348	1.62	.766
1.40	.504	1.76	.829
1.60	.639	2.00	.915
1.80	.759	2.20	.945
2.00	.848	2.40	.973
2.25	.940	2.75	.986
2.50	.970	3.00	.998
2.75	.995		
3.00	.999		

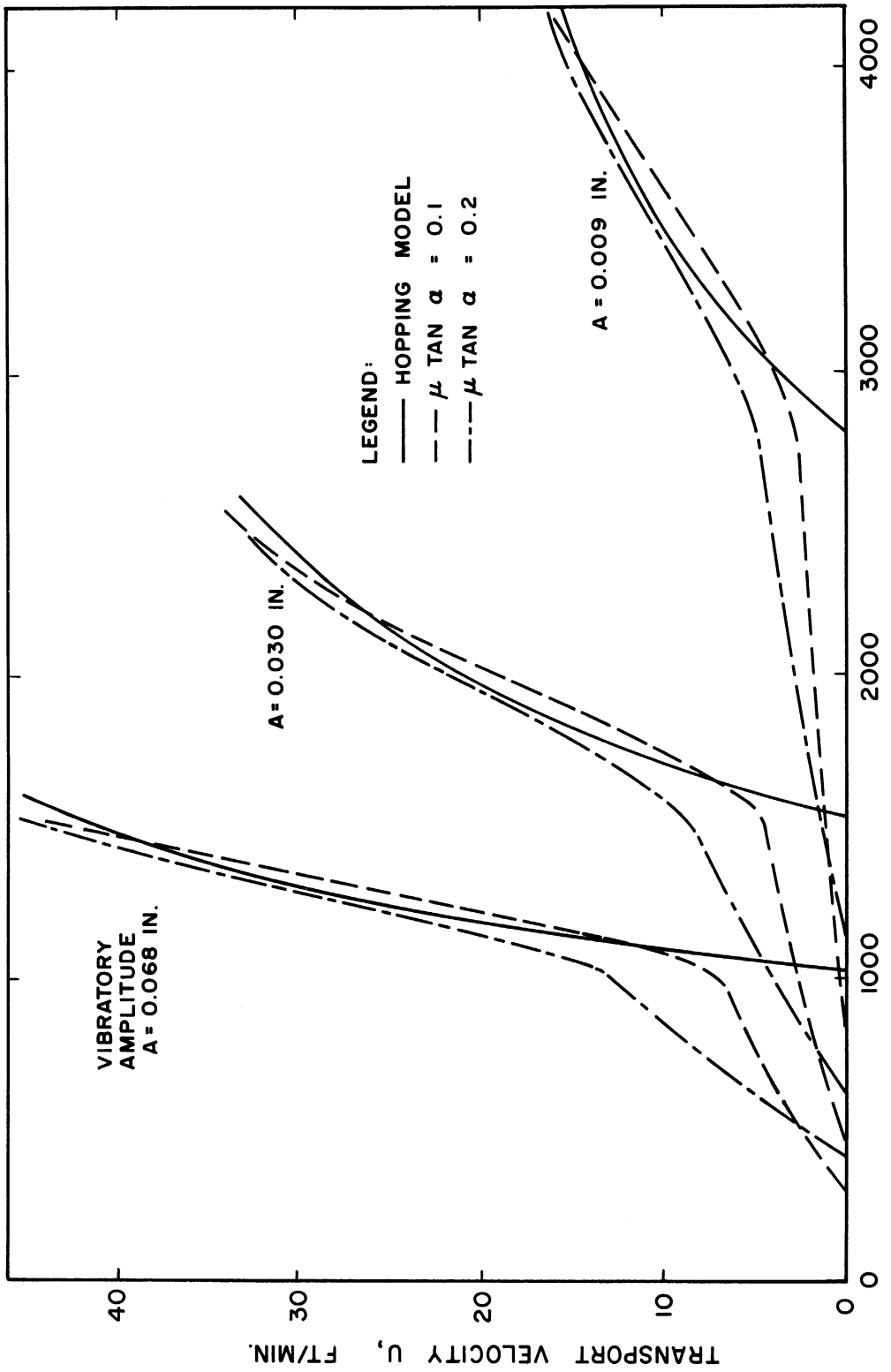

Figure 13. Effect of Material Slide on Predicted Performance of Vibratory Conveyor with 30 Degree Vibration Angle.

E. The Porous Plate Model

In the foregoing analyses the transport material has been likened to a single particle which for conveyor accelerations greater than 1.0 g loses contact with the surface during part of each vibrating cycle. During these intervals it has been assumed that the particle obeys the laws of free fall and is acted on by no force other than that of gravity. As discussed earlier, this idealization of the transport material and its motion may be valid where the atmosphere offers little resistance to relative vertical motion of the material layer. However, a more sophisticated model may be necessary and useful to accurately predict the transport behavior of fine-grained aggregates where air drag on the material is appreciable. Such a model is considered in this section.

1. Effect of Air Resistance

In order to assess the effect of air resistance in as simple a manner as possible, it will be assumed that the transport material consists of a collection of mass particles bonded together to form a uniformly porous but rigid plate capable of transmitting air flow. The motion of this equivalent porous plate relative to the conveyor surface will be studied, as in the case of the particle model, by considering its horizontal and vertical components separately. In this connection, all horizontal components of air drag on the material will be neglected so that many of the equations of motion developed for the particle models apply directly to the porous plate. On the other hand, because of the finite extent and permeability attributed to the porous plate, its

vertical behavior can differ markedly from that of the particle.

A piston-cylinder arrangement shown in Figure 14(a) can be visualized to study the purely vertical components of motion in the porous plate model. Here the cylinder undergoes a vertical vibration and represents the conveyor surface. The frictionless, tightly-fitting disc represents an element of transport material and the axial capillary hole in the disc accounts for the porosity of the material. During operation at acceleration levels above 1.0 g, separation of the disc and cylinder can occur by virtue of air flow through the capillary hole.

The flow characteristics of the porous plate model must be related to those of the transport material. In general the expression describing the flow of any viscous fluid through an element of a porous medium is known as Darcy's law which relates flow rate to fluid viscosity, flow area, path length, and pressure difference through an empirical property of the medium known as permeability. For the purpose of this analysis, the following modified version of Darcy's law will be used to describe the vertical flow of air through the porous plate of transport material:

$$w = KS\,\frac{p - p_o}{h} = \frac{KSp_o}{h}\left(\frac{p}{p_o} - 1\right) \tag{39}$$

Here w is the instantaneous upward mass flow rate of air, S is the gross surface area normal to the flow, h is the thickness of material in the direction of flow, p is the underside air pressure, p_o is the ambient air pressure, and K is a permeability coefficient that characterizes a particular transport material.

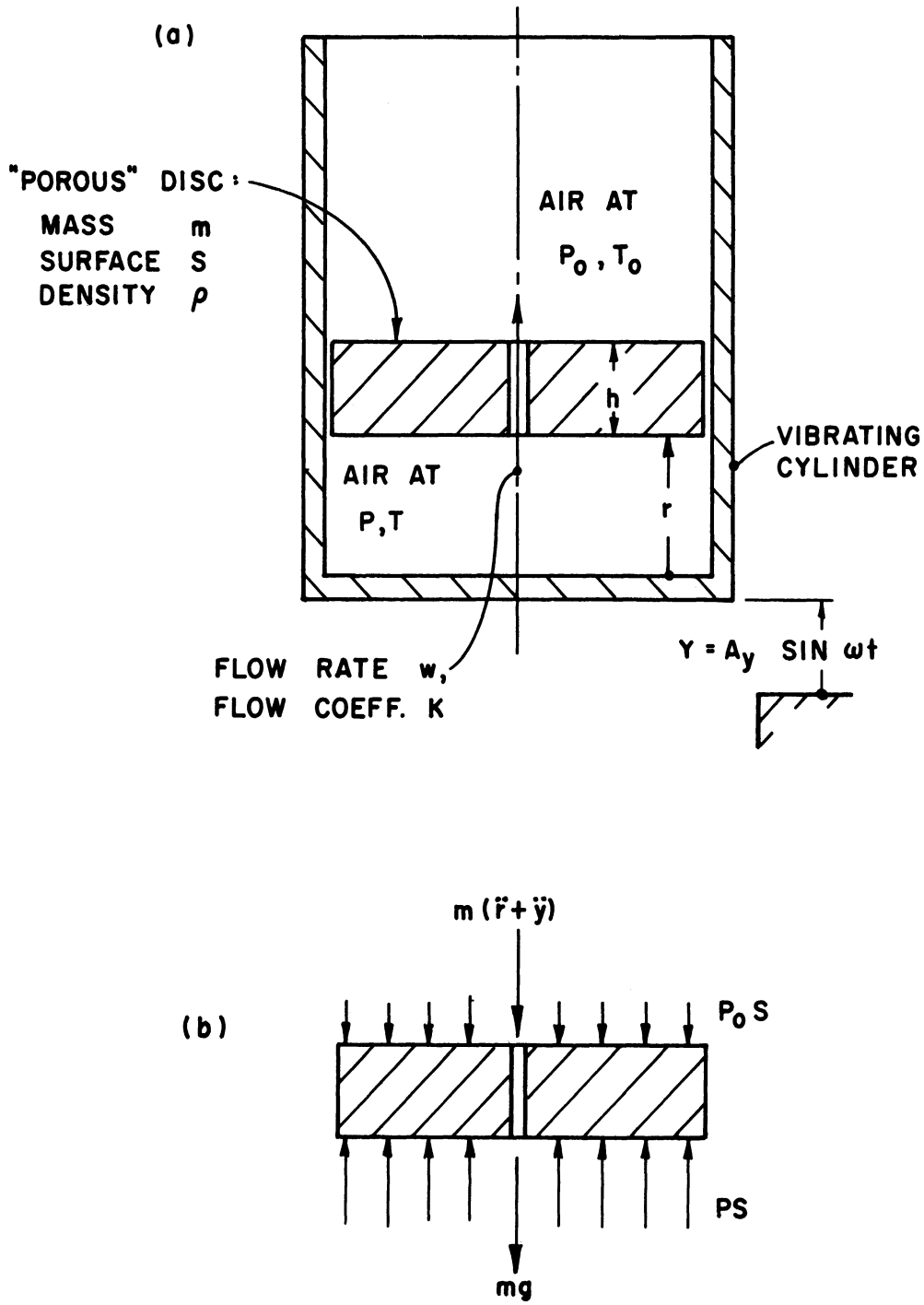

Figure 14. Idealization of Transport Material as a Rigid Porous Plate.

2. Criteria for Vertical Motion

For a typical displaced configuration of the model system, the instantaneous forces on the porous plate are as shown in Figure 14(b). These include pressure forces $p_o S$ and pS from the air on either side of the plate, gravity force mg, and an inertia force formed of the product of the mass m of the plate and its absolute acceleration $(\ddot{r} + \ddot{y})$, where r and y are the displacements defined in Figure 14(a). The balance of forces on the plate thus yields

$$m(\ddot{r} + \ddot{y}) + Sp_o \left[1 - \frac{p}{p_o} \right] + mg = 0 \qquad (40)$$

The mass of air occupying the clearance space of the model at any instant can be expressed in terms of pressure, volume, and temperature, as $M = pSr/RT$ by using the equation of state for a perfect gas. By assuming that changes of state of the air occur isentropically such that $Tp^{(1-k)/k}$ is a constant and noting that the ambient air density is $\rho_o = p_o/RT_o$, one can rewrite $M = \rho_o Sr(p/p_o)^{1/k}$. From continuity considerations, the outflow of air from the clearance space is related to the mass inside by $w = - dM/dt$ so that in terms of pressure and displacement,

$$w = - \rho_o S \frac{d}{dt} \left[r \left(\frac{p}{p_o} \right)^{1/k} \right] \qquad (41)$$

The foregoing three equations relate the three operating variables of displacement r, air flow w, and separation pressure p for the porous plate model. However the nonlinear form of Equation (41) makes the solution for the plate motion difficult if not impossible by ordinary methods. A reasonable way out of this trouble is to assume that the pressure

ratio p/p_o is never far from unity and that the air flow is incompressible. On this basis Equation (41) becomes simply $w = - \rho_o S\dot{r}$, and when this is equated to Equation (39) one obtains

$$\frac{p}{p_o} = 1 - \left[\frac{\rho_o h}{K p_o}\right] \dot{r} \tag{42}$$

This value for p/p_o and also the relation $m = \rho Sh$ can now be substituted in Equation (40) to obtain a single equation of motion for the plate as follows:

$$\ddot{r} + \left[\frac{\rho_o/\rho}{K}\right] \dot{r} = - \ddot{y} - g \tag{43}$$

A better form of this equation can be obtained by changing the independent variable from t to $\varphi = \omega t$, using $v = \dot{r}/\omega A_y$ as a relative velocity ratio, noting that $\ddot{y} = - \omega^2 A_y \sin \varphi$, and making use of Equation (4), whereupon

$$\frac{dv}{d\varphi} + \lambda v = \sin \varphi - \sin \varphi_a \tag{44}$$

This first-order differential equation gives the relative velocity ratio v of the porous plate as a function of vibration angle φ. It is valid from $\varphi = \varphi_a$ when separation first occurs at 1.0 g acceleration until the plate resumes contact with the vibrating surface. The nature of the place velocity described by Equation (44) depends not only on the conveyor acceleration level $V = 1/\sin \varphi_a$ as in the case of the particle models, but also on the damping factor λ defined by

$$\lambda = \frac{\rho_o/\rho}{K\omega} \tag{45}$$

For a transport material that is extremely permeable to air flow the coefficient K defined by Equation (39) is very large, making λ very small. In such a case the velocity predicted by Equation (44) is practically the same as that given by the particle model analysis. On the other hand, for fine-grained materials of limited permeability, λ may be appreciable in which case the vertical motion and ultimate transport of the material may be severely affected by the air pressures built up during separation. The other factors appearing in Equation (45), i.e. material density ρ and conveyor speed ω, apparently have the same influence on the predicted motion as the permeability.

3. Correlation with Particle Models

As far as the transport analysis is concerned, Equation (44) can be used to find, for a relatively impermeable material, an equivalent angle φ_b marking the end of the separation or hopping phase of the porous plate motion. This angle can be compared with values of φ_b obtained from Equation (9) of the particle analyses, and thus the permeability of the material can be taken into account in a quantitative way.

Equation (44) can be integrated to obtain the plate velocity v as a function of vibration angle φ. For an initial value of $v=0$ at $\varphi=\varphi_a$ the solution contains exponential, cosine, and constant terms given by

$$v = \left[\frac{\sin(\varphi_a+\alpha)}{\lambda\sqrt{1+\lambda^2}}\right] e^{-\lambda(\varphi-\varphi_a)} - \frac{\cos(\varphi+\alpha)}{\sqrt{1+\lambda^2}} - \frac{\sin\varphi_a}{\lambda} \qquad (46)$$

where $\alpha=\tan^{-1}\lambda$. A typical numerical solution obtained from this equation

is plotted in Figure 15. It is seen that separation of the plate from the vibrating surface begins at $\varphi_a = 42$ degrees and that the plate velocity relative to the surface after that instant rises to a maximum, falls to zero, and then becomes negative. The corresponding relative displacement or separation r of the plate, shown in Figure 15 as a ratio r/A_y, was obtained by a graphical integration of the velocity curve. As one might expect, the displacement curve passes through a maximum when the velocity becomes zero, then drops to zero at $\varphi = 215$ degrees where the plate rejoins the vibrating surface.

In order to get a quantitative evaluation of how far and for how long the porous plate representing the transport material rises above the conveyor surface, a series of Equation (46) solutions was made for selected values of the acceleration and damping factors V and λ. For each combination of V and λ, the velocity solution was plotted to scale as in Figure 15. A planimeter was then used to measure the area under the velocity curve out to the zero crossover, and thereby obtain a value of the maximum separation attained by the plate. Finally, the area under the velocity curve was planimetered out to successively larger values of elapsed angle until a condition of zero net area was found. As indicated in Figure 15, the value of φ at this point corresponds to the landing angle marking the end of transport material hopping in the vibration cycle.

Values obtained from the porous plate model calculations are listed in Table V along with the corresponding results developed earlier for the hopping particle model.

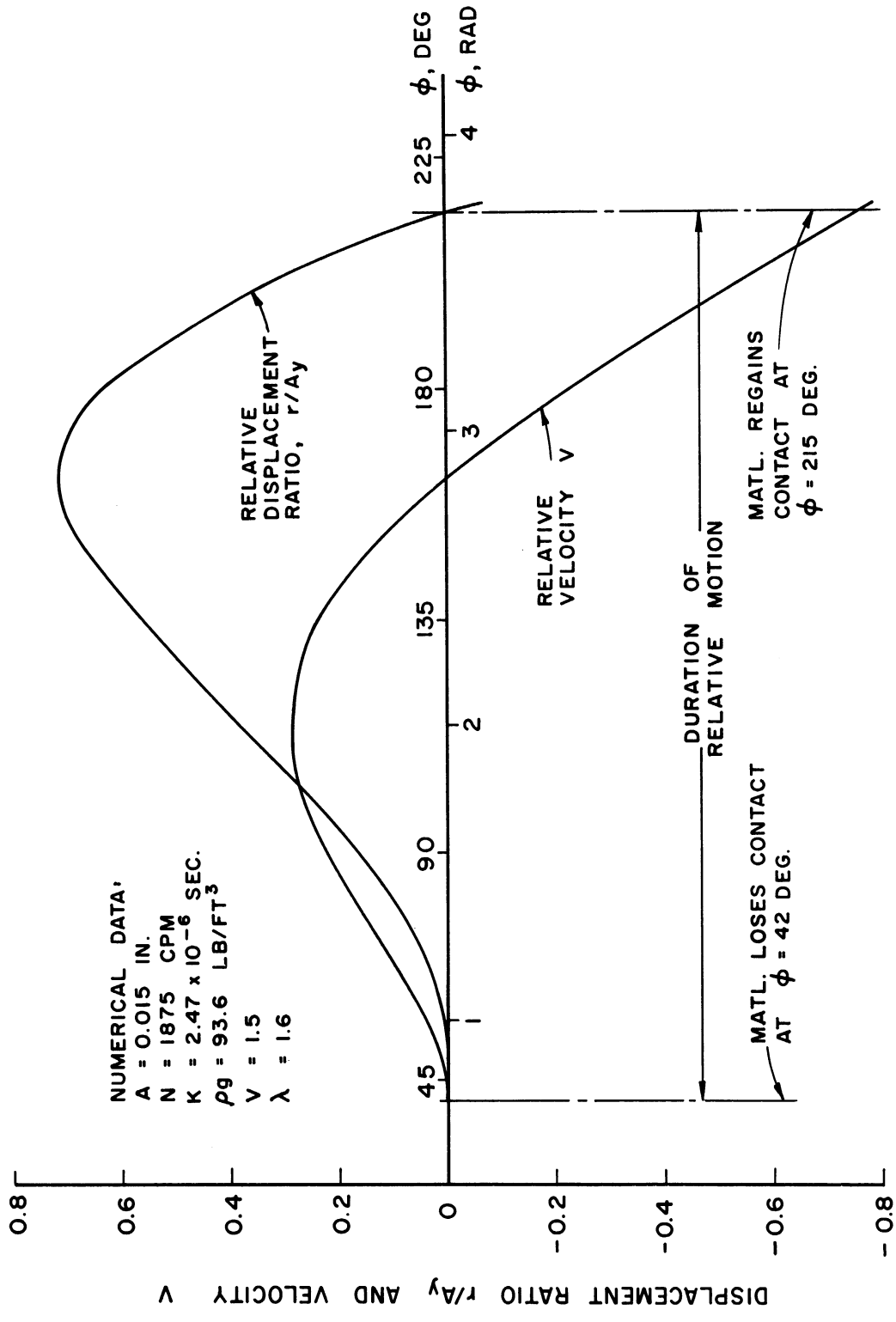

Figure 15. Typical Vertical Motion of Transport Material Predicted from Porous Plate Model.

TABLE V

COMPUTED RESULTS FOR POROUS PLATE MODEL

V	λ	φ_a	φ_b for		$(r/A_y)_{max}$ for		$U/\omega A_x$ for	
			Particle	Plate	Particle	Plate	Particle	Plate
1.50	.8	41.8	248	227	.55	.29	.68	.55
1.50	1.6	41.8	248	215	.55	.18	.68	.49
1.50	2.4	41.8	248	209	.55	.14	.68	.45
2.00	.7	30.0	298	256	1.27	.62	.86	.62
2.00	1.4	30.0	298	249	1.27	.39	.86	.58
2.00	2.1	30.0	298	241	1.27	.29	.86	.54
2.75	.6	21.3	348	331	2.15	1.11	.93	.65
2.75	1.2	21.3	348	275	2.15	.68	.93	.57
2.75	1.8	21.3	348	270	2.15	.50	.93	.55
4.00	.5	14.5	-	341	-	1.58	-	.65
4.00	1.0	14.5	-	310	-	1.03	-	.53
4.00	1.5	14.5	-	297	-	.76	-	.49

It is apparent that the more impermeable the transport material, the more attenuated its hopping motion becomes in comparison with that of a single particle. One must be cautious, however, in trying to generalize the respective influence of the conveyor acceleration factor V and the material damping factor λ on the transport mechanism since both factors contain conveyor speed ω. The specific relation between V and λ can be obtained by solving $V = A_y\omega^2/g$ for ω and substituting the result in Equation (45) so that

$$\lambda = \left[\frac{\rho_o/\rho}{K}\right]\sqrt{\frac{1}{V}}\sqrt{\frac{A_y}{g}} \tag{47}$$

From this equation and the preceding analysis it is possible to predict the performance of a hypothetical conveyor that operates like the porous plate model, and to contrast this performance with that of other theoretical or experimental models.

The dotted curves of Figure 16 show how the maximum separation and the transition angles vary with vertical acceleration in the typical porous plate model. It has been assumed for this model that the material is fixed and gives a value of $\rho_o/\rho K = 310$ sec in Equation (47), and that the amplitude A_y also appearing there is fixed at .035 inch. Values of the same quantities for the particle model are given by the solid curves.

F. Comparison of Theoretical Results

The foregoing theoretical analyses make it possible not only to predict some apparent practical limitations of the vibratory transport mechanism but also to assess the relative importance of operating variables

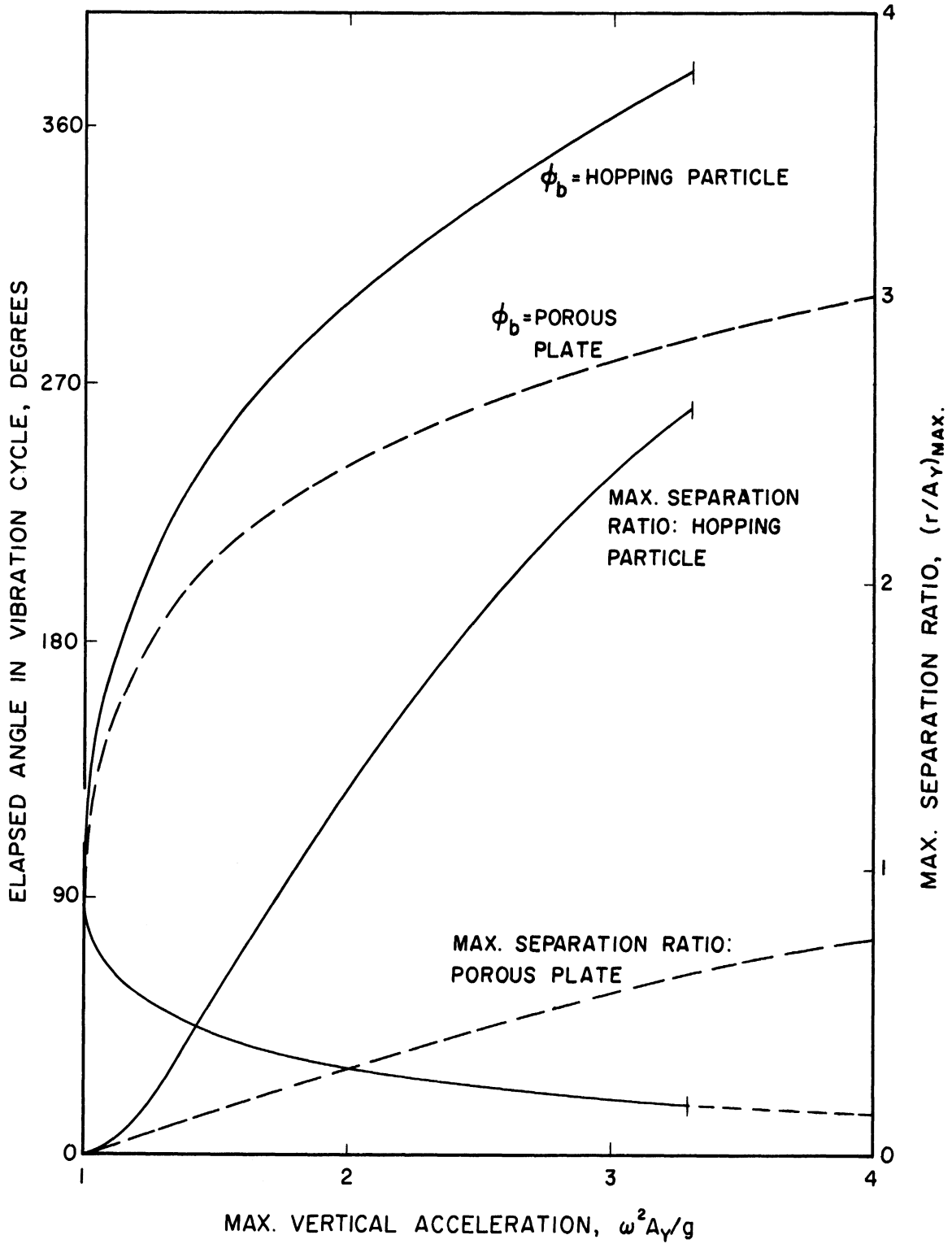

Figure 16. Comparison of Predicted Vertical Motions of Transport Material (A_y = .035 in).

and material properties that affect conveyor performance.

Despite the crude assumption made for the hopping particle model, its analysis establishes the vertical acceleration amplitude V of the vibrating surface as the most influential factor in conveyor performance. The results of Figure 4 show that for $V > 1.0$ g , the transport velocity increases at a practically exponential rate with acceleration level. Near $V = 3g$, the predicted material velocity U levels off asymptotically at a value equal to the horizontal velocity amplitude ωA_x of the vibrating surface. For accelerations above 3.3g, the analysis indicates a non-periodic type of motion for which the hopping displacements of the particle may extend over more than one vibration cycle but for which there is no corresponding increase in flow velocity.

When the particle model of the transport material is capable of sliding with dry friction on the conveyor surface, a considerably different picture of the transport mechanism appears. Results of the sliding particle analysis shown in Figures 8 and 11 indicate that for increasing accelerations below 1.0 g a forward sliding phase occurs first, then increments of both forward and backward sliding, and finally a continuous but predominantly forward sliding motion. As seen in Figure 12, the transport velocities attained by pure sliding depend on the friction factor $\mu \tan \alpha$, but level off near $V = 1$ at the onset of hopping action. Above $V = 1$, Figures 12 and 13 show that the existence of sliding produced transport velocities that can either exceed or fall below those predicted from the hopping particle model.

In any case, the large velocities achieved at high accelerations are evidently due mainly to the hopping action of the particle with frictional effects playing a secondary role.

The porous plate model affords a quantitative way of finding the effect of air flow through the conveyed material on the transport mechanism. This presumably becomes an important factor only for accelerations great enough to produce hopping action and for relatively impermeable materials. On this basis, the analysis indicates that a damping factor $\lambda=\rho_o/\rho K\omega$ has a pronounced effect on the periodic separation of the material from the vibrating surface.

In general, for a given acceleration level $V > 1$, low density ρ and permeability K for the material will combine to reduce the duration and magnitude of the hopping motion from that predicted by the particle models. Also, for a given material and acceleration level, the same effect can be expected at relatively large vibration amplitudes. Figure 16 and Table V show the quantitative results of the porous plate analysis in comparison with those of the hopping particle. These results indicate further that transport velocities for relatively light impermeable materials can fall well below the values predicted from the particle models and become almost independent of the acceleration level.

III. EXPERIMENTAL PROGRAM

In order to study the vibratory transport mechanism under controlled conditions and obtain experimental relations between the operating variables, a test conveyor and auxiliary apparatus for bulk material handling were assembled. This chapter describes the features of the test apparatus and its use in measuring conveyor performance with a given transport material.

A. The Material Transport System

Figure 17 shows an assembly drawing of the experimental conveyor which is seen to be a unit about 8 inches wide by 16 inches high by 32 inches long. For the performance tests the conveyor was secured firmly to a heavy metal base and became a component part of the system shown in Figure 18. Transport material was stored in a large hopper A that opened into a continuous feeder B whose flow rate was adjusted by controller C. The material was allowed to fall onto the input end of the test conveyor D and at the output end was deflected into a receiver E. Conveyor output was weighed on scale F synchronized with an electric timer G. A variable speed drive and electric motor, obscured by the test conveyor in Figure 18, served as a power source.

1. Description of the Test Conveyor

The general configuration of the test conveyor, as indicated by Figure 17, is very similar to that of its kinematic model described earlier in Figure 1. A heavy welded frame, (part 1) of steel plate supports the parallelogram linkage which guides the vibrating plate (2).

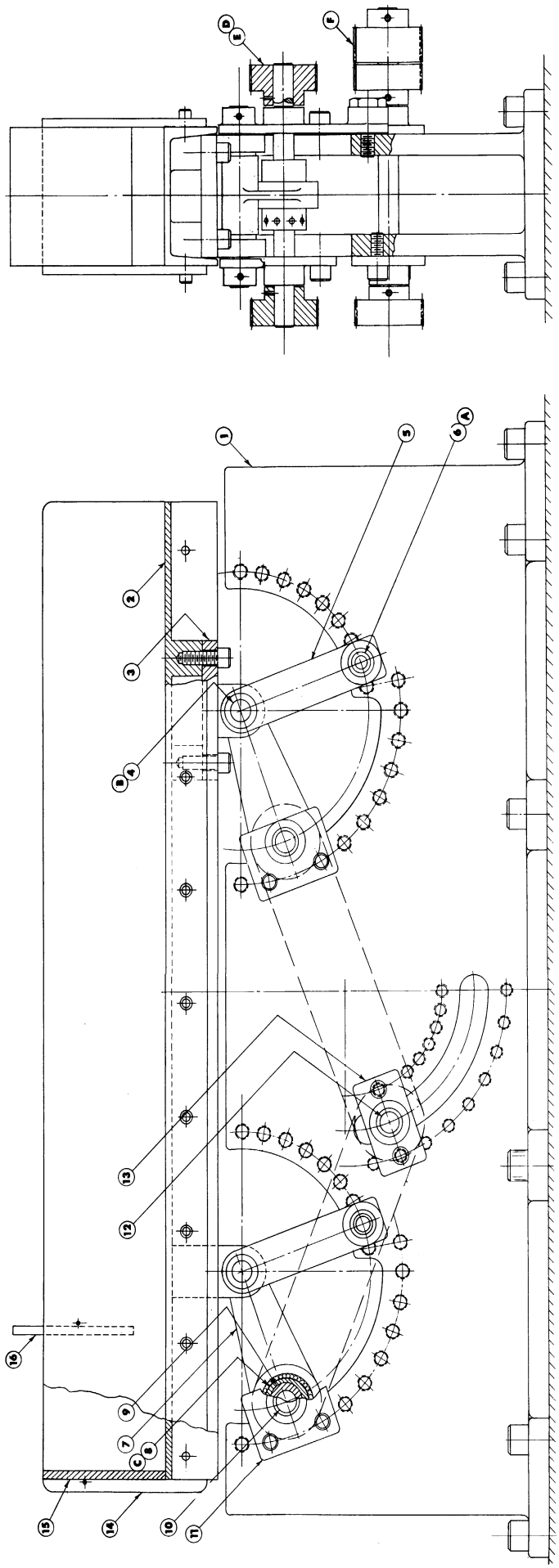

Figure 17. Assembly Drawing of Experimental Conveyor.

The four arms (5) of the linkage, two on either side of the frame, are hinged to both the frame and the underside of the vibrating plate. Two connecting rods (7) at right angles to the arms transmit to the plate a small back-and-forth motion from the set of double eccentrics (8,9) carried on shaft (10). Synchronization of the identical fore and aft eccentrics is achieved through the use of a common drive shaft (12) and a system of timing (toothed) belts and pulleys (D,E). Anti-friction bearings (A,B,C) are used throughout.

The inclination angle α of the plate vibration can be varied by 10 degrees increments from 10 to 90 degrees by attaching shaft brackets (11,13) and pins (6) at the appropriate hole locations in the frame. The double eccentrics permit stepwise adjustment of the vibration amplitude A (half the total displacement) in approximately .010 inch increments up to 0.100 inch. Both of the foregoing adjustments require shutdown of the conveyor. A Link-Belt Company type HM P.I.V. variable speed drive with an integrally-mounted 2 hp electric motor supplied power to the test conveyor drive shaft through a timing belt and pulley(F), and vibratory speeds from 700 to 4200 cpm were attainable. During test runs, however, an arbitrary upper limit of 8 g's was imposed on the conveyor acceleration in order to avoid excessive inertia loading and possible damage in the eccentric drive train.

2. The Vibrating Channel

In Figure 17, the vibrating plate (2) is actually a 28-inch length of 4-inch steel channel mounted horizontally with the flanges extending downward. The upper surface was machined to an rms roughness

level of 50 micro-inches lengthwise. Transparent Lucite panels (14) attached to the side of the channel form a rectangular trough for the transport material. The inlet end of the trough is closed off by a transverse panel (15) and a second transverse panel (16) nearby forms an adjustable gate under which all the conveyed material must pass during operation.

Figure 19 shows the inlet end of the actual test conveyor in position underneath the feeder discharge chute A. The vibrating surface B, carrying a layer of transport material, and gate C are both visible through the transparent side panel. The belt and pulley shown transmit motion of the main drive shaft to the rear eccentric shaft D, and a similar arrangement on the far side of the conveyor frame drives the front eccentric shaft E. Also apparent in Figure 19 are the rear parallelogram arms F and a displacement transducer G.

3. Input and Discharge Equipment

A Syntron Company model FM-010-3 dry feeder unit consisting of a hopper A, electromagnetic feeder B, and flow control unit C as shown in Figure 18 was used to supply the test conveyor with a constant supply of transport material. No mechanical connection existed between the feeder unit and the test conveyor. Instead, material deflected by a chute fell by gravity into a surge chamber formed on the conveyor trough by the end panel and gate as shown in Figure 19. The height h of the opening under the gate was considered to be the nominal depth of flow since the level of material in the surge chamber was always maintained slightly above the edge of the gate during operation.

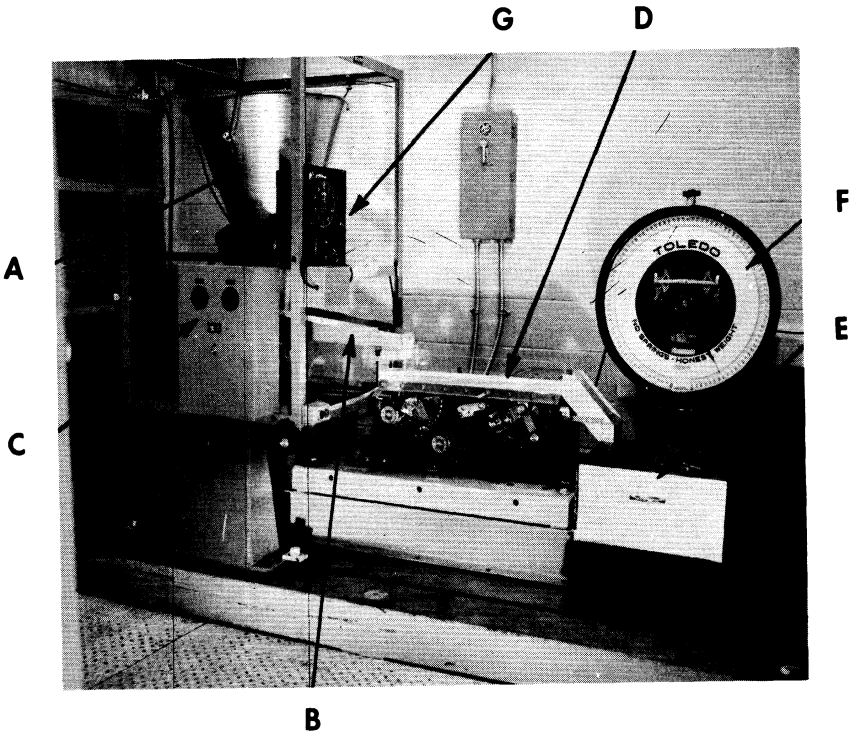

Figure 18. Test Arrangement for Measuring Performance of Experimental Conveyor.

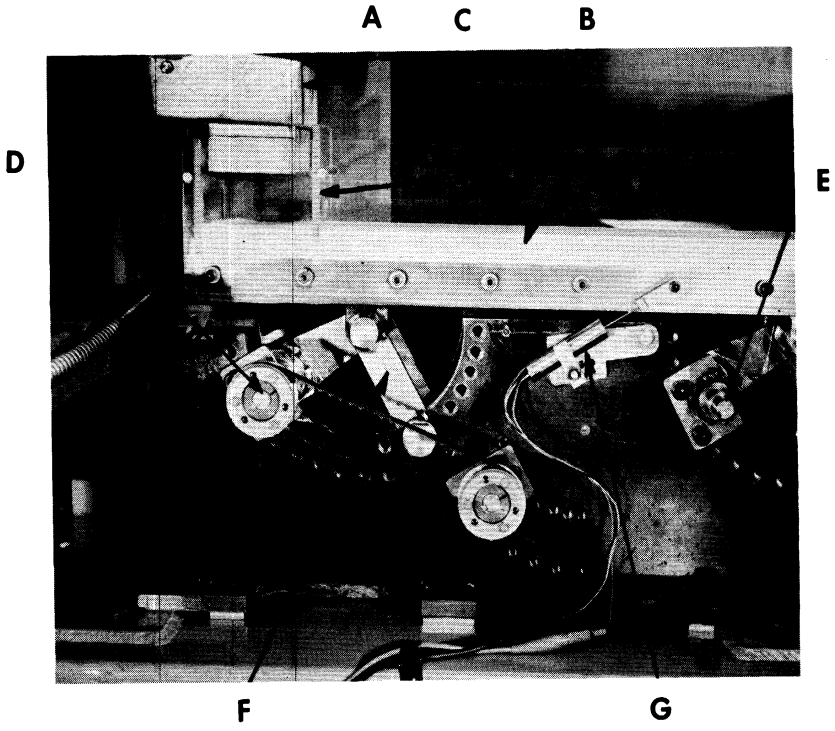

Figure 19. Inlet End of Experimental Conveyor.

As indicated in Figure 18, material discharged from the conveyor during a test run was weighed directly in 5, 10, 15, or 20 lb increments on F, a Toledo Scale Company 0-100 lb direct reading platform scale equipped with a pair of mercury switches. As a given weight increment was being collected in receiver E, these switches would successively energize and de-energize the timer-counter components of G, a Standard Electric Time Company chronotachometer unit, thus permitting flow rates to be accurately measured. Periodic restoration of the transport material from the receiver E back to storage hopper A was made by the author.

4. Instrumentation

In order to obtain an electrical signal proportional to the vibratory displacement of the trough for timing purposes a Sanborn Company model 7DCDT-250 differential transformer was used. As shown by G in Figure 19, the stator of this instrument was clamped to the conveyor frame and the moving core to the vibrating surface. A second electrical signal was obtained from a Kistler Instrument Corporation model 401 pressure pickup carried on the vibrating surface in such a way that the transport material came into direct contact with the pressure-sensitive face.

The output of the pressure pickup was amplified in a Kistler model 651 piezo-calibrator. Both transducer signals were displayed during operation on a Tektronix Incorporated model 502 dual-beam oscilloscope. A photographic correlation of the displacement and pressure traces with the actual transport mechanism was obtained from high speed motion pictures taken with a Beckman and Whitley Company model 333 Magnifax camera.

B. The Transport Material

All the experimental work of this investigation was performed with a single kind of bulk material. In selecting this material, consideration was given to the fact that most commercial vibrating conveyors are rated for capacity on the basis of their output of sand having a density of about 100 lb per cu ft, and that grain size distribution, being related to permeability, plays an important part in the transport mechanism. On this basis a stable, sand-like aggregate obtainable in various reproducible grain sizes was sought for test purposes.

After some preliminary comparisons, the material selected was Minnesota Mining and Manufacturing Company's "Superbrite" glass beads, commonly used as reflective granules in highway markers, tape, and paint. The glass beads were of the class B variety having an average diameter of .008 inch, a density of 93.5 lb per cu ft, and almost perfect sphericity. Specifications indicate a very narrow size distribution for this class, i.e., 10, 40, 40, and 10 percent retention respectively on U.S. No. 60, 70, 80, and 90 sieves.

1. Friction Coefficient

An approximate value for the friction coefficient between the bulk material and surface was determined by standing a short length of 2-inch diameter glass tubing on the conveyor deck, partly filling the tube with test material, and then finding the net force required to drag the tube steadily along the surface. A cloth ring was cemented to the lower end of the tube to prevent leakage of the material, and a simple spring scale was used for force measurements.

2. Air Flow Permeability

Figure 20 shows the simple test apparatus used to find the permeability characteristics of the test material. A sample A of the material is retained in the lower end of a glass tube by a fine-mesh screen cemented in place. Air at a constant upstream pressure indicated by manometer B flows downward in the tube and out through the sample. The air flow rate can be determined from the operating conditions and area of a tiny plate orifice installed in the line at fitting C. Constant pressure shop air is the flow source and enters the line through an adjustable pressure regulator D.

Suppose the supply air upstream of the small orifice is throttled by the regulator to stagnation conditions p_s and T_s and the downstream manometer pressure $p \ll p_s$. Then the orifice flow w is choked and from compressible flow theory

$$w = .532\, C_w A_w \frac{p_s}{\sqrt{T_s}} \tag{48}$$

where C_w and A_w are the orifice discharge coefficient and area, respectively. All of this air flow passes through the material sample which has a known area S and thickness h. Thus by operating this apparatus over a range of regulator settings and sample sizes, one can determine numerical values for the permeability coefficient from

$$K = \frac{wh}{S(p-p_o)} \tag{49}$$

a rearranged version of Equation (39) appearing in Section E of Chapter II.

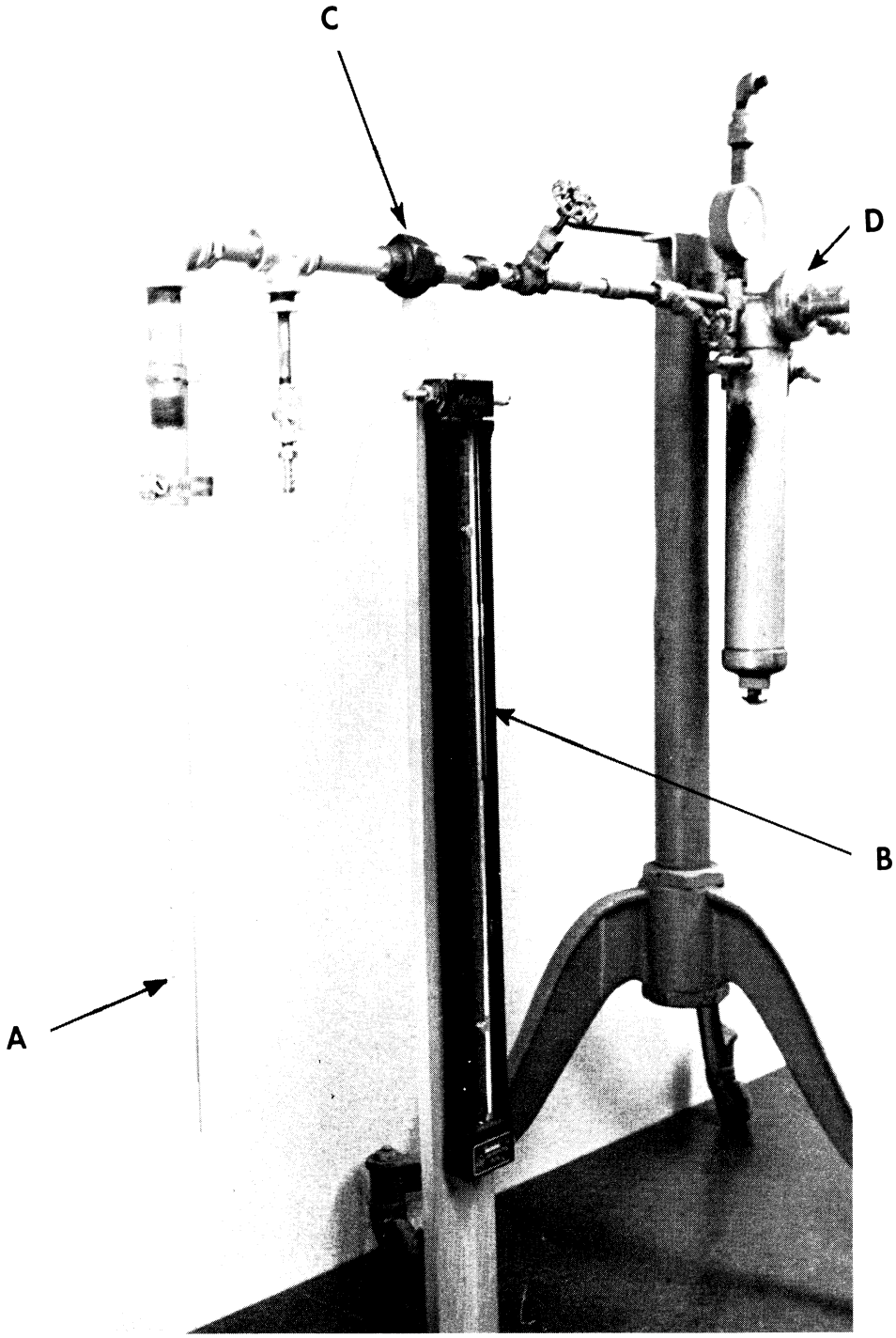

Figure 20. Apparatus for Measurement of Transport Material Permeability.

C. Experimental Procedure

After some exploratory tests of the conveyor system, a systematic measurement of transport flow rate as a function of vibration frequency, amplitude, and inclination angle was made with the glass bead material. Then certain details of the transport mechanism related to the transport material properties were observed.

1. Conveyor Performance Characteristics

The first series of test runs was made with the conveyor assembled at $\alpha = 20$ degrees, the eccentrics set at $A = .068$ inch, and the flow depth $h = 0.5$ inch. For each run the conveyor was started and allowed to reach a steady flow condition at a low speed. Next a fixed weight of discharged material was collected and the elapsed time and number of cycles recorded. Additional runs were then made at successively higher speeds up to the design limit of the conveyor.

The second series of tests was similar to the first except that a smaller vibratory amplitude was used. In all, the performance at five different amplitude settings was observed, then the conveyor was reassembled at $\alpha = 30$ degrees and all test runs repeated. The vibration angle was varied, and complete test data recorded, up to $\alpha = 60$ degrees in 10 degree increments. Selected tests were also run at flow depths other than 0.5 inch.

2. Vertical Vibration Observations

The theoretical aspects of vibratory transport discussed in Chapter II suggest that the vertical components of motion are not directly coupled to the horizontal, and that an examination of a purely vertical

model might therefore be worthwhile. On this basis, the test conveyor was modified and assembled for operation at $\alpha = 90$ degrees as shown in Figure 21. The glass tube A, partly filled with the glass bead material, is cemented directly on the vibrating surface at the location of the Kistler pressure pickup whose lower end is visible at B. A flat plate attached to the conveyor deck by long vertical rods supports the upper end of the tube.

During vertical vibration at large accelerations, the pressure pickup responds to variations in contact force at the material-surface interface. The corresponding signal is fed into Kistler Amplifier C and can then be displayed on the same time base as the signal from the Sanborn displacement transducer D. The arrangement of Figure 21 was also used to obtain high-speed motion pictures of the vertical vibration.

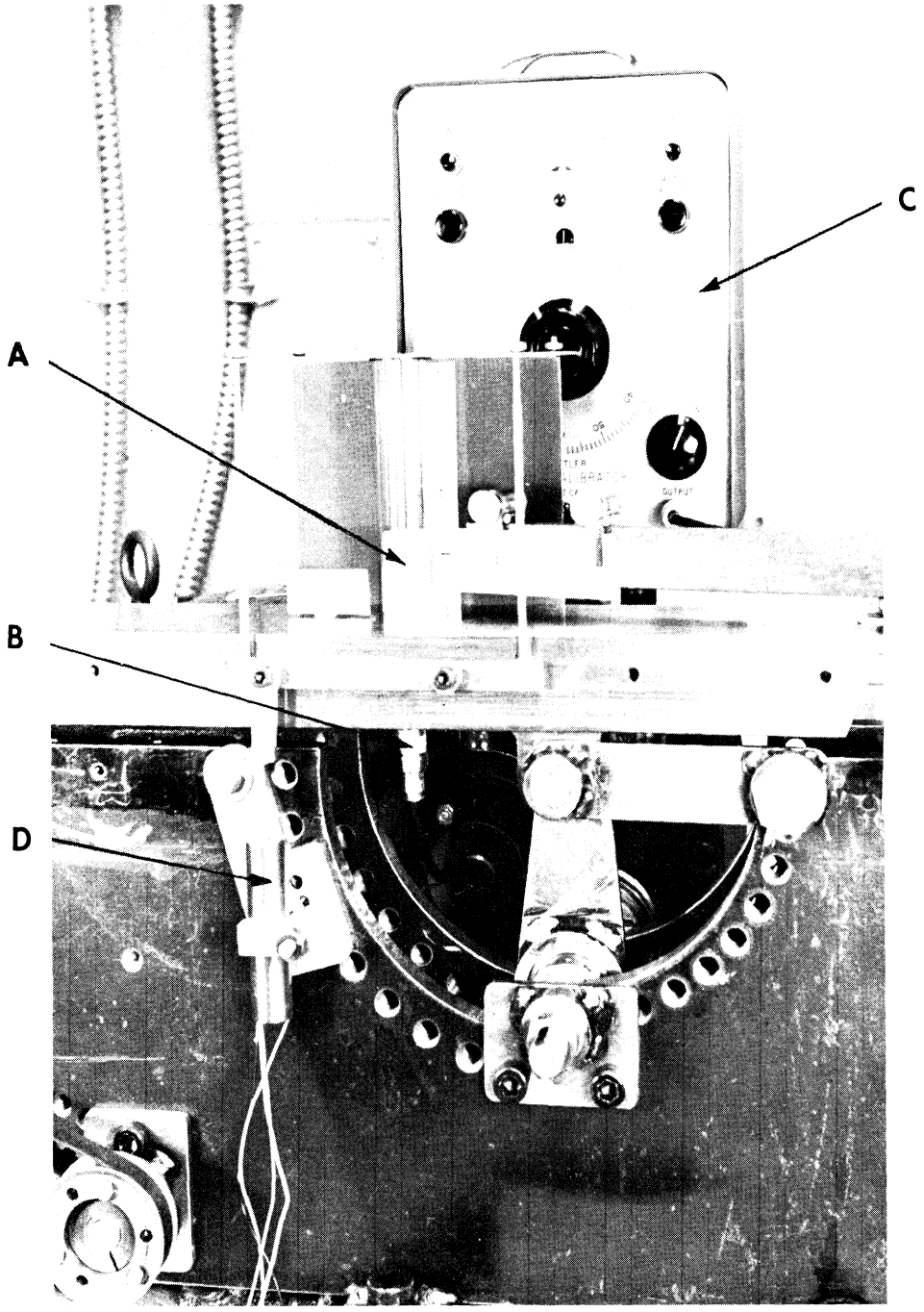

Figure 21. Test Arrangement for Observing Transport Material Behavior During Vertical Vibration.

IV. EXPERIMENTAL RESULTS AND DISCUSSION

In this chapter the test results are reported and put into a form suitable for comparison with the results predicted from idealized models of the transport mechanism. Since only one test material was used for all tests, quantitative comparisons are based on numerical values obtained for the characteristic properties of that particular material and to an extent on the results of other investigators.

A. Transport Material Parameters

Two samples of glass bead material differing only in grain size were tested for frictional drag with the results shown in Figure 22. Here the net horizontal drag force, i.e., the gross force less the drag of the empty container, is plotted for various sample weights of each material. In both cases virtually no static increment of force was required to start the steady motion (about 10 ft per min) during which measurements were made. Therefore it can be concluded that there is a negligible difference between the static and dynamic friction coefficients as in the case of Hurst's experiments.[12]

The test data indicate the linear dependence of drag on normal force that is characteristic of dry friction, and the value of μ corresponds in each case to the slope of the curve. As seen in Figure 22, the test material A had a higher coefficient than the finer-grained comparative material B. This result appears to disagree qualitatively with handbook data where angles of slide of coarse aggregates on an inclined surface are usually lower than those for fine aggregates of the

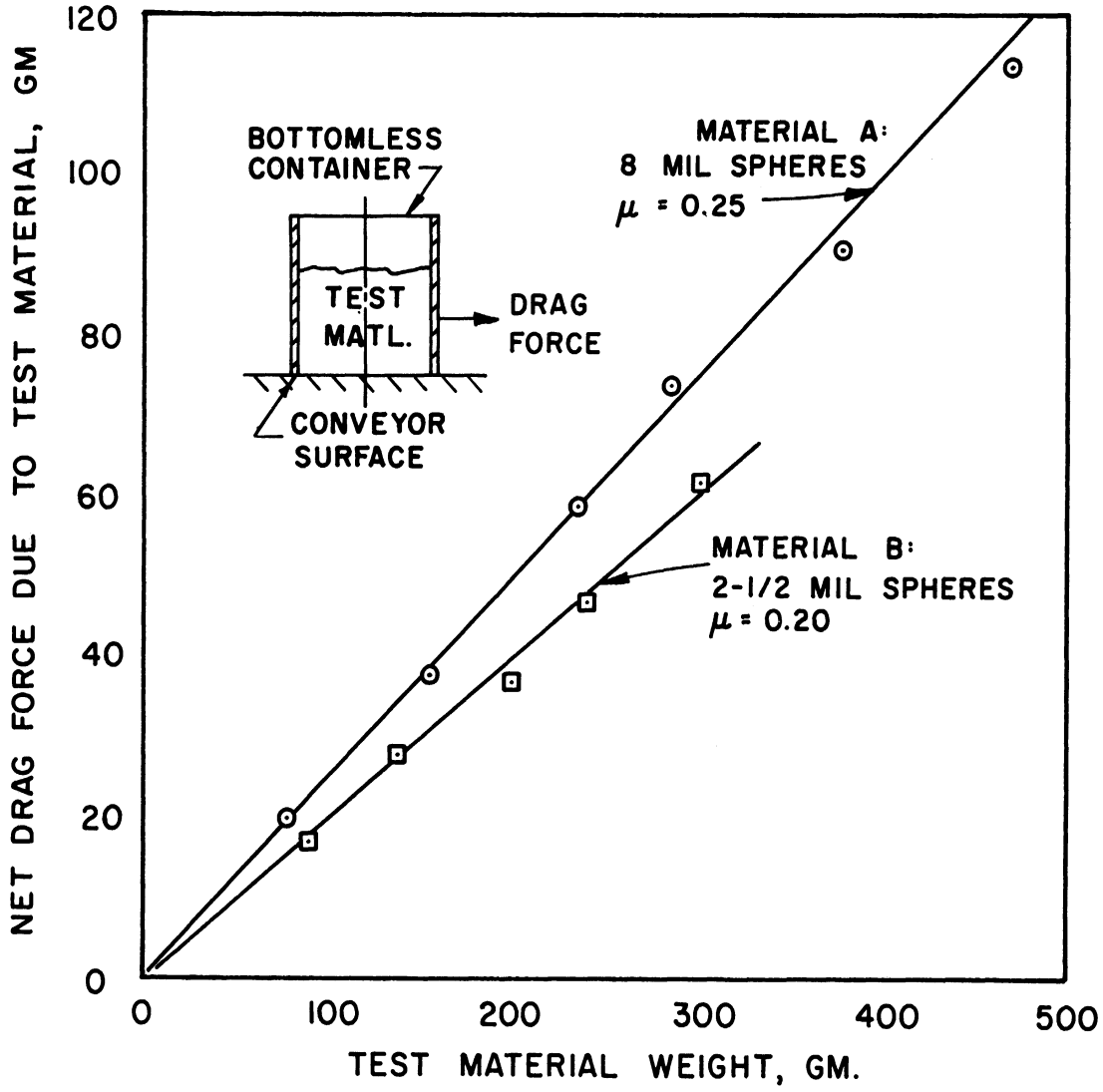

Figure 22. Results of Frictional Drag Tests on Transport Material

same material. However the detailed action of the material in inclined plane tests is quite different from that in the drag tests of Figure 22.

Test results obtained from the permeability apparatus of Figure 20 are shown in Figure 23. For a constant mass flow rate w of air it is seen that the pressure drop across the glass bead transport material varies linearly with sample thickness h. For these tests the orifice at D in Figure 20 was a sharp-edged, .010-inch diameter hole having a discharge coefficient $C_w = .84$, and the sample tube diameter was 7/8 inch. Values of specific flow rate w/S in Figure 23 were calculated from Equation (48) for 70 deg F shop air and pressure regulator settings of 30, 50, and 80 psig. When used in Equation (49), these numerical values give a permeability coefficient $K = 2.54 \times 10^{-6}$ sec for the glass bead test material.

An attempt was made with the same apparatus to find the permeability of the material with respect to an upward flow of air. It was found that the results were unchanged for low pressure drops, but when the equivalent upward force of the air on the underside of the sample exceeded its weight, air passed through the material in slugs analogous to large bubbles rising through a boiling liquid. This action is probably related to the ebullition noted by Böttcher[3] in conveyor tests with powder-like transport materials, and will be discussed later in this chapter.

B. Conveyor Performance Characteristics

Numerical data from the conveyor performance tests are tabulated in Appendix C. The same grade of glass bead material and gate

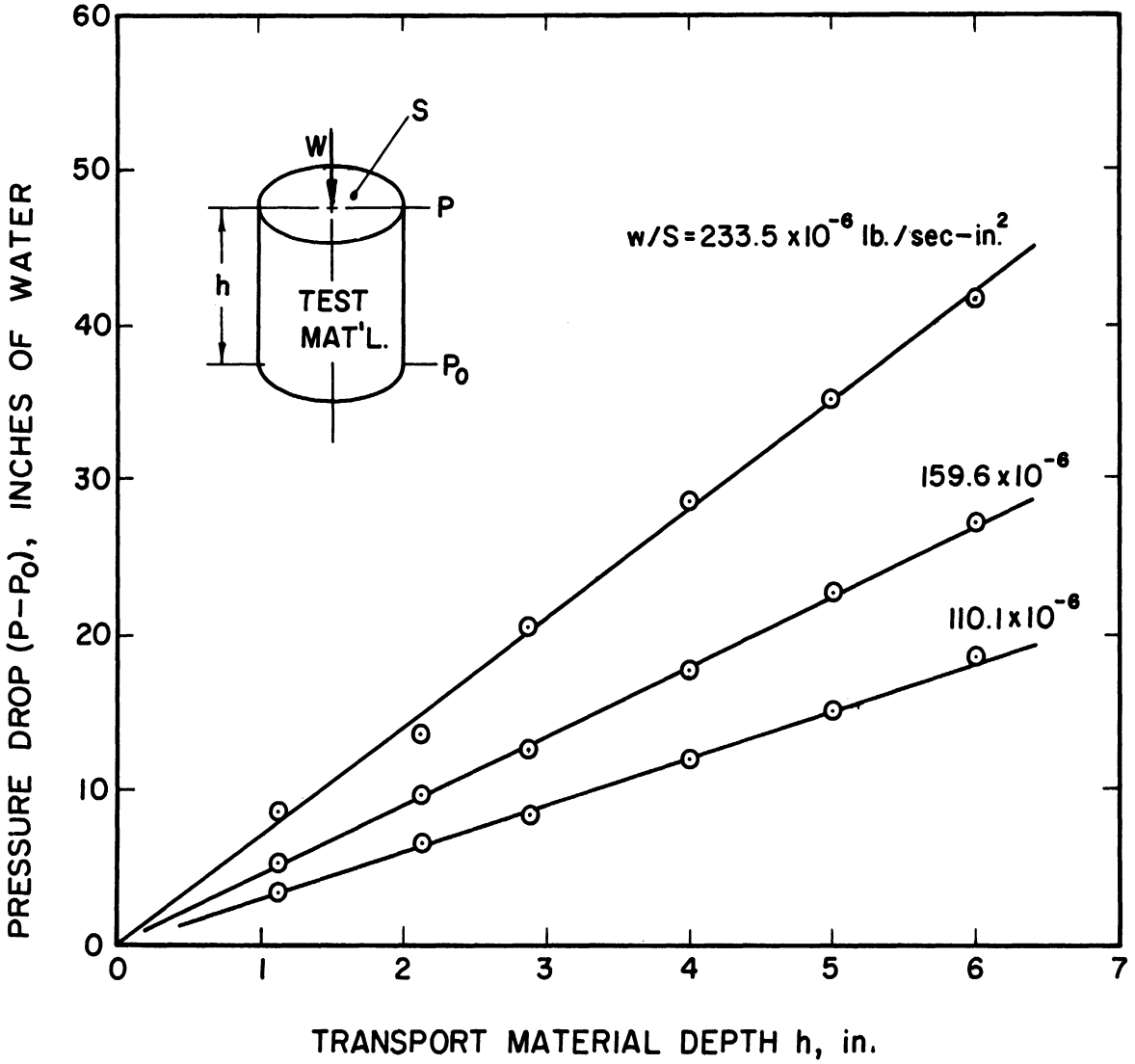

Figure 23. Pressure Drop Across Transport Material Under Constant Air-Flow Conditions.

setting of $h = 0.5$ inch were used in all tests. Values of vibration frequency N and material flow rate W were obtained from the data by taking account of the run duration Δt. An average transport velocity was then calculated from a simple continuity relation as follows:

$$U = W/\rho g b h \tag{50}$$

1. Transport Velocity Curves

A general picture of the test conveyor performance can be obtained from Figures 24-28, inclusive. Each of these curve sheets shows flow rate as a function of frequency for a given value of vibration angle, and the data points along each curve represent operation at constant vibration amplitude.

It is seen that for a given amplitude, the conveyor output increases almost linearly with frequency over much of the operating range and that the rate of increase depends directly on the amplitude. In much the same way the output at any given frequency depends directly on the amplitude, and this dependence increases with increasing frequency. The implication is that except for very low output levels the material flow rate is linearly related to the product of vibratory speed and amplitude.

The effect of vibration angle on conveyor performance can be observed by comparing the curves for a given amplitude in each of the five figures. In all cases the tests show that as the angle increases from $\alpha = 20$ degrees, the curves shift to the left and at the same time become less steep. At the larger angles, say $\alpha = 60$ degrees, it is evident that the conveyor output is greatly reduced over a wide range of speeds, but this effect is less noticeable in the 20 to 30 degrees range.

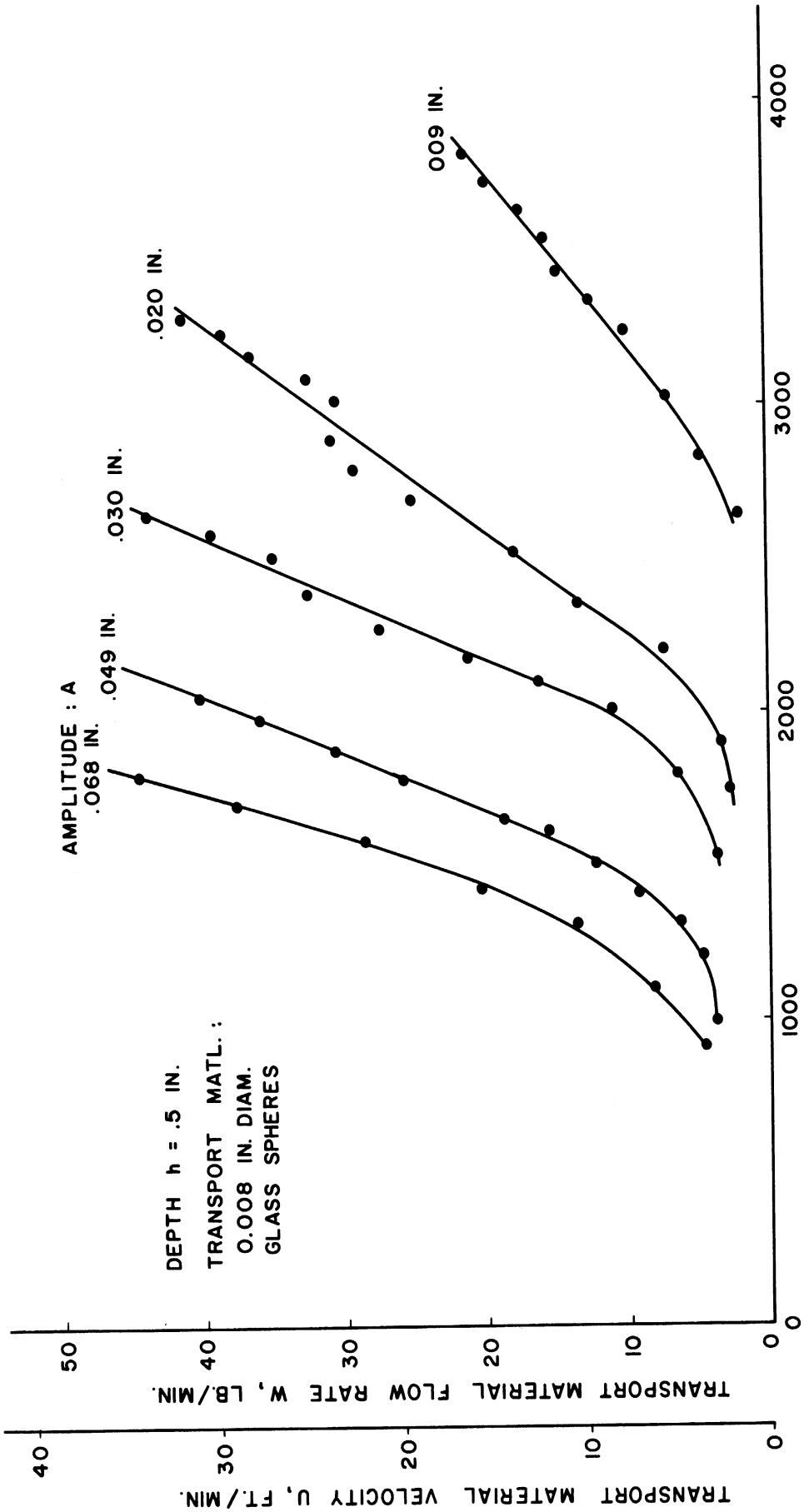

Figure 24. Performance Characteristics of Experimental Conveyor for a 20 Degree Vibration Angle.

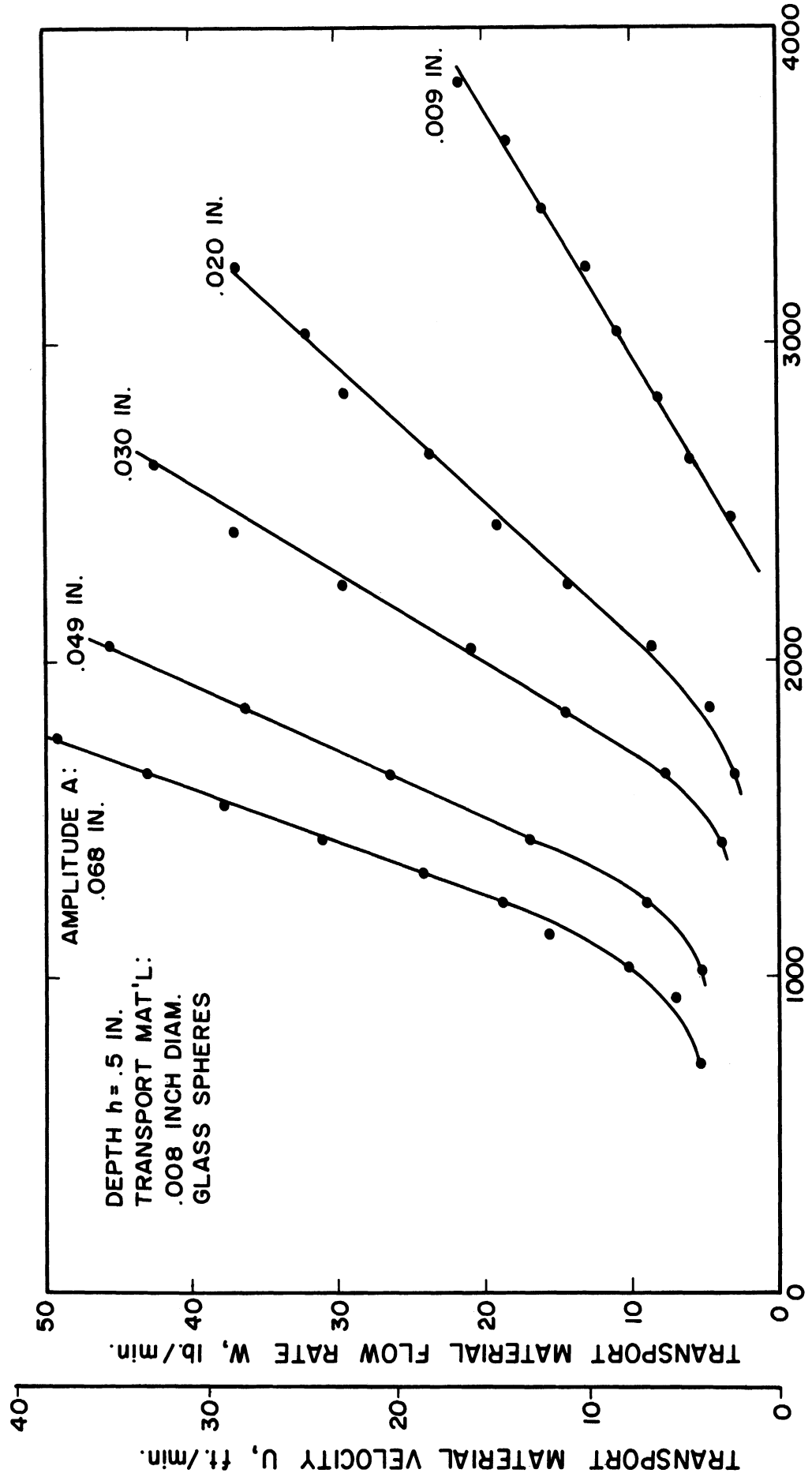

Figure 25. Performance Characteristics of Experimental Conveyor for a 30 Degree Vibration Angle.

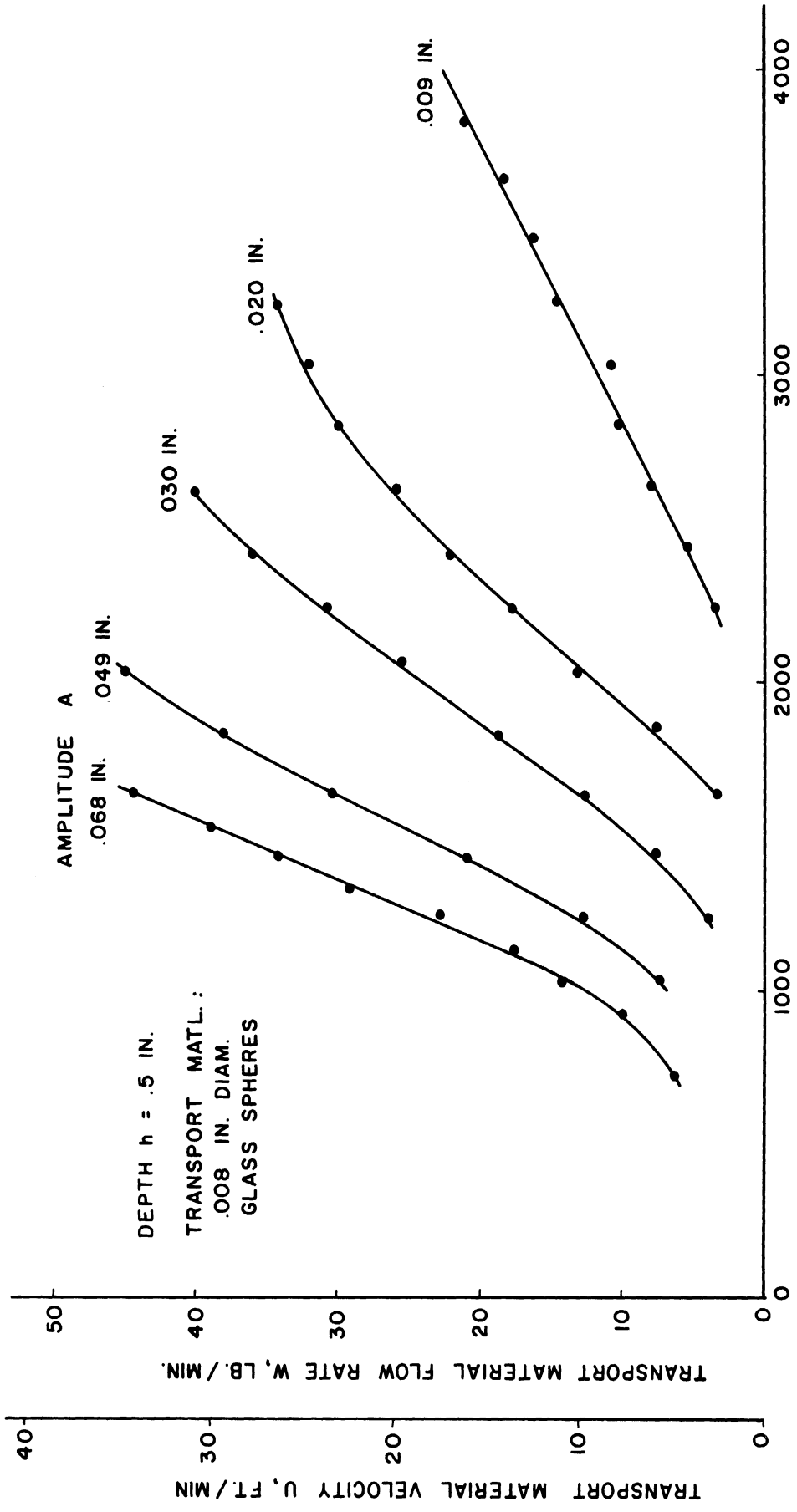

Figure 26 Performance Characteristics of Experimental Conveyor for a 40 Degree Vibration Angle.

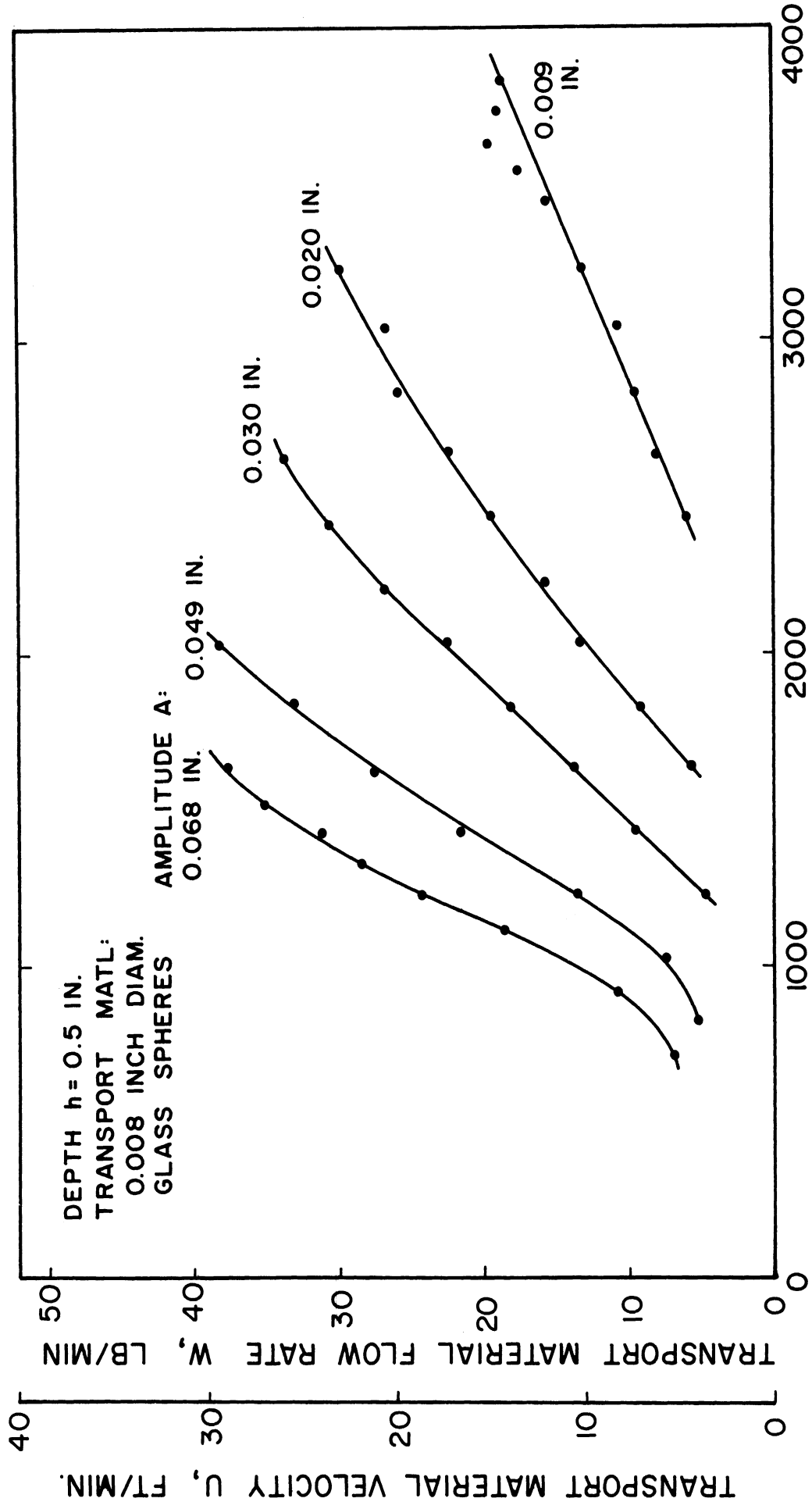

Figure 27. Performance Characteristics of Experimental Conveyor for a 50 Degree Vibration Angle.

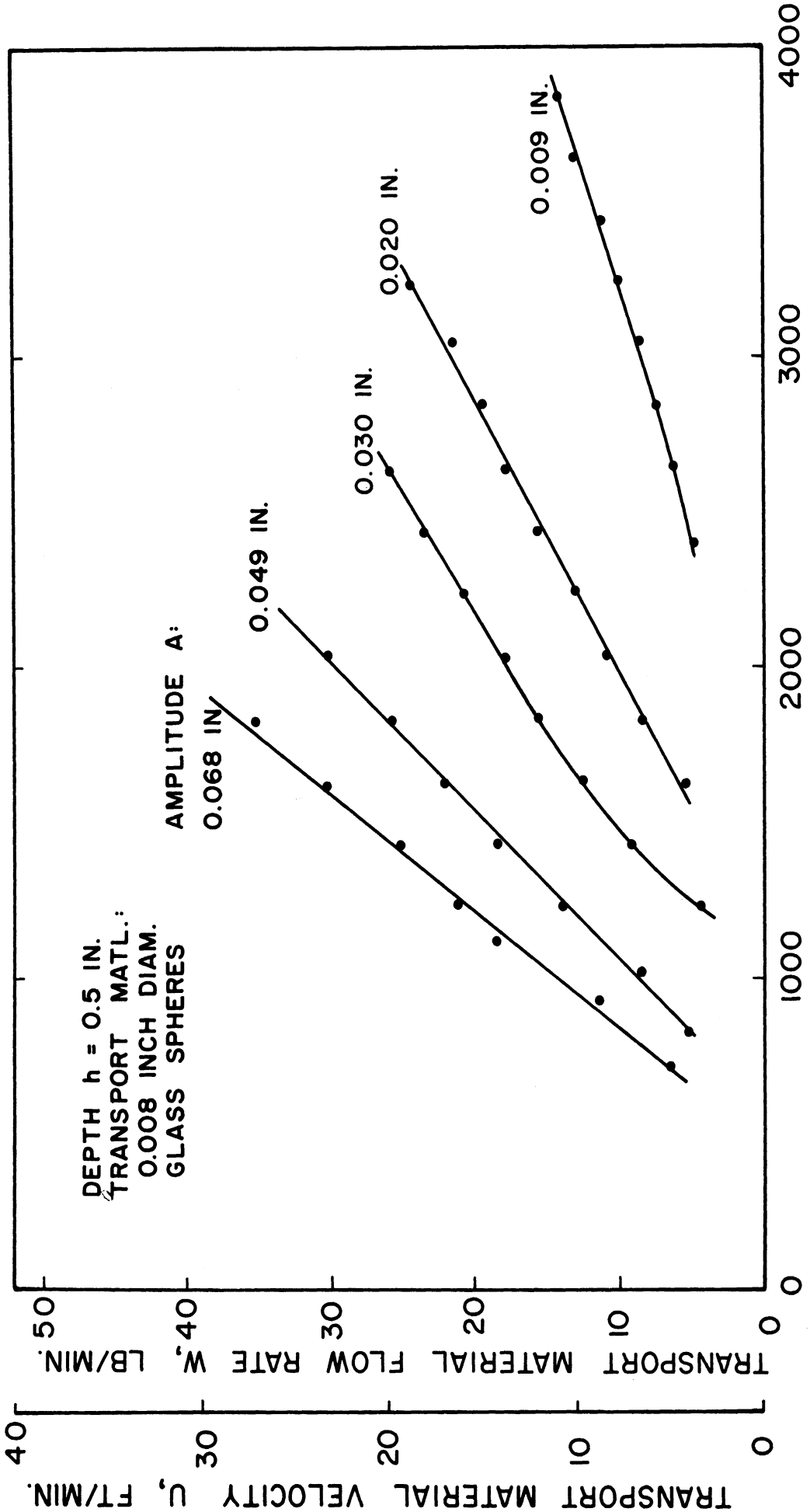

Figure 28. Performance Characteristics of Experimental Conveyor for a 60 Degree Vibration Angle.

2. Effects of Flow Depth and Angle

A preliminary series of tests was undertaken to determine how flow depth of the material as controlled by the gate setting affected total flow rate for conveyor operation at constant vibration angle, amplitude, and frequency. Typical results are shown in Figure 29 where despite some scatter in the test data, the flow rate W is seen to be essentially proportional to material depth h. This means either that the transport velocity of the material does not vary appreciably with distance above the vibrating surface, or if such a vertical velocity gradient does exist, that it is unaffected by the depth of transport material.

In any event, the results appeared to justify the elimination of flow depth as an independent variable in measuring conveyor performance. Consequently, a constant value of h = 0.5 inch was used for the tests reported in Appendix C.

A somewhat clearer picture of the effect of vibration angle is given in Figure 30 where flow rate W has been cross-plotted versus angle from the performance characteristics of Figures 24-28. The resulting constant speed curves are seen to reach a maximum flow value at a particular setting of the vibration angle, but this optimum condition changes with speed and undoubtedly amplitude as well.

Figure 30 bears out the use of 20 to 40 degree vibration angles in most commercial vibratory feeders where practical considerations generally require both a fixed angle and speed. The problem of selecting an optimum vibration angle has been studied theoretically by Böttcher for conveyor frequencies of 25, 50, and 75 cps in terms of the

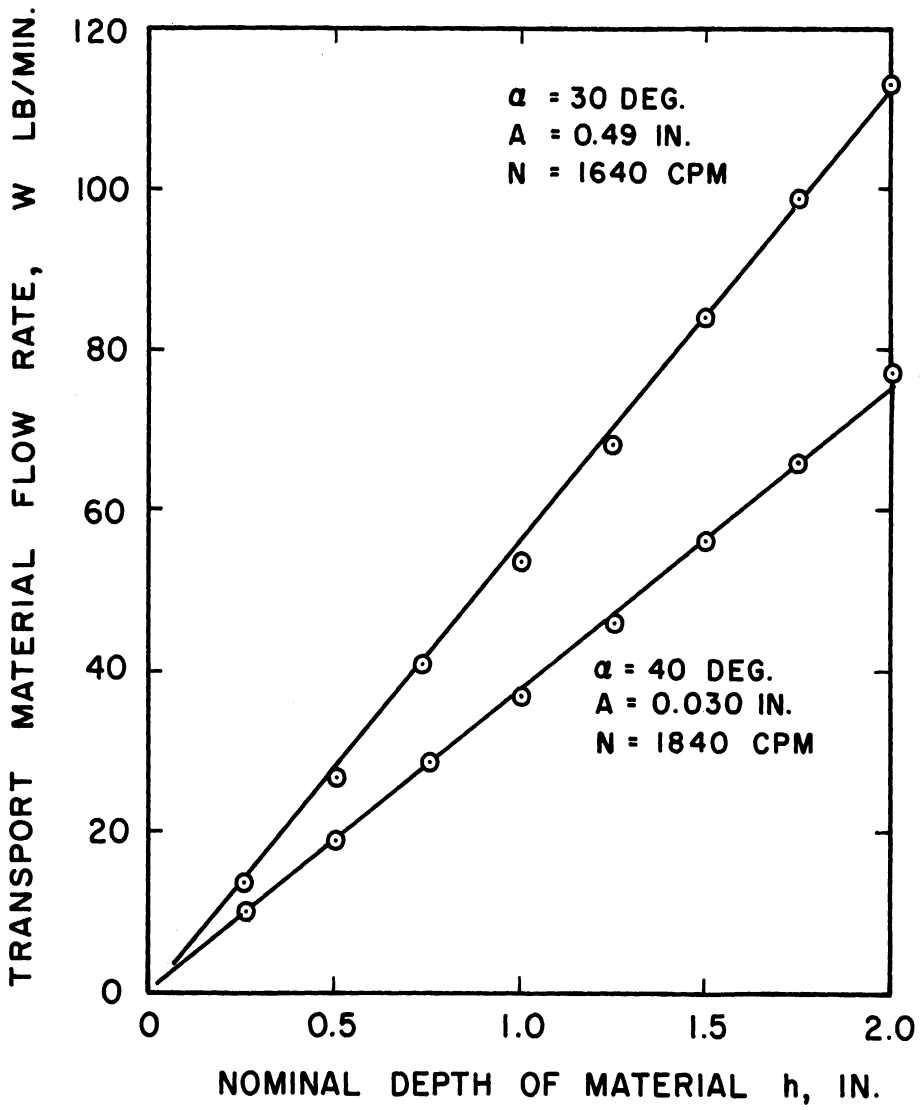

Figure 29. Typical Variation of Material Flow Rate with Flow Depth.

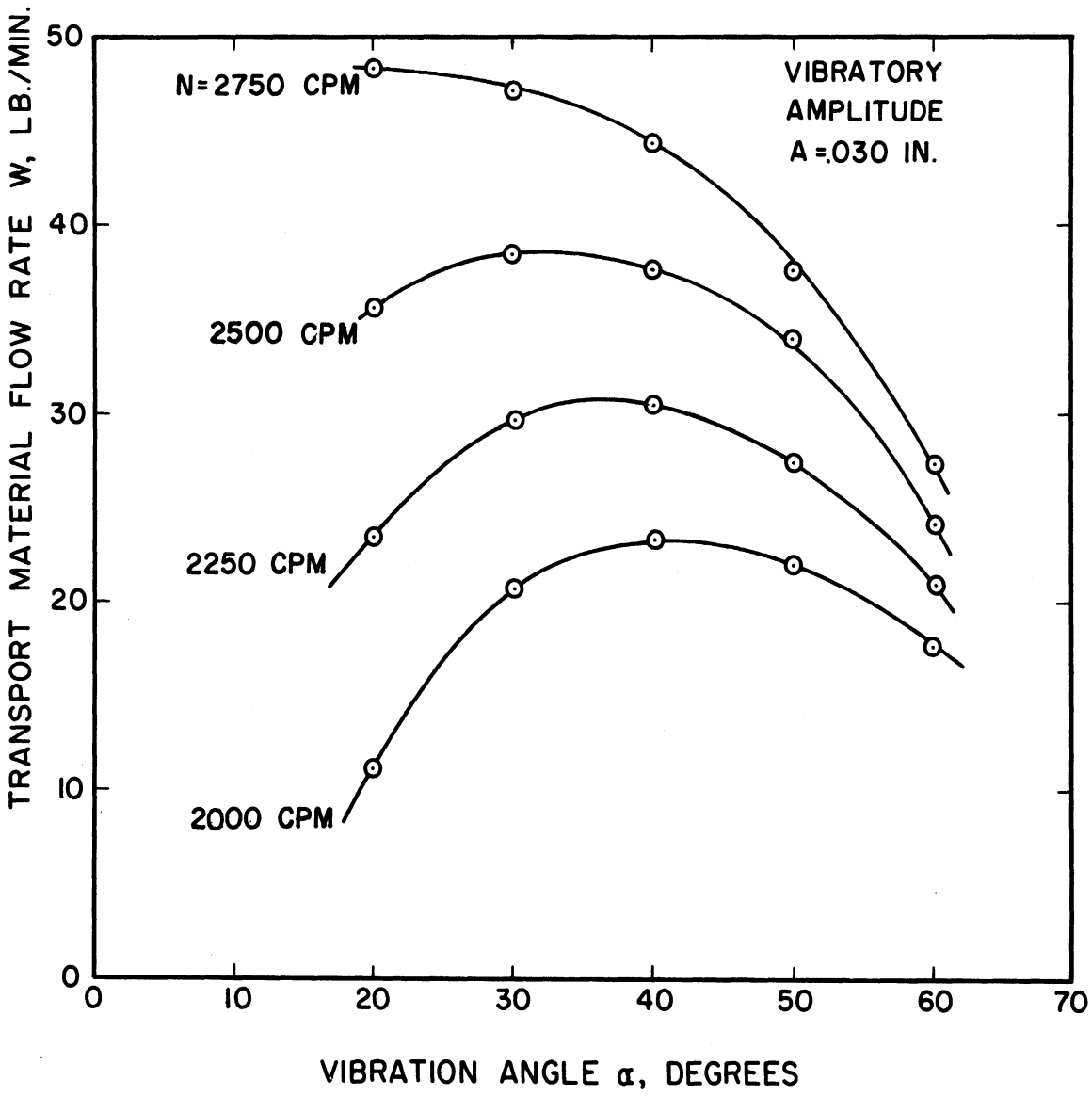

Figure 30. Variation of Material Flow Rate with Angle of Vibration in Experimental Conveyor.

hopping particle analysis of Chapter II, Section C. His results indicate that for operation at constant speed and amplitude, conveyor output is relatively insensitive to vibration angle in the 20 to 40 degree range.

C. Comparison of Experimental and Calculated Results

The foregoing performance results can now be compared with predictions calculated from the model analyses of Chapter II. The test results for a vibration angle of $\alpha = 30$ degrees will be used as the basis of comparison since a comprehensive study has shown these results to be completely typical of the entire body of performance data. In addition, since the test material has a measured friction coefficient of $\mu = 0.25$, representative values of friction parameter $\mu \tan \alpha$ will be taken as 0.1 or 0.2 for purposes of calculation.

1. Particle and Plate Models

The transport velocity ratio $U/\omega A_x$ of a hopping particle conveyor has been shown in Chapter II to depend only on the vertical acceleration ratio $A_y\omega^2/g$. One can calculate the numerical values of these ratios for each run of the test conveyor by noting the definitions of A_x, A_y, U, and ω in terms of the test variables W, N, A, and α. The resulting experimental results for $\alpha = 30$ degrees are given by the solid-line curves in Figure 31. The dotted line curve indicates the predicted behavior of the hopping particle model re-plotted from Figure 4.

It is immediately apparent that while the test results follow the general trend predicted by the theoretical model, the test points

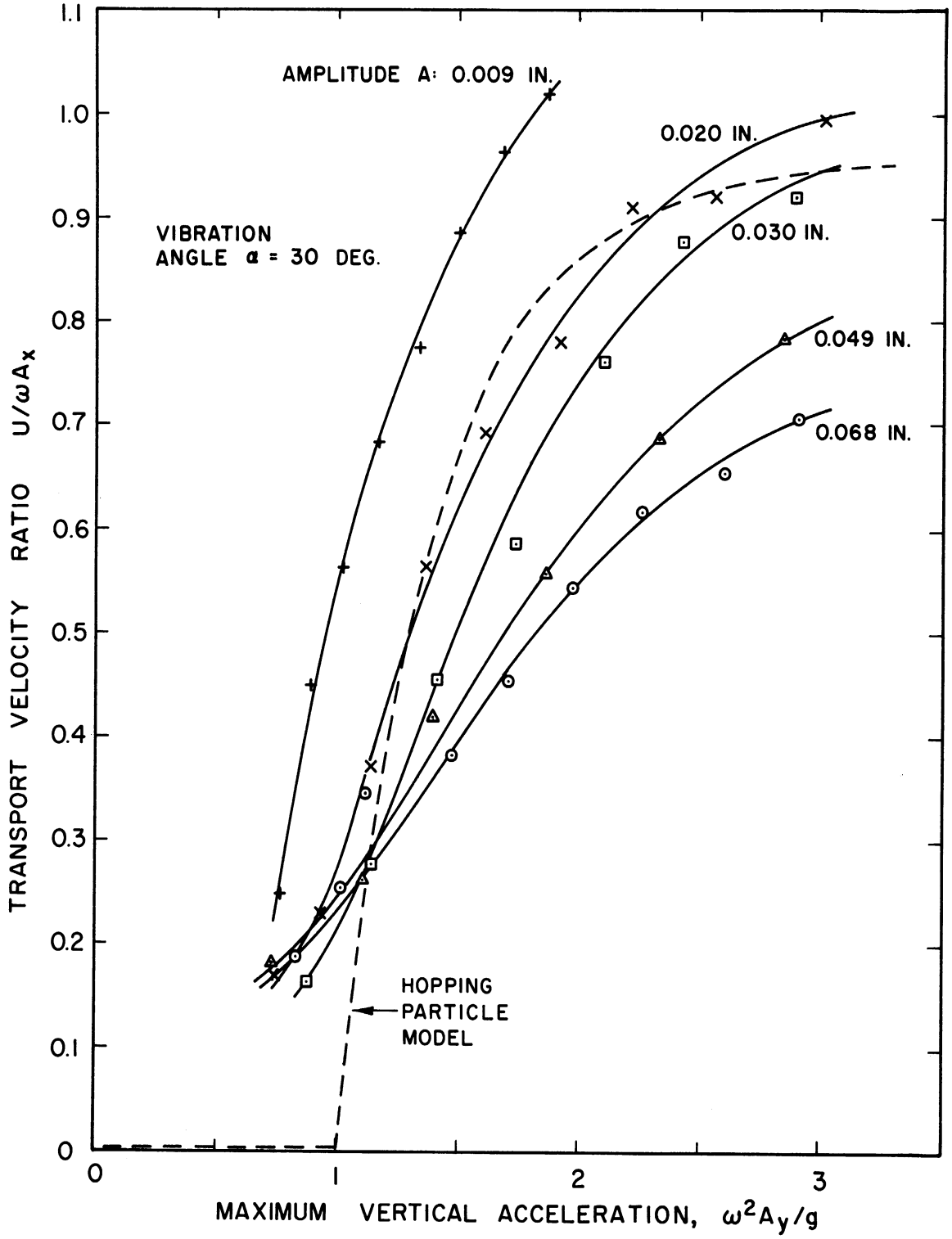

Figure 31. Comparison of Test Results with Those Predicted from Hopping Particle Model.

themselves do not fall on a single line. Instead, they form a family of curves for which the parameter is vibration amplitude as shown. This spread in the test results is not attributable to dry friction effects since the transport material, conveyor surface, and vibration angle remained unchanged for the test runs plotted. It is quite probable however that the permeability characteristic of the transport material may be responsible, and if so, a qualitative explanation should be evident from the porous plate model analysis given in Chapter II, Section E.

The theoretical effect of permeability on transport velocity ratio can be predicted by first noting in Equation (47) that when a porous plate conveyor is operated with a single material ρK and at constant vertical acceleration V, the damping coefficient λ varies directly with amplitude A. Then from Table V it is seen that transport velocity in the porous plate model is adversely affected by increases in λ. Returning to Figure 31, one can therefore conclude that the divergence of test data into a family of curves is due to the fine-grain, impermeable nature of the material and that the resulting reduction of the transport velocity is greatest at large vibration amplitudes.

Although it is possible to justify Figure 31 qualitatively from the porous plate model, the numerical values for transport velocity in Table V do not indicate a successful quantitative correlation with the test results except near $V = 1$. The selected values of λ in Table V were calculated from the measured permeability of the test material and the range of amplitude values shown in Figure 31. Yet the theoretical transport velocity ratios of Table V, unlike the test values, are virtually independent of conveyor acceleration above $V = 2$ and do not show as much

sensitivity to amplitude as the test results. This indicates that the assumptions made to simplify analysis of the porous plate model were not entirely valid.

2. Effects of Friction and Sliding

It is evident from the test points of Figure 31 that considerable transport velocity can be obtained at acceleration levels less than 1.0 g where the hopping particle analysis predicts zero flow. Since it is physically impossible for any separation of the material to take place in this range of operation, the observed flow must take place by the mechanism of sliding or horizontal shear.

The sliding particle analysis of Chapter II, Section D, shows that finite friction between the conveyor surface and transport material not only permits flow below 1.0 g but also can affect conveyor performance at higher accelerations as well. Figure 12 shows a plot of transport velocity ratios calculated for the hopping and sliding particle models in which the values of $\mu \tan \alpha$ are comparable to the test material and conveyor surface at $\alpha = 30$ degrees. It is evident from the curves that above $V = 1$, combined hopping and sliding of the material can produce transport velocities either larger or smaller than those caused by hopping action alone. This is in qualitative agreement with Figure 31, where the experimental curves are seen to fall on both sides of the theoretical curve. Moreover, the test curves for .020 and .030 inch amplitudes in Figure 31 are almost identical to the calculated curve for $\mu \tan \alpha = .1$ in Figure 12.

A more direct comparison is shown in Figure 32 where test results from Figure 25 are superimposed on the analytical model results of

Figure 13. It is seen that the three hopping model curves in Figure 32 intersect the abscissa axis and thereby predict zero transport flow at frequencies corresponding in each case to an acceleration of 1.0 g. By comparison, the sliding model curves predict finite flow at frequencies well below these intersections, and in this region the test data are in good agreement with the results for $\mu \tan \alpha = .1$.

Above the 1.0 g acceleration level both the sliding model and experimental results indicate a virtually linear increase of transport velocity with conveyor speed. However the sliding model results predict considerably greater transport velocities than those actually observed at the larger vibratory amplitudes and somewhat lower transport flow at small amplitudes. Although specific calculations do not account precisely for this discrepancy, the porous plate model shows that for relatively impermeable materials, the air damping responsible for attenuation of transport action increases with vibration amplitude.

If permeability effects are indeed responsible for the comparative results shown in Figure 32, then it is apparent from the model curves that friction and sliding play a relatively minor role in the transport mechanism of bulk materials. This situation holds true of course only for operation at accelerations above 1.0 g, but appears to be almost independent of vibratory speed and amplitude. The conveyor test results reported by Hurst[12] for two values of dry friction bear out this contention as do the single-frequency conveyor experiments by Böttcher.[3]

Only a few test runs carried the experimental conveyor operation into a region where turbulence and secondary flow patterns appeared in the moving layer of transport material. In all cases this condition

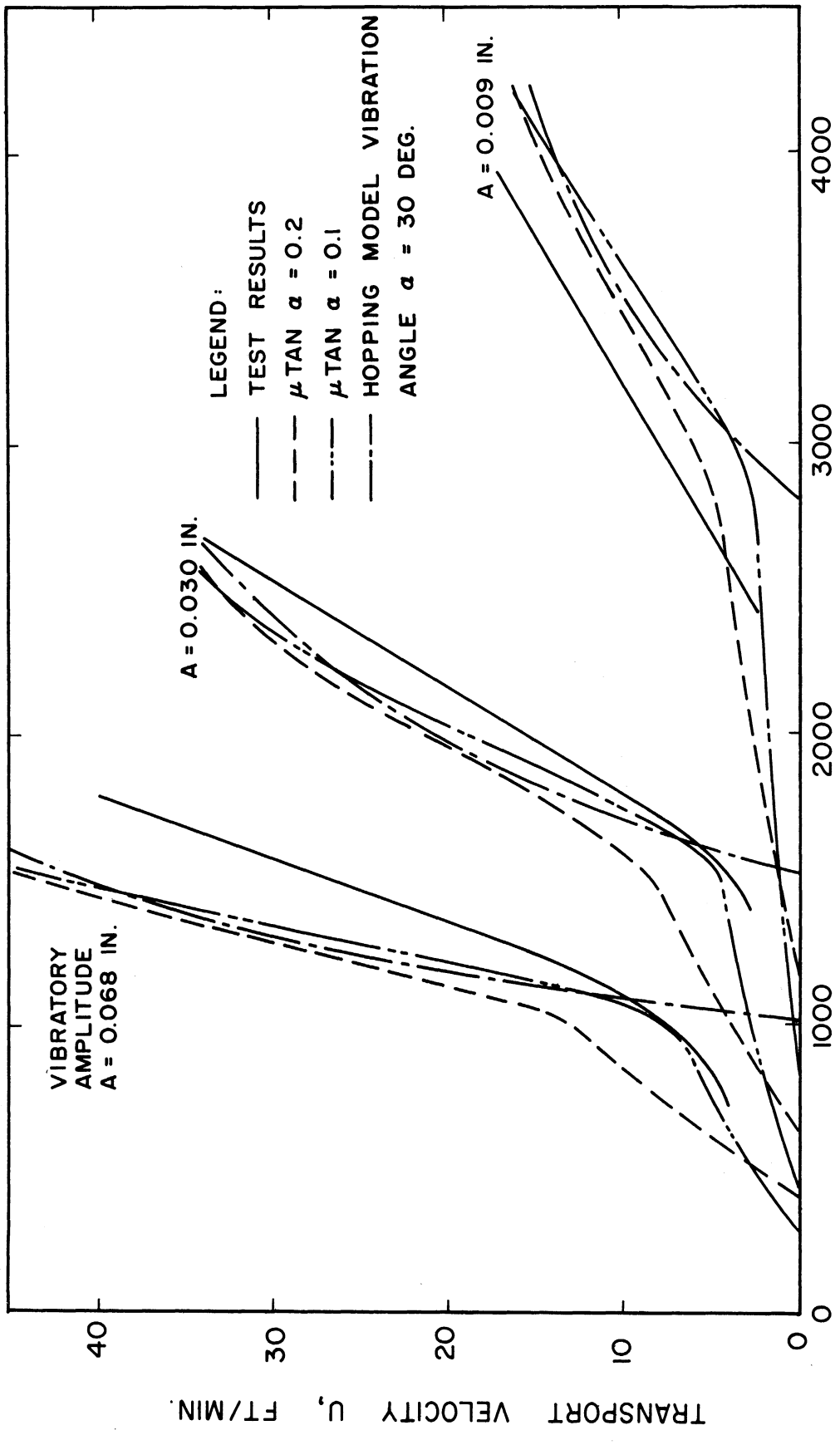

Figure 32. Comparison of Experimental Conveyor Performance with that Predicted from Particle Models.

occurred at high speed and amplitude levels and resulted in a reduced sensitivity of conveyor flow rate to changes in speed. As noted by other investigators it is difficult if not impossible to study conveyor operation quantitatively when the flow is disrupted by such turbulence and aeration. However some insight into this phenomenon may be obtained from the porous plate model.

It is possible to rewrite Equation (42) for the porous plate model to obtain an expression for the instantaneous air pressure p below the transport material as

$$p = p_o - (\rho g h \lambda V) v \tag{51}$$

From Figure 15 it is apparent that velocity ratio v reaches a large negative value v_b when the porous plate completes its hopping motion at $\varphi = \varphi_b$. Thus the maximum air pressure reached during the cycle is

$$p_{max} = p_o - \rho g h \lambda V v_b \tag{52}$$

where the upward pressure difference acting on the transport material is the last term in Equation (52). If this predicted pressure force is the same order of magnitude as the gravity force, it is logical to expect a disruption of the transport material due to upward air flow as observed during the permeability tests. By equating the pressure difference term of Equation (52) to the gravity pressure $\rho g h$, one obtains $v_b = 1/\lambda V$ which presumably defines the onset of ebullition.

Because the maximum velocity v_b is itself a function only of λ and V according to Equation (46), the dimensionless product λV may

be considered a rule of thumb index whose value indicates the tendency of a material to convey improperly because of air pressure effects. From the definitions of λ and V, the product can be written as

$$\lambda V = [\frac{\rho_o}{gK\rho}] A\omega \tan \alpha \qquad (53)$$

On the basis of the foregoing analysis it is seen that low permeability and density as well as large operating amplitudes, speeds, and vibration angles all contribute to air flows in the material that can render the conveyor ineffective at acceleration levels above 1.0 g.

D. Vertical Vibration of Transport Material

The observations made of a sample of test material subject to a purely vertical vibration permit some direct comparisons with results predicted from the porous plate model. For this purpose, the hopping motion of the material was detected by a force transducer and motion pictures were made at selected operating conditions.

1. Impact Determination

The conveyor apparatus arranged as in Figure 21 was operated at three different amplitudes, three acceleration levels, and three material depths. For each run, signals from the displacement and force transducers were displayed on the oscilloscope across a common time base. Two pairs of typical traces are shown in Figure 33 where the smooth curve of each pair represents conveyor surface displacement and the other indicates force on the surface.

The displacement curve is seen to be essentially sinusoidal and to thereby establish a convenient horizontal scale for the elapsed angle

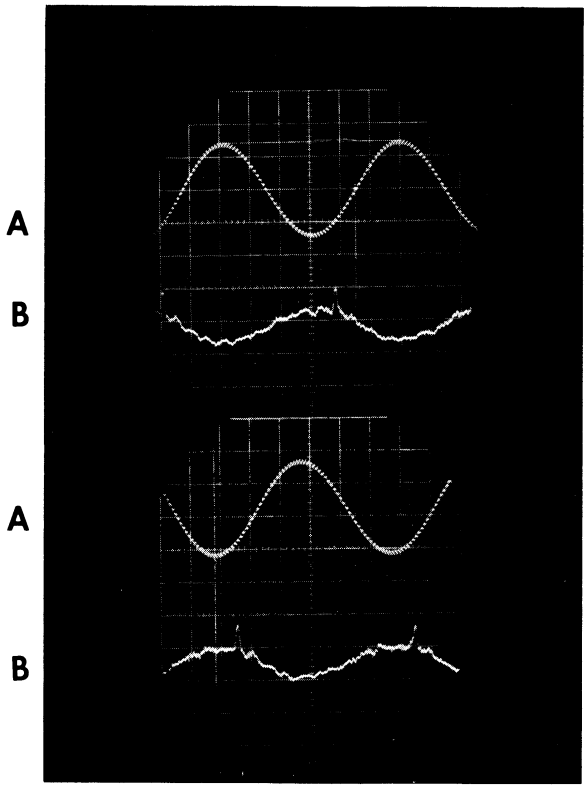

Figure 33. Typical Oscilloscope Traces Representing (a) Displacement of Vibrating Surface and (b) Signal from Force Pickup, Both as a Function of Time.

φ in the vibration cycle. The force curve has a wave shape similar to the displacement but 180 degrees out of phase with it. This variation does not represent a force change but instead is an unwanted acceleration signal arising from the fact that the transducer is mounted in a moving platform. However the small spike appearing once each cycle on the force signal does represent the impact of the transport material as it reestablishes contact with the vibrating surface after each interval of hopping. The location of the spike in the vibration cycle is thus the measured value of angle φ_b used earlier to denote the end of hopping. A list of these angles taken from oscillograms for the test runs is shown in Table VII.

TABLE VII

IMPACT ANGLES FOR VERTICAL VIBRATION

		Observed Angle φ_b (deg)		
h(in.)	V(g's)	A = .030 in.	A = .049 in.	A = .068 in.
1	1.5	-	324	326
	2.0	294	308	296
	3.0	258	270	274
2	1.5	330	333	331
	2.0	305	315	296
	3.0	270	280	270
3	1.5	330	337	328
	2.0	314	319	310
	3.0	276	270	286

2. High Speed Photographic Observations

The individual glass beads comprising the test material could behave much like a porous plate, i.e., have identical trajectories, if

they were vibrated vertically in a vacuum and internal damping eliminated any tendency to rebound. However, the surrounding medium and induced air flow will affect the motion of both the bulk mass and the individual particles of the test sample.

In order to discover the order of magnitude of particle separation and distributed mass effects in the material, high speed motion pictures were made of the vertical tube arrangement of Figure 21 during operation. A succession of photographs showing a typical vibration cycle projected directly from the motion picture film is presented in Figure 34. The conveyor frequency and amplitude were set at 1270 rpm and .068 inch respectively, so that the vibration has a vertical acceleration of 3g. The test material has a height of 1.5 inch.

It is apparent from these pictures that the test material exhibits a fairly large amount of "accordion" action, but that this motion is periodic with only small random changes from cycle to cycle. That this effect is due to air flow through the material is apparent from the top-most layers of the sample: they are seen to thin out periodically and to have a much larger amplitude of motion than could be accounted for by dynamic action alone.

The bottom layers of the material appear to move as a rigid body. It is seen that they separate cleanly from the vibrating surface during the interval of hopping and undergo no apparent rebound after landing. The maximum amount of separation is judged from the vertical scale to be about 1/32 inch. This is in good agreement with

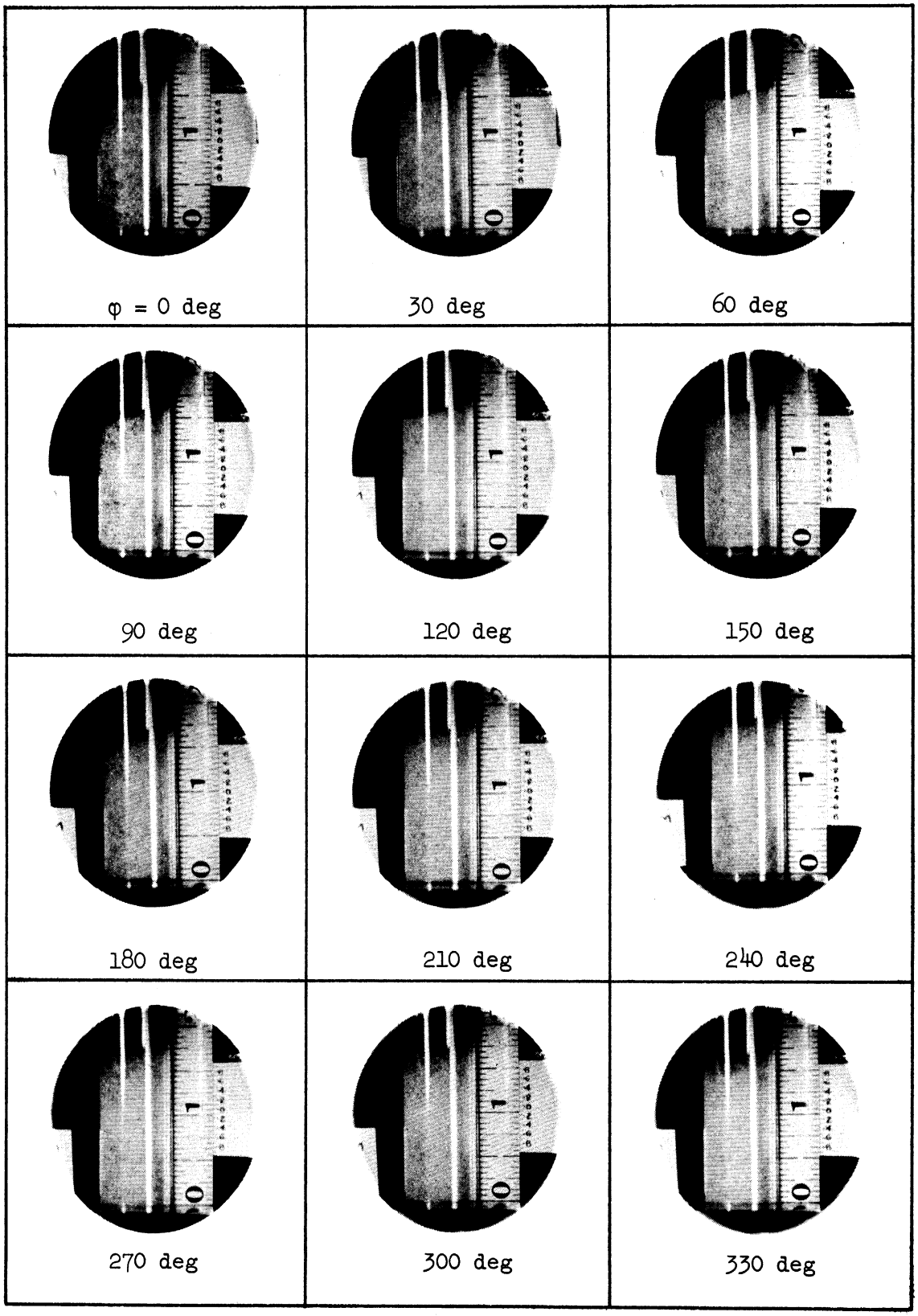

Figure 34. Sequence of High-Speed Photographs Showing Typical Dynamic Action of Transport Material.

the value of .029 inch predicted for the given operating conditions from the porous plate model analysis. By contrast, a maximum separation about 5 times larger (.167 inch) is predicted from the hopping particle model which takes no account of air flow effects.

It is very difficult to obtain accurate values for the takeoff and landing angles φ_a and φ_b from inspection of the motion pictures. However, in Figure 34 there is no visible separation of the material from the surface prior to φ = 90 deg, whereas the theoretical value of φ_a for a 3g vibration is only 19 deg. Also, the material appears to have completed its flight in Figure 34 by φ = 240 deg, but the landing angles calculated from the particle and plate models, φ_b = 360 and 270 deg respectively, occur much later in the cycle. These values may not represent typical discrepancies between actual and predicted operation but do suggest the qualitative effect of distributed-mass dynamics in the material motion

3. Comparison with Porous Plate Model

The results obtained for the landing impact angles φ_b as given in Table VII indicate that the depth of material had little effect on the vertical motion of the material. This is in agreement with the porous plate analysis where the damping coefficient λ defined by Equation (45) and hence the motion of the plate predicted by Equation (46) are not functions of plate thickness h. It is also evident from Table VII that an increase of vibration amplitude at constant acceleration level produced only a random change in the

observed landing angle φ_b, whereas the porous plate analysis as seen from Equation (47) and Table V indicates that φ_b decreases with amplitude.

The sharp contrast between the calculated and experimental values of the material landing event in the vibration cycle is shown in Table VIII. Here average measured values of angle φ_b taken from Table VII are listed for three acceleration levels along with calculated values from the particle and plate model analyses.

TABLE VIII

COMPARISON OF VERTICAL VIBRATION ANGLES

V(g's)	Vibration Angle φ_b (deg) from		
	Particle Model	Plate Model	Impact Tests
1.5	245	205	330
2.0	295	235	305
3.0	360	270	270

The largest calculated angles, and hence the most optimistic transport velocities, are predicted by the particle model; and hopping of the material persists later in the vibration cycle as the acceleration level increases. The porous plate results suggest that although the interval of material flight is severely reduced by air flow effects, hopping increases with acceleration level. An opposite trend is evident from the impact test results, however, with the landing event occurring earlier in the vibration cycle as acceleration is increased.

Since the photographic observations indicate that the test material completes its hopping action during the third quadrant of the vibration cycle and thus are in general agreement with the porous plate results, there is some doubt as to the validity of the impact measurements. It is quite possible that the pressure pickup used for the tests did not actually signal recurrence of material contact in the cycle but responded instead to a later impulse set up in the distributed elements of material overhead. On the other hand, the pickup traces may well indicate the point of equivalent solid-body impact of the test sample with the conveyor surface.

In any event, the results indicate the inherent shortcoming of the porous plate as a dynamic model of the transport material whose vertical motions become increasingly those of a distributed-mass system at high accelerations. On the other hand, both the porous plate model and the vertical vibration experiments demonstrate that cyclic motions of bulk transport materials are possible at conveyor accelerations above the 3.3 g limit predicted by the simple particle model. There is in addition the photographic evidence that hopping of the bulk material does not begin at the instant the surface acceleration reaches 1.0 g but is delayed considerably by dynamic effects carried over from the previous cycle.

V. SUMMARY AND CONCLUSIONS

A. Objectives of the Investigation

This research was undertaken to (a) study the mechanism by which a bulk material can be conveyed across a level surface undergoing an inclined sinusoidal vibration; (b) determine the relation between operating variables and performance in an experimental conveyor for a given granular material; (c) compare experimental results with those predicted from idealized dynamic models that account for the density, friction, and porosity of the test material; and (d) seek optimum conditions of operation and design limits in the vibratory transport of bulk materials.

B. Over-all Results and Conclusions

The results of this investigation show that for a specified combination of material, surface, and conveyor vibration, the material flow rate can be predicted with engineering accuracy from the analysis of an appropriate theoretical model of the transport system. It is shown that simple particle representations of the material can account for the characteristic hopping and sliding of the transport mechanism. In addition, the reduced flow rates observed in the transport of a relatively fine-grained material are correlated with the analysis of a porous plate model of the material. Specific results and conclusions are as follows:

1. The material flow rate produced by a vibratory conveyor is linearly related to the depth of material but reaches a maximum when the vibration is inclined at 20 to 40 deg with the horizontal.

2. The flow velocity attained by the material has a practical upper limit equal to the peak horizontal velocity of the vibrating surface.

3. Maximum vibratory transport is achieved primarily through the mechanism of cyclic hopping, and to a lesser extent sliding, of the bulk material; for this reason the most important conveyor operating parameter is the peak vertical acceleration of the vibrating surface.

4. For conveyor accelerations less than 1.0 g, material transport takes place entirely by sliding and the flow velocity depends not only on the acceleration level but also on the friction coefficient at the material-surface interface.

5. Above 1.0 g the flow velocity of a given material increases almost exponentially with conveyor acceleration, reaching its maximum value in the neighborhood of 3 to 5 g.

6. An inelastic particle capable of hopping and sliding motions can be used as an idealized dynamic model of the transport material to analyze conveyor performance characteristics.

7. For preliminary design purposes, the particle model analysis predicts the transport of all dry materials for conveyor accelerations in the zero to 1.0 g range, and of most coarse-grained materials above this range.

8. Cyclic hopping of a layer of bulk material on a conveyor surface, and therefore its vibratory transport, is made possible by cyclic transmission of air through the openings in the material.

9. A porous plate model is useful in studying the transport dynamics of fine-grained bulk materials, and the model analysis shows that the attainable flow velocities are indirectly reduced, particularly at large vibration amplitudes, by the lack of air permeability and/or low material density.

10. The cyclic hopping characteristics of a given material, on which the transport mechanism depends, can be observed as a one-dimensional motion by vibrating a material sample in the vertical direction only.

C. Areas Requiring Further Study

The results of this investigation suggest that further study might profitably be devoted to the following problems: (a) development of simple dynamic, rather than static, tests for bulk material friction and permeability so that measured values are more closely related to the transport mechanism; (b) refinement of the vertical vibration apparatus and its instrumentation as a possible test system for rating the conveyability of any given material; (c) comparison of conveyor performance with a series of test materials each differing only in grain size; and (d) investigation of non-sinusoidal and/or two dimensional surface vibrations as a means of improving the conveyability of fine-grained materials.

BIBLIOGRAPHY

1. Antwerpen, F. J. "Vibratory Equipment", Industrial and Engineering Chemistry, (June, 1940), 765-770.

2. Bachmann, D. "Beitrag zur Klärung des Schwingmahlvoranges". Unpublished dissertation, Technische Hochschule, Karlsruhe, 1939.

3. Böttcher, S. "Beitrag zur Klärung der Gutbewegung auf Schwingrinnen." (in three parts), Fördern und Heben, No. 3 (1958), 127-131; No. 4 (1958), 235-240; No. 5 (1958), 307-315.

4. Brickman, A. D. and Jenks, B. L. "Dynamic Analysis and Design Criteria for a Class of Vibration-Producing Machines", Transactions of the American Society of Mechanical Engineers - Journal of Engineering for Industry, (October, 1963).

5. Chahbandoor, J. "Vibrating Conveyors - Their Operation and Use", Foundry, (September, 1957), 160-162.

6. "Conveyor Vibrates at Natural Frequency", Chemical Engineering, LVIII (1951), 180-181.

7. During, K. "Berechnung der Amplituden von Electromagnetischen Schwingförderrinnen", Fordern und Heben, No. 8 (1962), 607-615.

8. Erisman, M. J. "Research in Bulk Materials Handling", Mechanical Engineering, (March, 1961), 55-59.

9. Flint, H. J. "Vibrating Conveyors", Modern Materials Handling, (March, 1954), 109-114.

10. Hagenbrook, L. D. and Hlinsky, E. J. "Analysis of a Shaker Motion for a Conveyor Application", Product Engineering, (April, 1952), 134-139.

11. Hinkle, R. T. Design of Machines. Englewood Cliffs, N. J.: Prentice-Hall, Inc., (1957), 83-91.

12. Hurst, C. J. "Effect of Surface Friction on Vibrating Conveyor Performance", Unpublished Master's thesis, The Pennsylvania State University, 1961.

13. Israelson, A. F. "Development and Uses of a New Line of Vibratory Feeders", Transactions of the American Society of Mechanical Engineers, No. 81 (1959), 384-352.

14. Jenike, A. W. "Gravity Flow of Bulk Solids", American Society of Mechanical Engineers Paper Number 60-WA-81, November, 1960.

15. Jenike, A. W., Elsey, P. J., and Woolley, R. H. "Flow Properties of Bulk Solids", Proceedings of the American Society for Testing Materials, No. 60 (1960), 1168-1180.

16. Jung, R. "Die Gleitbewegung auf der Schwingenden Ebene", Forschung auf dem Gebiete des Ingenieurwesens, No. 18 (1952), 13-24.

17. Klockhaus, W. "Fordergeschwindigkeit von Schwingrinnen und Schwingsieben", Erdol und Kohle, No. 5 (1952), 493-494.

18. Kneeland, F. H. "Jigging Conveyor Reduces Coal Mining Costs", Coal Age, (February, 1926), 287-291.

19. Kroll, W. "Über das Verhalten von Schuttgut in lotrecht schwingenden Gefaben", Forschung auf dem Gebiete des Ingenieurwesens, No. 20 (1954), 2-15.

20. "Oscillating Trough Conveyor", Steel, (April, 1946), 113-114.

21. "A Reciprocating Underground Coal Conveyor", Coal Age, No. 14 (October, 1918), 682-684.

22. Richmond, O. "Gravity Hopper Design", Mechanical Engineering, (January, 1963), 46-49.

23. Schraud, A. "Der Leistungsbedarf von Schwingförderanlagen", Forschung auf dem Gebiete des Ingenieurwesens, No. 23 (1957), 74-76.

24. Schultz, R. B. "The Performance Characteristics of a Horizontal Vibrating Conveyor". Unpublished Master's thesis, The Pennsylvania State University, 1959.

25. Sloane, W. W. "Controlling Inertia", Machine Design, (July, 1953), 154-158.

26. Thornton, C. A. "Use of Vibration as Means of Industrial Drive", Proceedings of the Institution of Mechanical Engineers, No. 157 (War Emergency Issue No. 25, 1947) 20-31.

27. Whitelock, J. H. "Solution to a Difficult Conveying Problem", Mechanical Handling, (October, 1947), 523-527.

28. Wolff, E. "The Motion of Bulk Materials on Vibratory Conveyors", American Society of Mechanical Engineers, Paper No. 62-WA-41, November, 1962.

29. Zilly, R. G. "Vibrating Conveyors", Modern Materials Handling, (November, 1958), 101-108.

APPENDIX A

CONTINUOUS SLIDING MOTION OF PARTICLE MODEL

1. Transition Angles

Variations in the velocities of both the material particle and vibrating surface for this type of conveyor motion are shown in the lower part of Figure 9. During the forward slide phase of the cycle the force diagram of Figure 2(a) applies and $F = \mu G$ because of the relative motion of the particle. Thus the equation of particle motion in the x direction is

$$m\ddot{x} = -F = -\mu G \qquad \text{(A-1)}$$

and in the y direction

$$m\ddot{y} = G - mg \qquad \text{(A-2)}$$

Since $\ddot{y} = \omega^2 A_y \sin\varphi$ and $V = A_y\omega^2/g$, (A-2) can be solved for G and the result substituted into (A-1) to obtain

$$\ddot{x} = -\mu g(1 - V \sin\varphi) \qquad \text{(A-3)}$$

The forward slide begins at φ_o when the particle and surface velocities are both $A_x\omega \cos\varphi_o$. Using this as a lower limit and noting that $A_y/A_x = \tan\alpha$, one can integrate (A-3) to obtain a dimensionless expression for the particle velocity $\dot{x}$ as follows:

$$\frac{\omega\dot{x}}{\mu g} = V\left(\frac{1 + \mu\tan\alpha}{\mu\tan\alpha}\right)\cos\varphi_o - V\cos\varphi - (\varphi - \varphi_o) \qquad \text{(A-4)}$$

The transition from forward to backward slide takes place at φ_1 when the particle and surface velocities as shown in Figure 9 again become equal at $A_x\omega \cos\varphi_1$. When $\dot{x}$ in (A-4) is replaced by this velocity and φ by φ_1, the resulting equation relates φ_1 and φ_o as follows:

$$\frac{\cos\varphi_o - \cos\varphi_1}{\varphi_1 - \varphi_o} = \frac{1}{V} \frac{\mu\tan\alpha}{1 - \mu\tan\alpha} \qquad \text{(A-5)}$$

During backward slip, the equation of particle motion changes from (A-1) to

$$m\ddot{x} = -F = \mu G \qquad \text{(A-6)}$$

because the relative velocity, and hence F, change sign. By using (A-2) which still applies and a lower velocity limit of $A_x\omega\cos\varphi_1$, one can obtain

$$\frac{\omega\dot{x}}{\mu g} = V\left[\frac{1 - \mu\tan\alpha}{\mu\tan\alpha}\right]\cos\varphi_1 + V\cos\varphi + (\varphi - \varphi_1) \qquad \text{(A-7)}$$

from an integration of the equation of motion. At the end of backward slip, the angle $\varphi = \varphi_o + 2\pi$ and the velocity $\dot{x}$ becomes $A_x\omega\cos\varphi_o$. Making these substitutions in (A-7) one obtains a second relation between φ_o and φ_1 as follows:

$$\frac{\cos\varphi_o - \cos\varphi_1}{\varphi_o + 2\pi - \varphi_1} = \frac{1}{V} \frac{\mu\tan\alpha}{1 - \mu\tan\alpha} \qquad \text{(A-8)}$$

This equation is Equation (36) in Chapter II, whereas Equation (35) is merely a simpler form resulting from the combination of (A-5) and (A-8).

2. Transport Velocity Ratio

During the forward slide phase $\varphi_o < \varphi < \varphi_1$ the relative forwardurd velocity $\dot{s}$ of the particle is $\dot{x}$ from (A-4) less the surface velocity $A_x\omega\cos\varphi$. This can be reduced to

$$\frac{\omega\dot{s}}{\mu g} = V\left(\frac{1 + \mu\tan\alpha}{\mu\tan\alpha}\right)(\cos\varphi_o - \cos\varphi) - (\varphi - \varphi_o) \qquad \text{(A-9)}$$

Similarly during the backward slide phase $\varphi_1 < \varphi < \varphi_o + 2\pi$ the relative velocity can be expressed from (A-7) as

$$-\frac{\omega\dot{s}}{\mu g} = V\left(\frac{1 + \mu\tan\alpha}{\mu\tan\alpha}\right)(\cos\varphi_1 - \cos\varphi) - (\varphi - \varphi_1) \qquad \text{(A-10)}$$

The net increment of displacement through which the particle moves in one complete cycle is obtained by integrating $\dot{s}(dt) = \dot{s}(d\varphi)/\omega$ between φ_o and $\varphi_o + 2\pi$. This must be done in two parts however, using the $\dot{s}$ of (A-9) in the integration from φ_o to φ_1 and the $\dot{s}$ of (A-10) from φ_1 to $\varphi_o + 2\pi$. The transport velocity U is then found by multiplying the net sliding displacement per cycle by $n = \omega/2\pi$. After considerable manipulation and the use of (A-5) and (A-8), the following transport velocity ratio results:

$$\frac{U}{A_x\omega} = \left(\frac{1 + \mu^2\tan^2\alpha}{2}\right)(\cos\varphi_o + \cos\varphi_1) + \left(\frac{\mu\tan\alpha}{\pi}\right)(\sin\varphi_o - \sin\varphi_1) \qquad \text{(A-11)}$$

APPENDIX B

HOP SLIDE MOTION OF PARTICLE MODEL

1. Transition Angles

As indicated in Figure 8, when the friction factor $\mu\tan\alpha$ is less than about .35, the particle motion can be one of continuous sliding on the conveyor surface for accelerations less than 1.0g. When the acceleration level exceeds 1.0g, this characteristic motion continues but its forward slide phase is regularly interrupted by an interval of hopping during $\varphi_a < \varphi < \varphi_b$. A velocity diagram for the hop-slide motion is shown in Figure 10.

Consider first the interval of forward slide starting at φ_o for which (A-4) gives the particle velocity $\dot{x}$. When this slide reaches the point of hopping at $\varphi = \varphi_a$, (A-4) gives the instantaneous velocity $\dot{x}_a$ as

$$\frac{\omega\dot{x}_a}{\mu g} = V\left(\frac{1 + \mu\tan\alpha}{\mu\tan\alpha}\right)\cos\varphi_o - V\cos\varphi_a - (\varphi_a - \varphi_o) \qquad \text{(A-12)}$$

At the end of the hopping event, $\varphi = \varphi_b$ and the sliding resumes according to equation of motion (A-3). Using $\dot{x}_a$ as a lower limit for the velocity and φ_b for the angle one can integrate (A-3) to obtain the subsequent sliding velocity $\dot{x}$ in the form

$$\frac{\omega\dot{x}}{\mu g} = \frac{\omega\dot{x}_a}{\mu g} - V(\cos\varphi - \cos\varphi_b) - (\varphi - \varphi_b) \qquad \text{(A-13)}$$

The forward slide persists as shown in Figure 10 until $\varphi = \varphi_1$ at which point the particle velocity $\dot{x}$ becomes equal to the surface velocity $A_x\omega\cos\varphi_1$, and (A-13) after some rearrangement yields Equation (38).

Because the backward slide interval begins immediately at φ_1 and proceeds without interruption until $\varphi_o + 2\pi$, Equation (36) developed above holds also for this case. Thus Equations (36) and (38) together yield unique values for the transition angles φ_o and φ_1 in this type of motion.

2. Transport Velocity Ratio

During each of the four phases into which the vibration cycle of Figure 10 is divided, the particle will realize some relative horizontal displacement along the vibrating surface. The algebraic sum of these displacements multiplied by the frequency n yields the transport velocity U.

In the following analysis, velocities and displacements of the particle corresponding to the four phases of motion will be designated by subscripts according to the following plan:

phase	duration	instantaneous x velocity		net relative x displ.
		absolute	relative	
1	$\varphi_o < \varphi < \varphi_a$	$\dot{x}_1$	$\dot{s}_1$	s_{m1}
2	$\varphi_a < \varphi < \varphi_b$	$\dot{x}_a$	$\dot{s}_2$	s_{m2}
3	$\varphi_b < \varphi < \varphi_1$	$\dot{x}_3$	$\dot{s}_3$	s_{m3}
4	$\varphi_1 < \varphi < \varphi_o + 2\pi$	$\dot{x}_4$	$\dot{s}_4$	s_{m4}

The development of an expression for the particle velocity $\dot{x}$ during each phase is similar to that of (A-4) and (A-7) in Appendix A. That is, one starts with the appropriate differential equation of motion

and integrates once with the lower limits of velocity and angle appearing in Figure 10. When this is done, one obtains

$$\frac{\omega\dot{x}_1}{\mu g} = V\left(\frac{1 + \mu\tan\alpha}{\mu\tan\alpha}\right)\cos\varphi_o - V\cos\varphi - (\varphi - \varphi_o) \qquad (A\text{-}4)$$

$$\frac{\omega\dot{x}_a}{\mu g} = V\left(\frac{1 + \mu\tan\alpha}{\mu\tan\alpha}\right)\cos\varphi_o - V\cos\varphi_a - (\varphi_a - \varphi_o) \qquad (A\text{-}12)$$

$$\frac{\omega\dot{x}_3}{\mu g} = \frac{\omega\dot{x}_a}{\mu g} - V(\cos\varphi - \cos\varphi_b) - (\varphi - \varphi_a) \qquad (A\text{-}14)$$

$$\frac{\omega\dot{x}_4}{\mu g} = V\left(\frac{1 - \mu\tan\alpha}{\mu\tan\alpha}\right)\cos\varphi_1 + V\cos\varphi + (\varphi - \varphi_1) \qquad (A\text{-}7)$$

The procedure for finding the increment of displacement s_m for each phase follows that employed in the Chapter II particle model analysis. That is, one first forms an expression for the relative velocity, e.g., $\dot{s}_1 = \dot{x}_1 - A_x\omega\cos\varphi$, then integrates this velocity over the appropriate interval, e.g., $s_{m1} = \int_{\varphi_b}^{\varphi_a} \dot{s}_1 d\varphi/\omega$. The resulting expressions for s_m can be simplified somewhat by the substitution of relations (A-5), (A-8), and Equations (4) and (9) but still involve a great many algebraic and trigonometric combinations of the transition angles as follows:

$$(s_{m1} + s_{m3})\frac{\omega^2}{\mu g} = V\left(\frac{1 + \mu\tan\alpha}{\mu\tan\alpha}\right)\left[(\varphi_a - \varphi_o)\cos\varphi_o - (\varphi_1 - \varphi_b)\cos\varphi_1\right]$$

$$+ V\left(\frac{1 + \mu\tan\alpha}{\mu\tan\alpha}\right)\left[(\sin\varphi_b - \sin\varphi_a) + (\sin\varphi_o - \sin\varphi_1)\right]$$

$$+ \frac{1}{2}\left[(\varphi_1 - \varphi_b)^2 - (\varphi_a - \varphi_o)^2\right] \qquad (A\text{-}15)$$

$$\frac{s_{m2}\omega^2}{\mu g} = \frac{(\varphi_b-\varphi_a)^2}{2\mu\tan\alpha} - (\varphi_b-\varphi_a)\left[V\left(\frac{1+\mu\tan\alpha}{\mu\tan\alpha}\right)(\cos\varphi_a-\cos\varphi_b) + (\varphi_a-\varphi_o)\right] \tag{A-16}$$

$$\frac{s_{m4}\omega^2}{\mu g} = \frac{1}{2}(\varphi_o + 2\pi - \varphi_1)^2\left[\frac{\cos\varphi_o+\cos\varphi_1}{\cos\varphi_o-\cos\varphi_1}\right] - (\varphi_o+2\pi-\varphi_1)\left[\frac{\sin\varphi_o-\sin\varphi_1}{\cos\varphi_o-\cos\varphi_1}\right] \tag{A-17}$$

Finally, numerical results from the four s_m equations can be added and transformed into a transport velocity ratio as follows:

$$s_m = (s_{m1} + s_{m2}) + s_{m3} + s_{m4} \tag{A-18}$$

$$\frac{U}{\omega A_x} = \left(\frac{s_m\omega^2}{\mu g}\right)\frac{\mu\tan\alpha}{2\pi V} \tag{A-19}$$

APPENDIX C

TABULATION OF EXPERIMENTAL DATA

TABLE VI

PERFORMANCE DATA FOR TEST CONVEYOR

α = 20 deg

A = .068 in.			A = .049 in.			A = .030 in.			A = .020 in.			A = .009 in.		
WΔt lb	Δt min	nΔt rev	WΔt lb	Δt min	nΔt rev	WΔt lb	Δt min	nΔt rev	WΔt lb	Δt min	nΔt rev	WΔt lb	Δt min	nΔt rev
20	4.375	3945	20	5.200	5172	20	5.486	8399	10	3.561	6200	10	4.754	12538
20	2.445	2690	20	4.090	4920	20	3.072	5533	20	6.163	11698	10	2.092	5934
20	1.545	1900	20	2.165	3065	20	1.783	3563	20	1.515	3593	10	1.422	4316
20	0.939	1345	20	1.616	2446	20	1.238	2596	20	1.120	2834	10	0.991	3208
20	0.698	1107	20	1.275	2049	20	0.903	1974	20	2.683	5900	20	1.624	5427
20	0.529	904	20	1.062	1769	20	0.727	1657	20	0.795	2149	20	1.383	4755
20	0.450	813	20	0.776	1389	20	0.617	1479	20	0.618	1916	10	0.647	2285
			20	0.652	1229	20	0.574	1442	20	0.484	1600	10	0.580	2113
			20	0.555	1103	20	0.509	1320	20	0.659	1988	10	0.515	1923
			20	0.498	1029	20	0.458	1219	20	0.649	1880	10	0.474	1809
									20	0.685	1919			
									20	0.550	1767			
									20	0.520	1690			

α = 30 deg

10	1.435	900	10	1.857	1896	10	2.442	2487	5	1.575	2578	5	1.556	3796
20	1.283	1444	10	1.076	1326	10	1.251	2049	10	2.065	3786	10	1.595	4199
10	0.967	988	20	1.160	1654	15	1.021	1870	15	1.725	3501	10	1.184	3353
20	1.058	1304	20	0.757	1243	10	0.475	964	20	1.380	3068	10	0.911	2765
20	0.825	1096	20	0.550	1009	20	0.668	1488	20	1.034	2504	10	0.750	2431
20	0.642	916	20	0.437	886	20	0.538	1292	20	0.839	2214	10	0.621	2132
20	0.529	808				20	0.471	1231	20	0.672	1903	10	0.538	1957
20	0.466	764							20	0.620	1880	10	0.458	1755
20	0.407	707							20	0.539	1743			

α = 40 deg

10	1.601	1148	10	1.342	1376	10	2.589	3188	10	2.876	4722	10	2.863	6405
10	0.996	920	20	1.579	1941	10	1.320	1896	10	1.319	2426	5	0.926	2252
20	1.405	1442	20	0.957	1369	20	1.565	2561	10	0.761	1549	10	1.254	3305
20	1.130	1270	20	0.657	1077	20	1.068	1962	20	1.119	2504	10	1.000	2833
20	0.878	1079	20	0.527	968	20	0.787	1602	20	0.900	2178	10	0.928	2817
20	0.693	918	20	0.445	908	20	0.653	1460	20	0.774	2037	10	0.687	2225
20	0.589	840				20	0.555	1344	20	0.673	1907	10	0.617	2120
20	0.506	775				20	0.503	1315	20	0.625	1898	10	0.543	1979
20	0.452	741							20	0.582	1882	10	0.474	1817

α = 50 deg

10	1.425	1028	10	1.335	1366	10	1.032	1477	5	0.879	1440	5	0.812	1976
10	0.918	849	10	0.730	900	5	1.047	1286	10	1.088	1994	5	0.614	1618
20	0.967	1085	20	0.933	1334	10	0.728	1191	10	0.755	1533	5	0.526	1490
20	0.882	1013	20	0.727	1188	20	1.096	2012	10	0.643	1434	5	0.471	1431
20	0.706	932	20	0.606	1113	20	0.892	1815	20	1.038	2526	5	0.258	936
20	0.641	916	20	0.524	1066	20	0.747	1653	20	0.900	2373	5	0.320	1103
20	0.570	869	5	0.925	763	20	0.649	1571	20	0.774	2197	5	0.383	1238
20	0.533	872				20	0.591	1554	20	0.754	2294	5	0.287	1014
									20	0.672	2175	5	0.267	998

α = 60 deg

5	0.751	540	5	0.939	770	5	1.160	1422	5	0.909	1482	5	1.013	2467
10	0.874	811	10	1.183	1213	10	1.084	1555	10	1.192	2181	5	0.800	2112
20	1.071	1202	10	0.718	885	10	0.799	1306	10	0.923	1872	5	0.668	1898
20	0.941	1158	10	0.544	780	10	0.637	1164	10	0.770	1717	5	0.589	1795
20	0.796	1138	10	0.452	738	10	0.561	1143	10	0.638	1553	5	0.500	1619
20	0.659	1065	20	0.663	1346	10	0.482	1073	10	0.561	1482	10	0.896	3083
20	0.566	1036	20	0.776	1423	10	0.425	1032	10	0.505	1465	5	0.381	1386
						10	0.377	993	10	0.464	1411	5	0.352	1352
									10	0.410	1326			